Thesis for The Degree of Doctor of Philosophy

Installation Effects on the Acoustics of Low-Pressure Axial Fans

Aspects of Source, Environment and Receiver

Michail Vourakis

Department of Mechanics and Maritime Sciences
CHALMERS UNIVERSITY OF TECHNOLOGY
Göteborg, Sweden 2025

Installation Effects on the Acoustics of Low-Pressure Axial Fans
Aspects of Source, Environment and Receiver
Michail Vourakis
ISBN 978-91-8103-333-5

Acknowledgements, dedications, and similar personal statements in this thesis, reflect the author's own views.

Doktorsandlingar vid Chalmers tekniska högskola
Ny serie nr 5790
ISSN 0346-718X
https://doi.org/10.63959/chalmers.dt/5790

Department of Mechanics and Maritime Sciences
Chalmers University of Technology
SE-412 96 Göteborg, Sweden
Telephone: +46(0)31 772 1000

Printed by Chalmers Reproservice
Gothenburg, Sweden 2025

Installation Effects on the Acoustics of Low-Pressure Axial Fans
Aspects of Source, Environment and Receiver
Michail Vourakis
Department of Mechanics and Maritime Sciences
Division of Fluid Dynamics
Chalmers University of Technology

Abstract

Low-pressure axial fans are employed in a wide range of applications, from industrial systems to domestic appliances. Their operation in proximity to humans necessitates the mitigation of noise emissions to prevent adverse health effects and promote comfort. The acoustic characteristics of these fans are influenced by installation effects, considered here in terms of inlet geometry, upstream obstructions, parallel fan operation, and the acoustic field of the test environment. Installation effects associated with the fan's local flow field modify the underlying aeroacoustic source processes, while the test environment influences sound propagation. Furthermore, the assessment of installation effects must consider human perception of noise.

In this work, installation effects on the acoustics of low-pressure axial fans are investigated experimentally. A round robin test of a benchmark fan is first conducted to evaluate both the aerodynamic and acoustic measurement capabilities of a bespoke fan performance facility. In addition, the influence of room-acoustical effects is examined, along with the estimation of sound power and directivity using a spherical harmonics scheme of the half-space.

A series of case studies on a low-pressure axial fan with rotating ring, investigates the effects of inlet geometry, upstream obstructions, and spacing in parallel fan operation on the system's acoustic performance. Psychoacoustic metrics are also evaluated with respect to the installation conditions.

Finally, seven 3D-printed fans are employed to investigate the influence of blade loading distribution and hub-to-tip ratio on aeroacoustic performance. The interaction between the examined rotor design parameters and installation effects, in particular inlet geometry and upstream obstructions, is also studied.

This work advances the understanding of installation effects on the acoustics of low-pressure axial fans, considering the aspects of source, environment, and receiver. The findings provide guidance for the evaluation and abatement of noise emissions from installations of low-pressure axial fans.

Keywords: low-pressure axial fans, installation effects, aeroacoustics, psychoacoustics, room-acoustical effects, inlet geometry, upstream obstructions.

Παιγνίδια εγωκεντρισμού με το στανιό θα παίξεις,
οπλίσου δυνατή καρδιά σα θες να τα αντέξεις!
Μ.Β.

Acknowledgments

It is said that *"words mean nothing, it is the actions that count"*. I tend to agree with that saying and, thus I hope that I have managed through my actions to show some gratitude to all these people that I got the chance to work and interact with during the period of my doctoral studies. However, I must acknowledge my faulty nature so I will try to set things right in the following lines.

I would like to begin by expressing my gratitude to my supervisors Sassan Etemad, Niklas Andersson, Mikael Karlsson and Elias Zea for giving me the opportunity to take part in this project, and supporting me throughout. I think you make a versatile, capable, winning team and consider myself lucky working under your guidance. I cherish the many discussions we had of both technical and informal nature. The encouraging and positive atmosphere you created made this work rewarding and provided breathing space for my growth as a researcher. I aspire to many of the traits you showcased throughout, or to put it better you may consider me a fan!

I would like express my gratitude to Mats Åbom, who has not only instilled in me the curiosity for the field of aeroacoustics but has also mentored my professional steps during and after my masters, including the undertaking of my doctoral studies.

I would also like to express my gratitude to Franz Zotter and Eric Brandão for collaborating in part of this work. Despite the limited amount of online encounters I enjoyed the collaborative environment you promoted and the constructive feedback you provided. Thinking back to it, I would not say I am surprised about this fruitful collaboration since Elias was the one that orchestrated it.

I would also like to thank Hans Bodén for the insightful discussion at my licentiate seminar, which was especially rewarding given his pivotal role in my master's education in sound and vibration.

I would like to thank all the people at VOLVO TRUCKS who supported and delivered solutions for the measurements conducted there. Thank you Andreas Lygner for always providing robust solutions when it comes to the tested fan installations and Antonio Ortiz for facilitating special design requests for many parts of the setups tested. Thank you Jan Niklasson, Carl Levenstam and all the other engineers and technicians at the vehicle workshop for fabricating and putting up with our demanding requests. Thank you Roger Carlsson, Eric

Persson and all the engineers and technicians who helped with any problems that arose during the measurements at the Fan Test Rig. Thank you Torbjörn Ågren, Frédéric Wullens, Theresia Manns and all the other members of the steering committee group for providing feedback throughout this project. I would also like to extend my gratitude to the members of the steering committee group from VOLVO CARS for providing feedback during this work and especially Randi Franzke for making the LDA measurements at the Fan Test Rig a reality. On the same note I thank Mats Herbert for his support with the LDA system and David Sedarsky for providing advice concerning measurement settings.

Thanks to all the tutors and classmates involved in the courses I enrolled at during my PhD studies, your passion and expertise made learning more enjoyable. Special shootout to all the people involved at ASSA in Eindhoven. My gratitude is also extended to all the students at Chalmers I interacted with. I hope that I have been of some assistance.

Thanks to Paul, Angelica, Christina and all the other motivated colleagues I worked with during my time at DS. Your passion for contributing to a better life for PhD students and the kindness you brought along is inspiring and makes me hopeful for the future of academia.

To my colleagues and senior faculty at the Division of Fluid Dynamics, thank you for finding the time to talk with me about research, politics and any other topic at hand. Your contribution to me feeling a part of this division is probably higher than you think. Special shout-out to Valentin for tolerating me at his office over these years and to Debarshee for our research collaboration and most importantly his active support in the beginning of my PhD studies, despite me making a quite bad first impression.

A warm thank you to Kostas and all the other people I have hiked with, as well as Suvi, Adam, Jacob and rest of the climbing gang. You helped me lots in maintaining a balanced life on the face of these challenging years.

Θερμές ευχαριστίες σε όλα τα παιδία από Ελλάδα: Παρή, Γιώργο, Στράτο, Ρωμανό, Μίνω, Παπαζώτο, Κατερίνα, Ντάτση, Πωλίνα, Ευδοκία, Αρχοντούλα, Κούτρα και λοιπούς που κρατάνε ψηλά το λάβαρο της φιλίας ανεξάρτητα αποστάσεων και συνθηκών. Ειδική μνεία στον Σταύρο και στην Αντωνία για την γεναιόδωρη και έμπρακτη φιλία τους (συμπεριλαμβανομένης συμβουλευτικής βοήθειας).

Ευχαριστώ την Βαγγελιώ, το Γιώργο και την ανιψία μου για την αγάπη τους.

Παππού Αποστόλη, γιαγιά Βαγγελιώ σας ευχαριστώ για όλα, σας κουβαλάω όσο αναπνέω.

Ότι αποκάμω στη ζωή όσο μακριά και αν φτάσω, πυξίδα βάνω την καρδιά αγάπη να κεράσω. Γιάντα έτσα με μάθατε Μανώλη-Κωνσταντίνα, να είμαι γεναιόδωρος κι ας μην τα έχω φίνα. Μου δώσατε τη δύναμη να στέκομαι στο κόσμο, να προπαθώ να διεκδικώ για το δικό μου δρόμο.

Thank you Minerva, for your generous love and care. You inspire me and make me a better person. Odotan innolla, mitä seuraavaksi tulee!

The herein work was carried out at the Division of Fluid Dynamics, Department of Mechanics and Maritime Sciences at Chalmers University of Technology, as part of the project: eFan, a key enabler for eMobility, Part 2. The collaborators of the project are: Chalmers University of Technology, KTH Royal Institute of Technology, Volvo Group Trucks Technology and Volvo Car Corporation. Funding was provided by the Swedish Energy Agency. All measurements were performed at the facilities of Volvo Group Trucks Technology.

Michail Vourakis
Göteborg, December 2025

List of Publications

This thesis is based on the following appended papers:

Paper 1. Vourakis, M., & Karlsson, M. (2022). *A round robin test of a low-pressure axial fan.* In International Congress on Fan Noise, Aerodynamics, Applications and Systems 2022, 27-29 June, Senlis, France, 2022. https://doi.org/10.26083/tuprints-00021703

Paper 2. Vourakis, M., & Karlsson, M. (2023). *Aeroacoustic interaction effects between parallel low-pressure axial flow fans.* In Tenth Convention of the European Acoustics Association, Forum Acusticum (pp. 3865-3872). https://doi.org/10.61782/fa.2023.0424

Paper 3. Vourakis, M., Zea, E., Etemad, S., Karlsson, M., & Andersson, N. (2025). *Impact of distorted inlet flow on axial fan psychoacoustics.* In International Congress on Fan Noise, Aerodynamics, Applications and Systems 2025, 9-11 April, Antibes/Juan-les-Pins, France, 2025. https://www.fan2025.org/doc/FAN2025%20-PROCEEDINGS%20-%20ISBN%20978-1-905941-32-2.pdf

Paper 4. Vourakis, M., Zotter, F., Brandão, E., & Zea, E. (2025). *Aeroacoustic source characterization at fan test facility with spherical harmonics of the half-space.* JASA Express Letters, 5(5). https://doi.org/10.1121/10.0036723

Paper 5. Vourakis, M., Zea, E., Karlsson, M., Andersson, N., & Etemad, S. (2025). *Installation effects on axial fans: Combined aeroacoustic and psychoacoustic perspective.* Applied Acoustics, 240, 110872. https://doi.org/10.1016/j.apacoust.2025.110872

Paper 6. Vourakis, M., Ghosh, D., Andersson, N., Etemad, S., Karlsson, M., & Zea, E. (2025). *Experimental investigation of installation effects on the aeroacoustics of low-pressure axial fans: on the impact of blade loading distribution and hub-to-tip ratio.* Manuscript.

Other publications

The following papers were published during my PhD studies. However, they are not appended to this thesis, due to contents overlapping that of appended publications or contents not directly related to the thesis.

Ghosh, D., Vourakis, M., Andersson, N., & Etemad, S. (2025). *Computational aeroacoustics of low-pressure axial fans installed in parallel.* Journal of Fluids Engineering, 147(2).
https://doi.org/10.1115/1.4066752

Ghosh, D., Vourakis, M., Boström, A., Andersson, N., Roy, A. & Etemad, S. (2025). *Evaluation of hybrid computational aeroacoustic methods applied to automotive cooling-fans.* In International Congress on Fan Noise, Aerodynamics, Applications and Systems 2025, 9-11 April, Antibes/Juan-les-Pins, France, 2025.
https://www.fan2025.org/doc/FAN2025%20-PROCEEDINGS%20-%20ISBN%20978-1-905941-32-2.pdf

Nomenclature

Abbreviations

LPAF	Low Pressure Axial Fan
TMS	Thermal Management System
FTF	Fan Test Facility
SWL	Sound poWer Level
SPL	Sound Pressure Level
LDA	Laser Doppler Anemometry
BPF	Blade Passing Frequency
CAD	Computer Aided Design
PMA	Phased Microphone Array
SHD	Spherical Harmonic Decomposition
BEM	Blade Element Momentum
SQAT	Sound Quality Analysis Toolbox
PA	Psychoacoustic Annoyance

Contents

Chapter 1

Introduction

Low-pressure axial fans (LPAFs), also denoted as low-speed axial fans, are characterized by high volume flow rates and small pressure gains [1]. These characteristics have been motivating their usage in a multitude of engineering applications. Applications include but are not limited to daily appliances such as heat and ventilation air conditioning systems, computer fans, and hair dryers, as well as thermal management of electric and internal combustion propulsion systems of vehicles, cooling towers, wind tunnels, and mine ventilation. In the case of mine ventilation, this was probably one of the first documented instances of LPAF usage, as noted by Castegnaro [2] with reference to Agricola [3].

Similar to other industrial devices, their energy efficiency, defined here as the ratio of work done by the fan on the fluid to the shaft power input from the motor, has been an important driver for the advancement of LPAFs [4]. This performance parameter has been primarily optimized with respect to the fan's aerodynamic design [1] where obtainable limits can be identified for simpler geometries [5] and standardized installations. Subsequently, the selection of an LPAF for a specific installation requires matching of the installation's pressure losses with the fan's pressure supply at the desired volume flow rate. The pressure losses originate from (mostly stationary) components of aerodynamic (e.g., inlet shroud, guide vanes) and/or application-specific roles (e.g., radiator, structural beam). An example case of an LPAF aerodynamic performance characteristic along with the characteristic of the installation (installation losses) is shown in Fig. 1.1. Ideally the fan is chosen so that the intersection point between the characteristic curves coincides with the fan's highest efficiency operation point as depicted in the figure.

1.1 Problem statement

Unfortunately, the operation of fans, and as such LPAFs, is accompanied by noise generation. Due to the health implications of noise exposure [6], [7], there has been an increased focus on reducing LPAF noise over the last few years [2], [4], [8]. The understanding of the sources of noise in axial fans, thus including LPAFs, was already well-advanced half a century ago, as depicted in

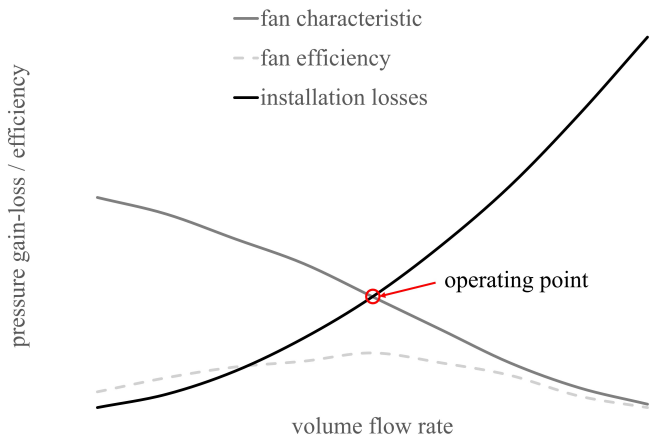

Figure 1.1: Aerodynamic performance characteristics of LPAF and system losses.

works like Sharland [9] and Mugridge with Morfey [10]. The distinction of noise mechanisms into the broadband and the discrete frequency components of the fan's noise spectrum was proposed. In particular, broadband noise was linked to vortex shedding at the trailing edges and the ingestion of large-scale turbulence found upstream of the blades or arising from secondary flows (e.g., tip clearance). Discrete noise components were associated with spatial non-uniformities in surrounding and/or aerodynamic interactions between the rotating blades and stationary obstructions (e.g., upstream bearing support, stator, inlet guide vanes). A further classification of noise mechanisms, present specifically in low tip-speed axial fans (i.e., LPAFs), was given by Longhouse [11]. Two noise mechanisms were considered predominant: rotational and non-rotational noise. The former was attributed to inflow distortion and turbulence effects, while the latter was related to blade tip clearance vortex effects. In terms of character and operating scenarios, rotational noise is tonal and relevant at high flow coefficients, while non-rotational noise is of broadband character and important at high fan loading. The acoustic spectrum of axial fans, according to Wright [12], recognized noise sources produced by steady blade forces as unavoidable due to the required fluid work. In the same analysis, the proposed generalized acoustic spectrum notably includes the rotor self-noise source, which can be characterized by a turbulent or laminar boundary layer. A subsequent overview by Neise and Michel [13] about aeroacoustic sound generation mechanisms in fans also adopts the distinction between steady and unsteady rotating forces, both of which represent dipole type sources. The steady forces include a uniform stationary flow mechanism of discrete character, which is considered negligible at low Mach numbers. The unsteady force mechanism has both broadband and discrete character, like secondary flows, vortex shedding, and non-uniform stationary or unsteady flow. Alternatively these mechanisms can be classified as self-noise and interaction noise according

to Blake [14]. Interaction noise arises from time-varying disturbances such as inlet flow distortion, whereas self-noise refers to sound generated under uniform flow conditions.

Mitigation of flow-induced noise in LPAF installations requires this understanding of noise sources. This understanding can be utilized in the aerodynamic design of LPAFs in tandem with modifications of installations, such as stator-rotor spacing and inlet geometry. However, two additional aspects must also be addressed when considering noise emissions from LPAF installations. These include acoustic propagation effects which are related to the radiation environment (near-field and far-field), and the sound quality that is perceived by the receiver. The former can depend on the application, for instance in automotive cooling systems condensers and radiators are typically found upstream of the fan (i.e., modify acoustic impedance of installation), while acoustic radiation occurs over hard reflecting surfaces (i.e., ground reflections). Consequently, evaluation of propagation effects aids in the minimization of noise emissions via appropriate modifications of the installations. Psychoacoustics examines sound quality as perceived by the listener and helps reduce annoyance from LPAF noise in a targeted way.

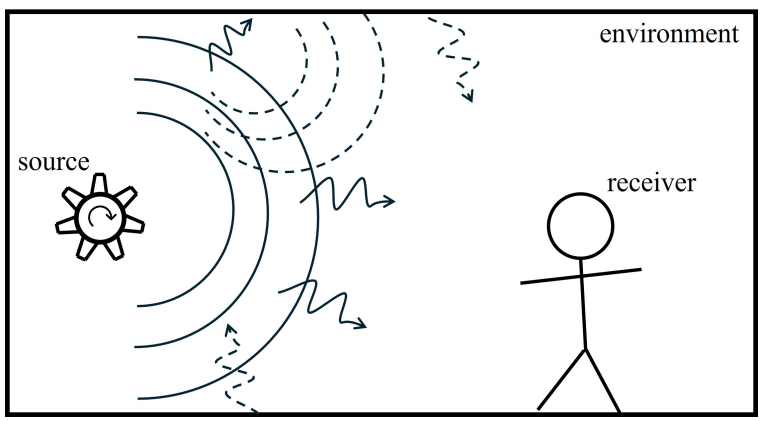

Figure 1.2: Schematic of the problem statement.

Considering the different aspects of noise emissions associated with LPAF installations, this acoustic problem can be described using the source-environment-receiver model (see Fig. 1.2). The source comprises the LPAF and installation components in the vicinity of the fan, such as the inlet shroud, stator and inlet guide vanes. These components may introduce installation effects on both aerodynamic and acoustic level. The former translates into modification of the flow field which consequently affects the flow-generated noise of the fan, while the latter concerns the acoustic properties of the installation which shape the source's radiation characteristics. The acoustic environment encompasses the boundary conditions imposed on the installation, which further affect reflection, absorption and transmission of propagating sound waves. Finally, the receiver represents the perceived noise at an observation point within the acoustic

environment.

1.2 State of the art

Research related to the previously stated problem can be reviewed in terms of the three components identified: environment, source, and receiver, herein corresponding to the test environment, the vicinity of the fan, and human perception. These perspectives, presented in the following sections, provide insights into research gaps and guide the definition of the work's objectives.

1.2.1 Installation effects in the test environment

Accurate characterization of aeroacoustic sources, such as low-pressure axial fans (LPAFs), requires a low background noise level and minimal influence from room-acoustical effects, including reflections [15]. The current landscape of wind tunnel facilities capable of such measurements can be broadly divided based on their test section [16] into open-jet and closed-test-section types. Open-jet facilities allow for acoustic treatment of surrounding boundaries, placement of microphones outside the main flow, and low background noise levels. As a result, they have been used in numerous experimental studies, including those involving airfoils [17], [18], rotors [19], [20], and propellers [21], [22]. Closed-test section wind tunnels provide better flow control and validation with numerical models [23], [24], while the absence of a shear layer enables accurate acoustic source localization. However, microphones can be exposed to flow-induced self-noise and source-unrelated sound waves, which can propagate into the test section because of the hard walls. Consequently, the source characterization process deteriorates due to coherent reflections and uncorrelated background noise. These issues can be minimized by modifying the test section near microphone installations [25]–[27] and/or by effective implementation of array processing techniques [28], [29].

Experimental investigations of LPAF noise, such as that generated by ventilation and cooling fans, are mainly conducted in duct configurations, within plenums, or in anechoic chambers [24], [30]. The latter configurations have enabled investigations [31]–[35] with minimal influence from acoustic propagation effects, but are limited to free-discharge conditions. Duct configurations in accordance with ISO 5136:2003 [36] and ISO 5801:2017 [37] allow acoustic investigations under varying loading conditions [38], [39]. However, as noted by Bilka et al. [30], results can be affected by duct scattering and casing boundary-layer effects, while investigations using plenums [40]–[42] face challenges in controlling the operating point and inflow conditions. A multi-chamber configuration within an anechoic chamber, evaluated according to ISO 3745:2012 [43] and used by Bilka et al. [30], is reported to address most of the aforementioned challenges. Two-chamber configurations have also been used in experimental investigations of low-pressure axial fan aeroacoustics, including combinations of reverberant and anechoic chambers [44], [45], reverberant and semi-anechoic chambers [46], and reverberant and plenum chambers [47]. Additionally, semi-anechoic chambers combined with ducts featuring anechoic terminations [48], as

well as acoustically transparent ducts combined with adjustable throttles [49], have also been utilized.

Experimental assessment of both aerodynamic and acoustic properties of low-pressure axial fans can also be conducted by modifying fan performance facilities. Zenger et al. [50] used a standardized inlet test chamber according to ISO 5801:2017 [37], which was constructed as an anechoic chamber with absorbing walls. This setup enabled sound localization studies and the estimation of sound power in accordance with ISO 3744:2010 [51]. Furthermore, for small axial fans, experimental setups following the guidelines of ISO 10302:2011 [52] have been employed in both semi-anechoic environments [53] and laboratory settings [54], enabling acoustic investigations in accordance with ISO 3745:2012 [43] and ISO 3744:2010 [51], respectively. It is also noted that a plenum designed in accordance with ISO 10302:2011 [52] was used by Canepa et al. [55] in conjunction with a semi-anechoic chamber for the aeroacoustic investigation of an axial automotive cooling fan under varying loading conditions.

Alternative strategies include conducting aerodynamic and acoustic investigations in separate facilities [56]–[58], which increase complexity and limits the loading conditions that can be investigated. Investigations have also been conducted in semi-anechoic chambers [59]–[61] and in sites treated with acoustic absorbent materials [62]. However, these setups present challenges associated with varying loading conditions and acoustic reflections.

It is noted that facilities featuring large upstream chambers, such as the cases mentioned above, are prone to the development of vortex-like flow structures [63], [64] at the fan inlet, especially when operated without inflow conditioners. Consequently, the tested fans can be subjected to distorted inlet flow, which can lead to tonal noise amplification, as has also been observed in more recent studies considering test environment effects on automotive cooling fan noise [46], [65].

1.2.2 Installation effects in the vicinity of the fan

While the test environment determines the accuracy of sound characterization for LPAFs and affects sound propagation, the installation conditions in the vicinity of the fan influence acoustic radiation, aerodynamics, and consequently aeroacoustics. These installation conditions involve shrouds, stators, support structures, inlets, and upstream or downstream components of the fan installation, such as radiators in automotive thermal management systems. These installation effects are discussed next.

A multitude of earlier studies [9], [10], [66]–[68] have laid the foundation for understanding the influence of turbulence ingestion at different scales on the noise spectrum of axial fans. Building on this work, more recent studies have focused on how blade design and specific blade features affect sound emission. In particular, the interaction between inflow conditions and blade characteristics, such as blade skew [50], [69], [70], leading-edge serrations [70], and permeable leading edges [71], has been investigated. Forward-skewed rotors have been found to exhibit greater sensitivity to distorted inflow, with amplified tonal and broadband noise linked to leading-edge interactions, com-

pared to backward-skewed designs [50], [69]. Although leading-edge serrations further reduce sound radiation under turbulent flow, this comes at the expense of aerodynamic efficiency, and the positive acoustic effects are not directly superimposed [70]. Similarly, permeable leading edges have been shown to provide notable broadband noise reduction under turbulent inflow, albeit also accompanied by a reduction in aerodynamic performance [71].

Inlet geometry strongly influences the aerodynamic performance of axial fans. Bellmouth intakes suppress separation and associated losses, whereas intakes featuring sharp edges result in larger separation regions and higher losses [72]–[74]. Since these modifications alter the inflow conditions, they inevitably affect acoustic emissions, motivating several studies on the interplay between inlet geometry and noise generation. Maaloum et al. [75] investigated the effect of a contoured duct and a lack of thereof for an axial fan installation. It was found that both discrete tonal components and broadband noise were influenced by the upstream flow organization imposed by the contoured inlet. Tian et al. [76] investigated the influence of inlet asymmetry on the aerodynamic noise of a cooling fan. The study showed that uneven inlet flow alters the size and distribution of unsteady blade loading, leading to periodic fluctuations as the blades rotate. Benedek et al. [77] studied the effect of inlet geometry on tip leakage flow noise for an axial fan operating at free-discharge conditions. The results indicated that a properly sized bellmouth inlet can moderate tip leakage flow, while eliminating double-leakage flow. The potential of aerodynamic noise reduction with short inlet ducts in axial fans was explored by Sun et al. [78]. It was found that short inlet ducts can suppress the upstream propagation of tonal noise by organizing multiple suction vortices into a single annular vortex, thereby weakening their interaction with the rotor blades. In a subsequent study, Sun et al. [60] investigated the use of sinusoidal-shaped inlet ducts for noise reduction in terms of acoustic mode modulation. They found that, compared with straight ducts, the sinusoidal-shaped design achieved greater reductions at the blade passing frequency and its first harmonic.

The reduction of tip clearance in low-pressure axial fan installations as a means of improving aerodynamic performance and reducing noise has been established in earlier studies [79], [80]. Subsequently, improved measurement methods have furthered the understanding on the aeroacoustic generation mechanism of tip clearance noise. Kameier and Neise [81] showed that a rotating blade instability at the blade tip, moving relative to the blade row at a fraction of the impeller shaft speed and present only under reversed flow conditions, is linked to tip clearance noise. Fukano and Jang [82] identified periodic velocity fluctuations as contributors to discrete tip clearance noise and blade passage velocity fluctuations as contributors to broadband tip clearance noise. More recently, detailed numerical simulations have complemented experimental insights. Zhu et al. [48] conducted a detailed modal analysis of the pressure field at the tip gap, revealing rotating coherent structures associated with the noise generation mechanism. Luo et al. [83] showed that the enhanced intensity of the blade tip vortex and its interaction with the blade surface are responsible for broadband noise amplification when tip clearance increases. More specifically, they linked low frequency broadband noise below 600 Hz to the blade tip vortex

and boundary layer instabilities interacting with the leading and trailing edges, while broadband noise above 1200 Hz was attributed to turbulent boundary layer fluctuations. Lendvai and Benedek [84] observed dominant noise sources at the blade tip leading-edge at low flow rates, associated with tip leakage flow. On the contrary, at higher flow rates, the turbulent boundary layer trailing edge noise, was identified as the dominant noise source.

Axial fan installations with upstream or downstream stationary components, such as inlet guide vanes and struts, are prone to interaction noise sources, designated as rotor-stator interaction [1], [85]. These sources can be identified as the cutting of upstream stator wakes by rotor blades, the impingement of rotor wakes on downstream stators, and the disruption of the rotor's pressure field by reflecting objects in the vicinity [85]. The effectiveness of these mechanisms is strongly affected by the number of rotor and stator blades [1], [85], [86]. Axial separation between the rotor and stator is less significant compared to blade count [86], although its optimal selection is nontrivial due to the simultaneous dependence of tonal noise on axial gap and rotation speed, according to Canepa et al. [87]. The effect of non-uniform distribution of stator [88] vanes or rotor blades [89] as a means of reducing rotor-stator interaction noise is more appealing in the automobile industry due to the desired compactness of the cooling module. In this context, Peng et al. [61] developed a theoretical model that considers non-uniform distribution of blades and vanes for evaluating the inherent discrete noise of automobile cooling fan modules in early design processes.

Axial fans in cooling modules often operate with significant upstream resistance from components such as radiators, condensers, and heat exchangers. These elements affect inlet flow conditions and associated aeroacoustic sources, as well as sound propagation, motivating ongoing research into their acoustic impact. Rynell et al. [44] studied the acoustic characteristics of an automotive cooling package with a shrouded axial fan and reported that the sound attenuation caused by the radiator is negligible. A similar observation was reported by Amoiridis et al. [32] after evaluating the acoustic emissions of an automotive engine cooling module with a radiator installed upstream of an axial fan. They found that, regardless of operating conditions, the radiator had a negligible influence on sound generation and propagation. Czwielong et al. [90] showcased that the heat exchangers influence the inlet flow field similar to flow straighteners, while the acoustic optimization of air conditioning systems should account for the interaction between heat exchangers and axial fans. In a subsequent study, Czwielong et al. [91] reported that a round heat exchanger geometry enhances the homogeneity of the flow field and, in turn, reduces sound emissions. Moreover, the tones at the blade passing frequencies exhibited a strong dependence on the heat exchanger geometry. Park et al. [92] investigated the effects of upstream condensers and radiators on the tonal noise generated by an axial fan. They found that these upstream components increased the tonal noise between the first and fourth blade passing frequencies, except under high loading conditions. It is noted that upstream obstructions can also be used as a control measure to reduce tonal noise. Gérard et al. [93] used a combination of upstream obstructions to reduce tonal noise at the blade

passing frequency through destructive interference. A combined installation of two lobed obstructions achieved significant overall spatial attenuation without compromising the fan's thermal performance.

Besides their association with tip clearance noise, ducts also play a pivotal role in the propagation of sound in axial fan installations. In applications such as automotive cooling modules, the ducts typically have lengths much shorter than the fan diameter, and therefore, the emitted sound field is only marginally influenced [1]. In contrast, in applications like tunnel ventilation systems, the duct length can be several times larger than the fan diameter, allowing significant sound amplification due to the excitation of cut-on duct modes [1], [85]. Regardless of the severity of the propagation effects imposed by ducts, noise reduction strategies can be integrated into their design. Czwielong et al. [94] studied the influence of a micro-perforated duct absorber on sound emission and performance of axial fans. The investigated micro-perforated duct absorber achieved up to a 16 dB noise reduction while maintaining fan performance, with the most favorable acoustic and aerodynamic results obtained when the fan was positioned downstream of the duct. Liu et al. [95] investigated the use of an open-cell metal foam casing to suppress tip leakage vortices and delay stall inception in a small axial fan. Their results showed that this casing treatment achieved up to a 10 dBA noise reduction under stalled flow conditions, with the improvement attributed to the aerodynamic weakening of the tip leakage vortex rather than direct sound absorption. More recently, Zhong et al. [35] explored the potential for tonal noise reduction in an electric ducted fan using over-the-rotor acoustic treatment, which included side-branch tubes and labyrinth-type acoustic metamaterials. A substantial reduction in the ducted fan's sound was achieved through precise tuning of the acoustic treatment's secondary sound field.

Installations using multiple fan configurations in close proximity, such as automotive cooling modules, are susceptible to challenges related to inlet flow interactions and acoustic wave interference. Recent studies have investigated noise reduction in multiple axial fan arrangements used in fuel cell vehicles. Guo et al. [96] investigated noise reduction in two parallel high-voltage axial fans by optimizing the outer ring structure, blade installation angle, and circumferential blade spacing. The results demonstrated improved aeroacoustic performance while preserving the system's aerodynamic efficiency. Dong et al. [97] analyzed the noise characteristics of a cooling system comprising two radiators with three- and two-fan parallel configurations respectively. They proposed a control strategy of a staggered duty cycle for reducing the total sound pressure level under different working conditions. In a subsequent study, Hu et al. [98] implemented a multi-physical field computational model for reducing noise in the same cooling configurations. By evaluating the field synergy angle and modifying four design parameters, they obtained a radiator system layout with improved heat dissipation performance and reduced noise emissions.

1.2.3 Human perception of axial fan noise

Understanding the installation effects on the acoustics of LPAFs (as described earlier) enables the development of effective noise mitigation strategies. However, these strategies cannot be evaluated solely based on overall sound pressure or sound power levels; they must also consider the human perception of noise. This can be achieved by using objective psychoacoustic metrics and conducting subjective assessments on axial fan noise. In this context, a growing body of research has focused on the intersection of psychoacoustics and axial fan noise.

Several studies have focused on identifying metrics and indices that capture the perceived annoyance from axial fan noise. Tang and Wong [99] conducted a survey to identify noise indices that describe the annoyance caused by domestic air conditioner noise in residential apartments. They found that Zwicker's loudness level and the 90% exceedance percentile level were the most effective indicators, while tonality was not a reliable measure of annoyance. Schneider and Feldmann [100] investigated a variety of axial and radial fan sound signals to find a psychoacoustic metric of fan noise that provides a single-number value of annoyance by combining relevant psychoacoustic parameters. A strong correlation was found between loudness and annoyance, and it was observed that tonality and fluctuation strength, especially near stall conditions, significantly increased perceived annoyance. Töpken and Van de Par [101] studied the perceptual dimensions of fan noise to develop relevant psychoacoustic indices. They identified six perceptual dimensions via principal component analysis and derived two indices by analyzing the specific loudness patterns of 35 different fan recordings. In a subsequent study [102], they quantified how varying the two indices impacts subject preference and loudness judgment. Moreover, they developed a regression model based on the ratio of loudness at high-to-mid-frequencies, which explained most of the variation in the evaluation fan noise data. More recently, Claaßen et al. [103] investigated the effects of reference sound level on loudness and preference judgments for fan sounds that were spectrally manipulated. A close relationship between loudness and preference judgments was observed at reference levels of 60 and 75 dB(A), whereas at 45 dB(A) the results indicated that equal loudness and equal preference are not synonymous.

The development of sound quality models has also been a topic of research interest. Rong et al. [104] investigated the relationship between subjective sound quality evaluations and objective psychoacoustic parameters to develop a predictive model for the sound quality of an installation with two axial cooling fans. Specifically, they developed two sound quality prediction models, one using multiple linear regression and another based on a backpropagation neural network, with the latter demonstrating superior prediction accuracy. Huang and Zheng [105] developed sound quality models for hairdryer noise by analyzing the contribution of various psychoacoustic metrics to perceived noise discomfort using partial correlation analysis. They found that loudness, followed by tonality, were the dominant factors influencing hairdryer noise discomfort.

Furthermore, researchers have investigated various fan design aspects and

their effects on sound quality. Cattanei et al. [59] investigated the impact of uneven blade spacing on the noise annoyance of axial fans. They found that fluctuation strength and roughness increased, while tonality values decreased. Zenger et al. [106] studied the effects of blade design on axial fan acoustic performance, including psychoacoustic assessment. They found that forward-skewed blades reduced loudness, whereas backward-skewed blades decreased both loudness and sharpness compared to the reference case without blade skew. Muiyser et al. [107] also demonstrated the quieter acoustic performance of axial fans with forward-swept blades compared to straight blades, including reductions in both tonal and broadband noise levels. However, they noted that improvements in subjective quality metrics depended on the loading conditions. More recently, Novaković et al. [39] investigated the impact of various geometric modifications on the psychoacoustics of small axial fans. The psychoacoustic metrics of loudness, roughness, and tonality showed the greatest variability among the fan designs considered, while the metrics of sharpness and fluctuation strength showed less sensitivity. In a follow-up study, Cerkovnik et al. [57] proposed a psychoacoustic annoyance model to correlate objective psychoacoustic metrics with the subjective assessments of computer fan users, based on recordings of nine different axial fans. Their results showed that fans with higher airflow ratings had increased low-frequency components which were perceived as powerful. In contrast, high-frequency components were strongly associated with negative perception.

1.3 Motivation and research objectives

The ongoing transition within the automotive sector from internal combustion engines [108] to battery electric, fuel cell, and hybrid-powered vehicles has introduced new demands for Thermal Management Systems (TMS). These needs include, but are not limited to: low-temperature circuits for thermally sensitive battery cooling; hybrid powertrain cooling in densely packed under-hood environments; downhill brake power cooling for heavy trucks; and battery cooling during fast charging. Consequently, a new generation of LPAFs, a core component in TMS, is being developed to meet these needs. Although the absence of internal combustion engines significantly reduces overall noise emissions at low speeds [109], [110], it also exposes noise sources from air-conditioning, power steering pumps, and TMS [109], [111], [112]. Consequently, LPAFs are not only expected to provide high cooling performance but also meet low noise criteria. In this context, the project eFan, a key enabler for eMobility, Part 2 has been initiated. *The main objective of the project has been the study of installation effects, such as inlet geometry, generic disturbances, and fan clustering, on the noise generation of eFans.* It is noted here that eFans refer to LPAFs driven by electric motors installed within the fan hub.

As described in Sec. 1.1 and in accordance with the literature review presented in Sec. 1.2, the main objective of this work is approached from the aspects of source, environment and, receiver.

The aspect of environment is motivated by the employment of a fan test facility (FTF) which was retrospectively modified for aeroacoustic investigations and thus does not constitute an ideal test environment for aeroacoustic measurements. Accordingly, the sub-objectives formulated are:

A to evaluate methods for characterizing the sound field of LPAFs and

B to identify room-acoustical effects at a FTF.

Objective *A* is addressed in Papers 1 and 4, while objective *B* is mainly addressed in Paper 4.

The literature review included in Sec. 1.2.2 highlights a range of installation effects in the vicinity of LPAFs (i.e.,aspect of source) which have been investigated. One of these effects concerns distorted inflow conditions, which have been studied under the impact of specific blade design features [50], [69]–[71]. However, the impact of hub-to-tip ratio and blade loading distribution on the aeroacoustic performance of LPAFs under system resistances remains largely unexplored. Moreover, studies concerning inlet geometry under varied loading conditions and multi-fan installations are scarce. Under this light, the sub-objectives concerning installation effects in the vicinity of LPAFs are:

Γ to investigate the impact of blade loading and hub-to-tip ratio on the aeroacoustic performance of LPAF under installation effects and

Δ to investigate the impact of inlet geometry on the aeroacoustics of single and parallel fan installations under varied loading conditions.

Objective Γ is addressed in Paper 6, while objective Δ is addressed in Papers 2 and 5. It should be noted that Paper 5 largely represents an extension of Paper 2, although Paper 2 includes aerodynamic measurements that are not reported in Paper 5. Furthermore, Paper 6, the only appended study that involves fan design, has been realized in association with the work from Ghosh [113].

The literature review on the human perception (i.e., aspect of receiver) of axial fan noise (see Sec. 1.2.3) highlights a focus on identifying metrics and indices that describe perceived annoyance, the development of sound quality models, and the influence of fan design on sound quality. However, studies investigating the interplay between installation effects and the sound quality of LPAFs remain scarce. Consequently, the sub-objective concerning the human perception of installation effects in LPAFs is:

E to investigate the impact of inlet geometry, parallel fan installation and upstream obstructions on the psychoacoustics of LPAFs.

Objective *E* is addressed in Papers 3 and 5.

Table 1.1 lists the contributions of the appended papers in accordance with the areas identified in the problem statement and the sub-objectives mentioned previously.

Table 1.1: Contribution areas and sub-objectives addressed by appended papers.

Area / **Paper No.**	Environment	Source	Receiver
1	**A**		
2		**Δ**	
3			**E**
4	**A**, **B**		
5		**Δ**	**E**
6		**Γ**	

1.4 Thesis outline

The thesis is divided in two parts: the introductory chapters and the appended papers. The overview of the introductory chapters is listed below:

Chapter 1 introduces and states the problem investigated in the thesis along with the state of the art and specific objectives in relation to the appended papers.

Chapter 2 presents methods utilized in this work. This includes the measurement environment, acoustic metrics, the method of spherical harmonic decomposition, concurrent aerodynamic measurements, system resistances, fan blade design and fan production as well as uncertainty considerations.

Chapter 3 discusses selected results from the appended papers concerning installation effects on the acoustics of LPAFs from the perspective of the environment, source and receiver.

Chapter 4 presents a summary of the appended papers.

Chapter 5 presents the summary of the thesis, and suggestions for future work.

Chapter 2

Methods

2.1 Test environment

The majority of the aeroacoustic measurements described in the appended papers were performed at a FTF (Fan Test Facility), owned by Volvo Group Trucks Technology. A schematic of the FTF is depicted in Fig. 2.1. The FTF incorporates a closed loop and plenum to plenum architecture. It facilitates control and monitoring of mass flow and pressure difference between the pressure and the outlet chamber which operates at atmospheric conditions. Moreover, it is equipped with a cooling system comprising of heat exchangers for temperature regulation. Thereby, it has been utilized for measuring fan performance, for research purposes and early-stage product assessment.

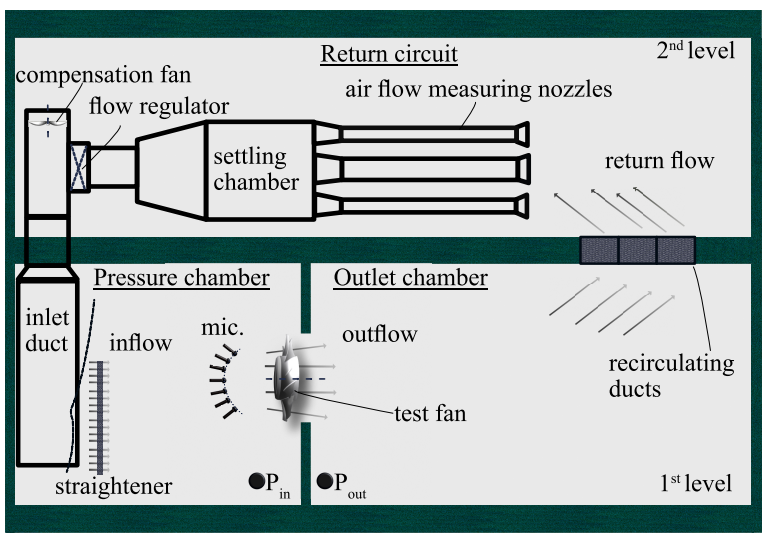

Figure 2.1: Schematic of FTF adjusted from Paper 5.

Verified accuracy values of selected parameters measured during the FTF operation are given in Table 2.1. More information including detailed operation of the FTF, further accuracy values and preceding research work are given by Gullberg [114].

Table 2.1: Verified accuracy of selected physical parameters [114].

Parameter	**Value**
Volume flow rate	±1.5%
Static differential pressure	±3 Pa
Temperature (pressure chamber)	±1 K
Atmospheric pressure	±50 Pa

The implementation of microphone measurements, a standard practice in experimental aeroacoustics, requires consideration of background noise and sound reflections. Signal to noise difference below 6 dB, challenges the retrieval of desired aeroacoustic noise sources from interfering noise, while the presence of reflections alters the measured sound spectra [15]. These considerations are of particular interest for this work, since the FTF was not designed under the consideration of aeroacoustic measurements.

An approach towards diminishing measurement interference from reflections, is by transforming the acoustic properties of the measurement space towards a free field. Prior to this work, the ceiling and side walls of the FTF's pressure chamber, have been acoustically treated with the installation of standard absorption material behind a perforate grid. This acoustic treatment, efficiently dissipates reflections above 200 Hz, while increasing the pressure chamber's critical distance. The latter prevents the contamination of the measured acoustic pressure signal from the hydrodynamic pressure fluctuations near the fan. Unfortunately the current acoustic characteristics of the pressure chamber do not conform to a semi-anechoic room according to ISO 26101-1:2021 [115], thus other approaches such as the ones described in ISO 3744:2010 [51] have been implemented for evaluating metrics like sound power and directivity. A different approach, which does not necessitate modification of the environment's acoustic properties is the utilization of a PMA (Phased Microphone Array) [15]. This approach has not been explored in this work.

Background noise at the FTF was evaluated against the 15 dB threshold from the investigated noise source (i.e., LPAF) in accordance with ISO 3744:2010 [51]. Besides the compensation fan (see Fig. 2.1) other background noise sources originate from engine durability testing in laboratories close to the FTF. The latter background noise sources concern frequencies below 200 Hz, which are unreliable for aeroacoustic investigations due to room-acoustical effects at the FTF. Another source of unwanted background noise is flow noise emerging from the nozzles on the second floor (see Fig. 2.1), under choked condition. Nonetheless, all investigations in this work were performed during constant

loading which translates into fixed nozzle positions. Last but not least, the industrial fan motor, only used in Paper 1, has been observed to emit unwanted noise of high amplitude within the investigated frequency range of the tested LPAF. Considering the above monitoring of background noise and identification of irrelevant noise sources has been performed for all acoustic investigations in this work.

2.2 Acoustic metrics

SWL (Sound poWer Level), is an acoustic metric which expresses the acoustic power radiated from a sound source. It is expressed as the logarithmic ratio of the source's emitted sound power (W) to a reference sound power (W_0). The standard reference power W_0 is 10^{-12} $Watt$ [116].

$$SWL = 10 \cdot log\frac{W}{W_0} \tag{2.1}$$

In theory the SWL of a sound source is independent of the acoustic environment it was measured in. On the contrary, the SPL (Sound Pressure Level), is sensitive to direction, distance and acoustic environment [116]. The mathematical expression (eq. (2.2) adjusted from [117]) of W, showcases the insensitivity of the SWL to the acoustic environment.

$$W = \iint_S \mathbf{I} \cdot d\mathbf{S} \tag{2.2}$$

W is estimated as the surface integral of sound intensity ($\mathbf{I}$) over a surface ($\mathbf{S}$) which completely encapsulates the sound source, thereby nullifying any acoustic environment effects. However, implementation of this expression in practice often involves SPL measurements prior to estimating the corresponding SWL. Thereby room-acoustical effects need to be accounted for when estimating SWL based on SPL measurements [117]. The selection of discrete measurement points, over the surface encapsulating the measured sound source, can be made in accordance with the acoustic environment.

Several standardized methods for estimating the SWL of sound sources over different acoustic environments are available. The ISO 3745:2012 [43] describes methods for precision level estimation of SWL in anechoic and hemi-anechoic rooms. Methods of lower accuracy, appropriate for free field over reflecting planes, are described by the ISO 3744:2010 [51]. For this standard the acoustic environment effects are accounted via the environment correction factor (K_2). Two procedures are outlined for calculating K_2:

- The first procedure, denoted as absolute comparison test, utilizes a reference sound source, usually with stable sound power output. Main

assumption of this method is that the acoustic environment influence is the same for the reference sound source and the sound source of interest. This procedure is compromised if there are significant dimension differences between the two sources or if the sound source of interest has strong directivity [117].

- The second procedure is based on the determination of room absorption. Room absorption can be estimated based on reverberation time, utilization of two measurement surfaces over the sound source of interest and a reference sound source. Although the second procedure includes three alternative approaches, the respective requirements for a valid estimation of K_2, are largely dependent on the dimensions of the measurement space.

SWL does not provide information about the directivity of the sound source, a property which expresses the spatial variation of SPL at certain distance from the acoustic center of a sound source. The directivity of the sound source, is the metric which entails the previous information [118]. Knowledge of this metric aids the understanding of present noise source mechanisms which in turn facilitates noise control [15]. This metric can be illustrated by a two-dimensional polar plot of SPL or estimated as a dimensionless factor. The directivity factor ($D(\theta, \phi)$) may be defined as the ratio of mean-square sound pressure ($p^2_{rms}(\theta, \phi)$) at a given distance from the sound source's center, to the mean-square pressure (p^2_S) of an omnidirectional sound source for the same distance and SWL [119].

$$D(\theta, \phi) = \frac{p^2_{rms}(\theta, \phi)}{p^2_S} \tag{2.3}$$

Another estimator used is the directivity index, which assesses the difference between the average SPL over all angles at a given distance to the SPL at a specific angle [43], [51], [118]. Realization of this metric via acoustic measurements is ideally translated to mapping the sound field over a virtual spherical surface surrounding the sound source. However, mapping the entire surrounding surface of the sound source is often not feasible due to space limitations and flow effects [15]. Further, the possibility of a symmetric noise field deem the complete mapping as redundant [15]. Instead mapping along a streamwise plane, spanning over angle ranges in the vicinity of half circle is often implemented [15], [120]. Distribution of measurement points along this plane is suggested to $\sim 10^\circ$ increments for many aeroacoustic investigations [15].

There exists a category of acoustic metrics concerned with the human auditory response to sound. These metrics are commonly employed in the field of psychoacoustics, where assessment of sound quality is of particular importance [119]. Sound quality metrics are relevant in product sound design and are therefore useful in automotive applications. In this context, automotive cooling fans, which can be dominant noise sources [109], [111], [112], are evaluated using

such metrics. In this work, the sound quality metrics of loudness, sharpness, roughness, tonality, fluctuation strength and psychoacoustic annoyance are considered. Estimation of these metrics has been carried out by the open-source toolbox SQAT (Sound Quality Analysis Toolbox) [121]. Brief definitions of each metric along with references to respective models utilized in SQAT are provided below:

- Loudness is a measure of a sound's strength as perceived by the listener under certain conditions. The calculation is performed according to ISO 532-1:2017 [122], using the Zwicker method for time-varying signals.
- Sharpness is a measure of the high-frequency content of a sound. This metric is estimated according to DIN 45692:2009-08 [123].
- Roughness is a measure of quick variations of the sound amplitude (modulation frequency above 20 Hz). Estimation is based on the model by Daniel and Weber [124].
- Tonality expresses the perception of a tone in relation to the total sound. It is estimated according Aures' model [125].
- Fluctuation strength is a measure of time-dependent fluctuations in amplitude and/or frequency content of a sound. The model by Osses et al. [126] is implemented for its estimation.
- Psychoacoustic Annoyance (PA) is a quantity (unitless) that expresses a combined annoyance of sounds based on the previous metrics. PA is estimated based on the model proposed by Di et al. [127] and is mainly influenced by the metrics of loudness and sharpness.

2.3 Spherical harmonic decomposition method

Spherical harmonic decomposition (SHD) is a well-established method within the field of acoustics [128]–[130]. Within the context of this work, spherical harmonic decomposition has been utilized for the identification of room-acoustical effects at the test environment (i.e., FTF) along with estimation of source's directivity and sound power.

Initially, the sound pressure field (p) radiated by a point monopole source in free field at a given observation point $\mathbf{r} = (x, y, z)$ and angular frequency ω in rad/s is considered [116],

$$p(\mathbf{r}, \omega) = \frac{\rho j \omega Q_0}{4\pi} \frac{e^{-\frac{j\omega|\mathbf{r}-\mathbf{r}_0|}{c}}}{|\mathbf{r}-\mathbf{r}_0|}, \tag{2.4}$$

where $k = \omega/c$ is the acoustic wavenumber in rad/m, ρ in kg/m^3 is the air density, j is the imaginary unit, c in m/s is the speed of sound in ambient conditions, $\mathbf{r}_0 = (x_0, y_0, z_0)$ are the point source coordinates, and Q_0 in m^3/s is point source's strength. It is noted that the time dependence, $e^{j\omega t}$, is omitted

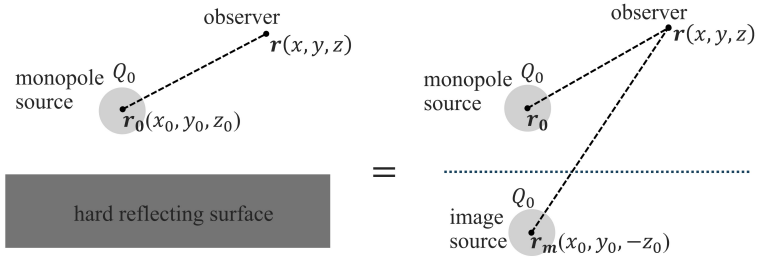

Figure 2.2: Image source principle for monopole radiation over hard reflecting surface.

throughout. As the next step, the imposed boundary conditions of a free field over a hard reflecting surface are applied, as depicted in Fig. 2.2.

In accordance with the image source principle [131] the total sound pressure field at the observation point is formed by the superimposition of two equivalent monopole sources mirrored across the (hard reflecting) surface's interface (see Fig. 2.2):

$$p(\mathbf{r},\omega) = \frac{\rho j\omega Q_0}{4\pi}\left(\frac{e^{-\frac{j\omega|\mathbf{r}-\mathbf{r}_0|}{c}}}{|\mathbf{r}-\mathbf{r}_0|} + \frac{e^{-\frac{j\omega|\mathbf{r}-\mathbf{r}_m|}{c}}}{|\mathbf{r}-\mathbf{r}_m|}\right), \tag{2.5}$$

where $\mathbf{r}_m = (x_0, y_0, -z_0)$ are the image source coordinates.

Subsequently, the sound pressure field in Eq. (2.5) is decomposed with the SHD method. Only half-space is considered due to the boundary conditions imposed at the acoustic environments of the pressure chamber (see Sec. 2.1). Then, according to Zotter et al. [132], it is possible to discard the odd harmonics and use the even spherical harmonics Y_n^{2l-n} as basis functions for the decomposition. It is remarked that even-harmonics decompositions include the zeroth order term, corresponding to an acoustic monopole in a free field.

The complex-valued spherical harmonics $Y_n^m(\theta,\phi)$ of order n and degree m are defined as implemented in [129]:

$$Y_n^m(\theta,\phi) = \sqrt{\frac{(2n+1)(n-|m|)!}{4\pi(n+|m|)!}}P_n^{|m|}(\cos\theta)e^{jm\phi}, \tag{2.6}$$

where P_n^m are the associated Legendre functions, θ is the zenith angle, and ϕ is the azimuth angle. Then, the SHD of the sound pressure at the observation radius r is written as [129]

$$p(kr,\theta,\phi) = \sum_{n=0}^{\infty}\sum_{m=-n}^{n} Y_n^m(\theta,\phi)\,\psi_{mn}(kr), \tag{2.7}$$

where ψ_{mn} is the n-th order spherical harmonic coefficient of degree m. For the even harmonics, with $m = 2l-1$, $l = 0,\ldots,n$, ψ_{mn} is considered to be non-zero.

The above-mentioned analysis can be implemented at a discrete set of M measuring locations (θ_i, ϕ_i) distributed over the surface of a hemisphere. Consequently a truncation order limit N is imposed, thus the infinite summation of Eq. (2.7) can be expressed as a set of linear equations:

$$\mathbf{p} = \mathbf{Y}\boldsymbol{\psi}, \tag{2.8}$$

where $\mathbf{p} \in \mathbb{C}^M$ is a vector of acoustic pressure at measurement points (M), $\mathbf{Y}$ is the $M \times L$ matrix of spherical harmonics at the corresponding measurement positions (M) containing only even harmonics, and $\boldsymbol{\psi} \in \mathbb{C}^L$ is the vector of the corresponding spherical harmonic coefficients. The dimension $L = [(N+1)(N+2)/2]$ corresponds to the number of even spherical harmonics up to order N. The overdetermined system can be solved for $\boldsymbol{\psi}$ using a least squares approach. The solution can be utilized for evaluating the directivity of the half-space via means of reconstruction.

Subsequently, the magnitude of the decomposed even harmonic coefficients can be considered for assessing the isotropy of the sound field in accordance with Nolan et. al [133]:

$$\iota(f) = \frac{|\psi_{00}(f)|}{\sum_{n=0}^{\infty}\sum_{m=-n}^{n}|\psi_{mn}(f)|}. \tag{2.9}$$

It is noted that the above expression has been adjusted from [133] by omitting the time-harmonic dependence.

As mentioned in the beginning of this section, SHD can be also used for estimating SWL. This is obtained via a composite SWL estimator according to Pomberger et al. [134]. The estimator combines a far-field estimate as suggested by ISO 3745:2012 [43] and a near-field estimate based on SHD. An adjusted expression from [134] is given in Eq. (2.10) below:

$$SWL_{comp} = 10\log_{10}\left(\min\left(\frac{1}{2\rho c}\frac{2\pi r^2}{M}\sum_{i=1}^{M}|p_i|^2,\ \ \frac{1}{2\rho c}\sum_{m,n}\frac{|\psi_{mn}|^2}{k^2|h_n^{(2)}(kr)|^2}\right)\right), \tag{2.10}$$

where p_i is the sound pressure in Pa at a measurement point. It should be noted that an assumption of hemi-anechoic conditions is made for the first term inside the min operator of Eq. (2.10).

2.4 Concurrent aerodynamic measurements

Implementation of PMAs coupled with beamforming techniques in aeroacoustic measurements, constitutes a proven method for estimating the strength and location of sound sources [23]. This method is often characterized as non-intrusive, while it may be applied even in cases of non-acoustic hard wall wind tunnels [15], [23]. There are several successful implementations of this

method in axial fan studies [77], [120], [135]–[138]. Still as the noise mechanisms in LPAFs are rooted in fluid mechanics, aerodynamic measurements are often carried out [77], [136], [137] in parallel for improved comprehension. Experimental studies without PMAs often utilize simultaneous aerodynamic measurements for the characterization of the inlet flow [50], [55], [63], [90], [91], [139]. Inlet velocity profiles, turbulence intensity and integral length scales are the main sought out parameters. To this end, several experimental methods are applicable such as LDA (Laser Doppler Anemometry) [50], [139], hot-wire anemometry [90], [91], pressure probes [55] and flow visualization [63], [91].

In Paper 2, acoustic measurements were complemented by velocity measurements at the fan's inlet, obtained via an LDA system. In this indirect measurement technique two monochromatic laser beams intersect in the measurement volume, creating a fringe pattern. A tracer particle passing through the measurement volume, perceives two light frequencies due to the Doppler effect. The scattered light from measurement volume is then collected by a stationary detector, also invoking the Doppler effect. Superimposition of the two light waves gives rise to the Doppler frequency, which is directly proportional to the particle's flow velocity perpendicular to the bisector of the two laser beams. Identification of flow velocity's direction is acquired by shifting the frequency of one beam via a Bragg cell [140], [141].

Table 2.2: LDA measurement volume dimensions.

beam wavelength in nm	488		514.5	
focal length in mm	400	800	400	800
$dx \cdot dy \cdot dz$ in mm	$0.1131 \cdot 0.113 \cdot 2.381$	$0.1192 \cdot 0.1191 \cdot 2.51$	$0.1142 \cdot 0.1141 \cdot 2.429$	$0.1204 \cdot 0.1203 \cdot 2.561$

A two-component LDA system, previously used for flow investigations in the underhood of vehicle TMS via Franzke [142], was utilized for the velocity measurements in Paper 2. It is noted that compared to the measurements performed by Franzke [142] in this work the LDA probe was fitted with achromatic front lenses of different focal length. The utilized LDA system incorporates an air-cooled 300 mW argon ion laser, a fiber flow transmitter, a two-component LDA probe in backscatter mode and a BSA processor F600. The two velocity components emit laser light with wavelengths of 514.5 and 488 nm respectively. Data processing during measurements was executed with BSA Flow software 6.72, provided also by the LDA system manufacturer Dantec Dynamics. The particle seeding was performed by the fog generator Viper NT (Look Solutions

USA), with glycol fluid (Look fluid regular-fog). The particle size is expected to be around 1 µm according to the manufacturer. The dimensions of the expected measurement volumes for the two achromatic lenses utilized are given in Table 2.2.

It should be pointed out that aerodynamic measurements and acoustic measurements included in this work [143] were acquired sequentially. However, they are conceived as being concurrent measurements because they were performed for the same test conditions. Conducting literally simultaneous acoustic and aerodynamic measurements is feasible, however the presence of the LDA system (i.e., traverse unit and probe) at the pressure chamber (see Fig. 2.1) introduces further acoustic propagation effects (e.g., scattering), while compromising the spatial range of the microphone grid due to space restrictions.

2.5 Installation losses

Installation losses or system resistances are inherent in LPAF installations and stem from components with aerodynamic or application-specific role, as discussed in Sec. 1. The curve of installation losses, also referred in literature as the plant characteristic [1], can be retrieved by driving flow through the installation without the fan placed. A good approximation of the plant characteristic is a quadratic parabola [1], which is showcased in Fig. 2.3 from measured cases acquired in Paper 6.

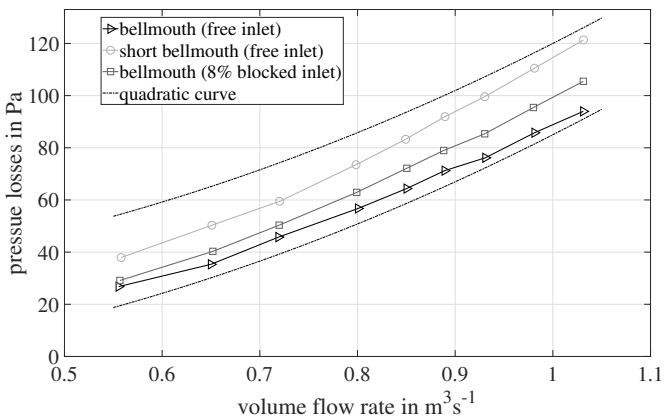

Figure 2.3: Curves of system losses for installations featuring bellmouth free and 8% blocked inlet, and short bellmouth free inlet. Image adjusted from Paper 6.

Subsequently, these losses can be accounted for when comparing characteristics of different installations (e.g. different upstream obstruction or different inlet geometry of Fig. 2.3) with the same fan, exemplified by Krömer [144] and Park et al. [92]. However, these corrections do not constitute a basis for a fair

comparison of acoustic pressure measurement in LPAF installations. Acoustic pressure is commonly evaluated as sound pressure level (SPL) [116]:

$$SPL = 10 \log_{10} \frac{\tilde{p}^2}{p_{ref}^2} \tag{2.11}$$

,where $\tilde{p}$ is the root mean square amplitude of the sound pressure in Pa and p_{ref} is a reference value of sound pressure ($2 \cdot 10^{-5}$ Pa). In the case of LPAFs the measured SPL is scaling with both volume flow rate and pressure rise. Consequently, comparison of measured SPL for different installations at the same conditions of volume flow rate and pressure rise (only possible after correcting characteristics [92], [144]) is unattainable. In literature it is common practice to compare at the same volume flow rates conditions [38], [50], [55], [90] or at free discharge [77] (i.e. zero loading albeit volume flow rates differ).

A non-trivial approach for accounting the different pressure rise at same volume flow rates of different LPAF installations, is replacing the reference value of sound pressure (see Eq. 2.11). In accordance with a method utilized for propellers by Quaroni et al. [145], the measured pressure rise (total-to-static pressure in Pa: Δp_{ts}) can be used for estimating a scaled SPL:

$$SPL_{scaled} = 20 \log_{10} \frac{\tilde{p}}{\Delta p_{ts}} \tag{2.12}$$

The effect of this scaling is demonstrated in Fig. 2.4 for the three LPAF installations previously presented in Fig. 2.3.

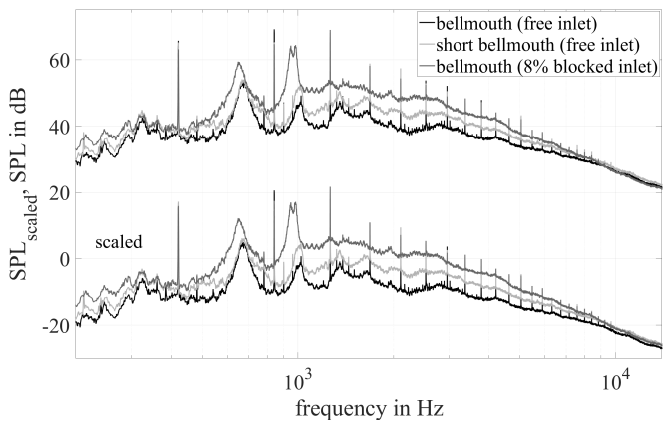

Figure 2.4: SPL and SPL_{scaled} of LPAF installations featuring bellmouth free and 8% blocked inlet, and short bellmouth free inlet. Image adjusted from Paper 6.

Aside from some small adjustments at low ($\sim$ 300 Hz) and high frequencies (above 7 kHz), it is observed that the scaled spectra (see Eq. 2.12) do not represent noteworthy deviations when compared to the standard spectra (see Eq. 2.11).

Another aspect which is inherent in installations of LPAF is flow-induced noise generated from components other than the fan (e.g. structural beam, radiator). This can be assessed by comparing the measured SPL of the installation without any components (i.e. only fan and inlet shroud) with the measured SPL of the installation with the components but without the fan placed. Figure 2.5 showcases the effects of self-noise for the installation corresponding to Fig. 2.3 and Fig. 2.4. The comparison is more representative at high volume flow rates, where amplitudes of LPAF spectra tend to be lower while the amplitudes of the spectra corresponding to system losses (i.e. installation without the fan placed) are higher.

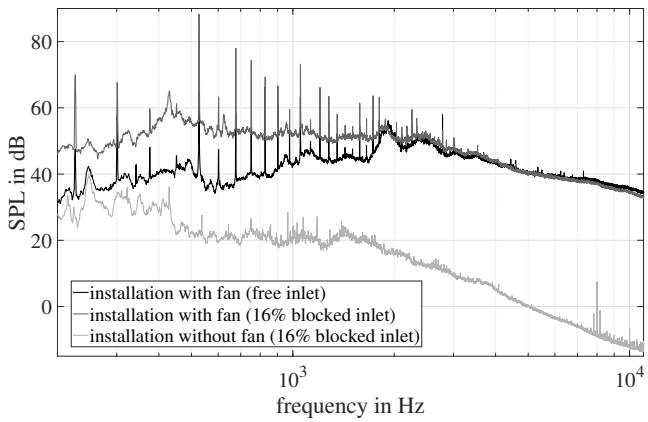

Figure 2.5: Evaluation of self-noise effects from upstream blockage. Image adjusted from Paper 3.

The spectra of the installation without the fan should be lower than the installation with the fan for dismissing self-noise effects. It should be noted that such evaluation is trivial under the condition of acoustically transparent components. The significant alteration of the system's acoustic impedance due to the presence of any components can potentially mask the presence of self-noise.

2.6 Fan blade design and fan production

The blades of the fans investigated in Paper 6 were designed based on the Blade Element Momentum (BEM) method for low-solidity LPAFs [1]. The implementation of the BEM method was performed via *C-Fan*, an in-house python code developed by Ghosh [113]. Since fan blade design is outside of the scope of this work, only a short summary of the utilized method along with relevant information about selected parameters and their values are presented in the following. Detailed information including the framework and equations implemented in *C-Fan* are provided by Ghosh [113].

The BEM method as implemented in *C-Fan* [113] can be summarized in the following steps:

1. **Determination of the design parameters**. The parameters to be determined include the volume flow rate, total-to-total pressure, rotational speed, fan diameter, hub diameter and blade count. Moreover, values of hydraulic efficiency and volumetric efficiency, typically chosen as 90 % and 95 % respectively, are assumed. In this work the selected design parameters correspond to fans utilized in contemporary automotive TMS. These values are given in Table 2.3, as also reported in Paper 6.

Table 2.3: Selected design parameters.

Design Parameter	**Value**
Volume flow rate	0.8 m^3/s
Total-to-total pressure	550 Pa
Rotational speed	3600 rpm
Fan diameter	320 mm
Hub diameter	$144 - 208$ mm
Blade count	7

2. **Segmentation of the blade**. During this step the blade annulus is segmented into elemental blade cascades, represented by coaxial sections. The segmentation is bounded by equal through-flow areas for all elemental blade cascades aside from the tip and hub cascades. In this work the blade has been segmented into ten elemental blade cascades. An example case of blade segmentation is illustrated in Fig. 2.6.

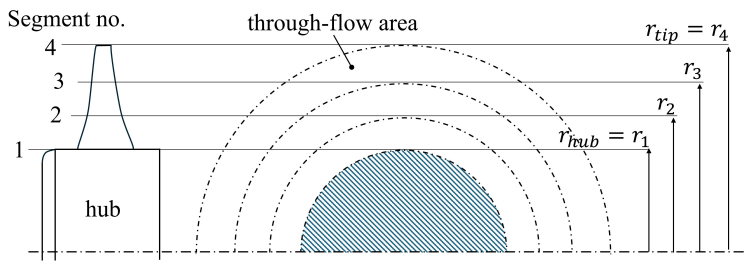

Figure 2.6: Example of blade segmentation. Image adjusted from [1].

3. **Determination of velocity triangles**. Firstly, the blade loading and the corresponding swirl distribution is selected. In this work the blade loading distributions investigated are: iso-energetic, linear, polynomial and parabolic. The iso-energetic represents constant blade loading and swirl distributions along the blade span (r), which necessitates larger circumferential velocity components at the hub ($r = 72 - 104$ mm) compared with the tip ($r = 160$ mm). Thereby, the larger blade twist required at the

hub (compared with the tip) increases the prevalence of flow separation and aerodynamic losses. The remaining blade loading distributions are radius-dependent. The linear and polynomial distributions constitute for higher specific work towards the blade tip. Consequently, this can result to increased tip blockage and earlier onset stall. The parabolic distribution features higher specific work at the mid section of the blade. For each swirl distribution the meridional ($u_{merid.,exit}$) and circumferential velocity ($u_{circum.,exit}$) components at the rotor exit are estimated via an iterative process in accordance with the values of the design parameters (see Table 2.3). Once the previous components ($u_{merid.,exit}$,$u_{circum.,exit}$) are estimated the remainder of the velocity triangles can be determined. The equations of the swirl distributions investigated along with their respective parameter values are given in Table 2.4, as also reported in Paper 6.

Table 2.4: Swirl distributions and parameter values.

Swirl distribution [blade loading]	**Parameter Value**
$ru_{circum.,exit} = b$ [Iso-energetic]	$b = 1.21$
$ru_{circum.,exit} = ar + b$ [Linear]	$a = 5, b = 0.55$
$ru_{circum.,exit} = ar^{m+1} + b$ [Polynomial]	$a = 3, b = 1.17, m = 1.1$
$ru_{circum.,exit} = a(r - d)^2 + e$ [Parabolic]	$a = -100, d = 0.128, e = 1.24$

4. **Determination of airfoil profile**. The airfoil profile of the blade segments is selected from the family of four digit NACA airfoils, which is supported by *C-Fan* [113]. In this work the NACA 3512 airfoil is utilized at the blade segments of the different rotor blades designed. The corresponding airfoil polar curves (for NACA 3512) are computed via XFOIL, a public domain code developed by Drela [146]. This computation requires inputs of: Reynolds number (Re), Mach number (Ma) corresponding to the blade tip, a range of angle of attack and the N-factor (i.e. amplification factor that controls the transition between laminar and turbulent flow over the airfoil surface). The eventual angle of attack is specified based on a minimum drag-to-lift ratio for all blade segments. Subsequently, the blade solidity (i.e. ratio of blade's chord length to blade spacing), blade spacing and blade chord length can be estimated at all blade spans. The estimated blade chord length allows the recalculation of the Reynolds number, since the initial Re input given at XFOIL represents an initial input guess. Following an iterative process the recalculated Re converges to the input guess (convergence limit is set at 0.1 % [113]). The final parameter to be estimated following the converged output from XFOIL is the twist of the blade along the blade span (i.e. summation of angle of attack and the vectorial mean flow angle [113]).

5. **Inspection of design criteria**. The final step of the blade design process concerns the inspection of certain design criteria. The De Haller [147] criterion accounts for the flow diffusion within the blade passage. According to De Haller [147] the ratio of the relative velocity at the rotor's exit

to the rotor's inlet should be lower than 0.75, across the blade span. Additional criteria considered in *C-Fan* [113] are the chord based Reynolds number and the blade solidity. The former is ideally maintained above 1.5×10^5 for suppressing flow separation effects, while the latter is kept below 0.7 for ensuring minimal interaction between subsequent blades.

The resulting blade design was incorporated into an equidistant-blade fan design. Subsequently the fan was 3D-printed via laser sintering (system EOS P 770) using polyamide (PA12) as the material. The produced result was evaluated via comparison of the CAD geometry with the scanned production fan. The equipment utilized for scanning the production fan was the ATOS Triple Scan, while the post processing of the acquired measurement was performed via Polyworks (InnovMetric). A representative result from a produced fan, with the longest blade span, is showcased in Fig. 2.7.

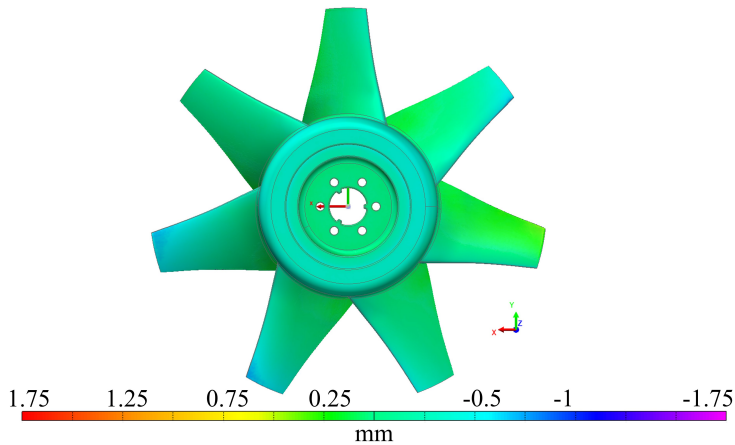

Figure 2.7: Example of CAD comparison with 3D scanning of produced fan. Image adjusted from Paper 6.

The diameter of these fans (see Table 2.3) enabled single-piece 3D printing in a horizontal orientation, resulting in small deviations from the CAD geometry and minor bending of the blades. In comparison, the reference LPAF investigated in Paper 1, which was produced via the same method, showcased greater deviations from the CAD geometry owing to its increased diameter.

2.7 Uncertainty considerations

The measurement chains employed in this work, for obtaining acoustic and aerodynamic parameters, comprise of several parts which contribute to the measurement uncertainty. The following includes uncertainty considerations for selected parts of these measurement chains, which have not been mentioned in earlier sections.

2.7.1 Sound pressure measurements

The measurement chain concerning sound pressure measurements can be viewed as a three part system. It comprises of the measuring sensor, the equipment for data acquisition and data processing. The measuring sensors used were condenser microphones, while the data acquisition was made by a Simcenter SCADAS system in Papers 1,2,4 and 5 while a DEWESOFT SIRIUS Modular system was utilized in Papers 3 and 6. Both data acquisition systems also acted as sensor power suppliers and signal analyzers. Data processing was handled in MATLAB.

Condenser microphones, which can be modeled as a capacitor having a moving and a stationary arm, may handle unsteady pressure fluctuations below ~ 200 Pa [148]. The directly measured voltage difference is converted to an indirect sound pressure measurement, provided the known sensitivity (ratio of voltage to pressure) of the microphone. Although this is initially provided by the manufacturer, the expected material degradation over time, necessitates repetitive calibrations. Two ways of calibrating sensitivity are the reciprocity technique and the usage of sound level calibrators. The former exhibits accuracy of ~ 0.1 dB based on the method used, while the latter ~ 0.3 dB [117] over measured SPL. It should be noted that sound level calibrators calibrate at a single frequency (often chosen as 250 or 1000 Hz), thereby their usage assumes an "overall" single value sensitivity over the measuring frequency range [149]. In this work sound level calibrators were used, a choice further motivated by the practical implications of operating measurement grids with a minimum of sixteen microphones.

The characteristics of microphones including type and diameter have also uncertainty implications. The free field type used in this work is best utilized in acoustic free fields, while being pointed towards the sound source [117]. Usage in different acoustic environments is feasible when free field corrections are applied on its frequency response [149]. These corrections also account for diffraction effects, present at frequencies corresponding to wavelengths comparable to the microphone's dimensions. Failing to consider these effects results in overestimation of sound pressure [117], [149]. Naturally smaller size microphones experience these diffraction effects at higher frequencies. To provide context, at 10 kHz the free field correction, for random incident angle wave at a 1/2 inch microphone, is ~ 1.5 dB over obtained SPL. In this work sound spectra beyond 10 kHz, produced by investigated sound sources, carried negligible acoustic energy.

Utilization of a finite number of microphone positions is a further cause of measurement uncertainty. For the case of SWL estimation this uncertainty (u_{mic}) can be evaluated according to ISO 3744:2010 [51] or ISO 3745:2012 [43]:

$$u_{mic} = \frac{1}{\sqrt{N_m}} \sqrt{\frac{1}{N_m - 1} \sum_{i=1}^{N_m} \left[L_{pi} - L_{pav}\right]^2} \tag{2.13}$$

Where N_m is the number of microphone positions, L_{pi} is the SPL at microphone position i and L_{pav} the arithmetic average SPL over all microphone positions. Figure 2.8 showcases u_{mic} for different number of microphone positions. Data from measurements at a semi-anechoic room for a monopole volume source conducted in Paper 4 has been used.

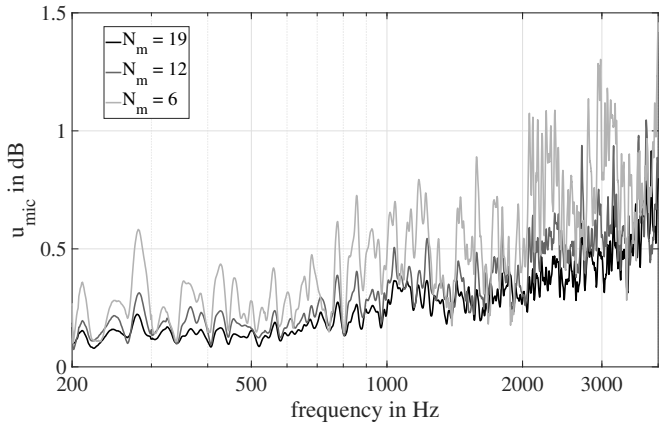

Figure 2.8: Uncertainty due to finite number of microphone positions. Data from measurements conducted in Paper 4.

As mentioned in section 2.2, estimation of SWL requires definition of a measurement surface. This surface is virtually encapsulating the sound source, with microphones being placed over the virtual surface at certain radius from the sound source. Discrepancies of radius in the order of 10 % may result in uncertainty contribution of up to 0.5 dB, according to ISO 3744:2010 [51].

Another source of uncertainty related to the data acquisition is sampling time. Longer sampling times enable segmentation of the principal recording to a higher number (M) of time segments. Subsequently, averaging power spectral density over a higher number of time segments according to Welch's method, induces better suppression of relative random error (ϵ_r) [150] as given by eq. (2.14):

$$\epsilon_r = \frac{1}{\sqrt{M}} \tag{2.14}$$

Where ϵ_r is expressed as the ratio of root mean square error to the signal's expected value. The effect of sampling time is further demonstrated in Fig. 2.9. Relative differences of SPL between a long (120 s) time sample and shorter samples are shown. It should be noted that all SPL estimates utilized the same

frequency resolution for the Fourier transform. The smoothing of the spectra as the sample length increases is apparent.

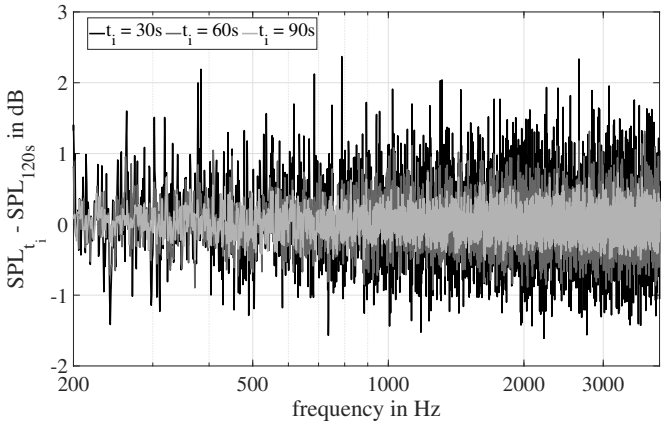

Figure 2.9: Relative difference of SPL between long and shorter sampling times. Data from measurements conducted in Paper 4.

Longer sampling time also translates into smaller frequency resolution for a given sampling rate. Consequently, a more precise estimation of spectra is feasible, although at the cost of data size and data processing times.

Last but not least, environment conditions and their effects have to be considered when assessing measurement uncertainty. The measurement environment's temperature and humidity affect the atmospheric sound absorption. Thereby correction of acquired sound pressure data to standard atmospheric conditions, may be performed [15]. Uncertainty evaluation of temperature and humidity variation, while estimating SWL, is given in ISO 3744:2010 [51]. The accumulated uncertainty level is below 0.5 dB, for the proposed range of measurement conditions.

2.7.2 Flow velocity measurements

As mentioned in section 2.4, seeding of flow with small particles is a prerequisite for LDA measurements. It is then no surprise that the accuracy of the measurement relies on the capability of these particles to follow the flow's fluctuations [151]. The particle size and its density mainly determine this capability [141]. In general smaller size particles may follow higher velocity gradients, however this undermines their light scattering ability which in turn compromises data acquisition. Typical particle diameters of materials eligible for air flows, range between 1 and 8 μm [152]. The attainable sampling rate is also strongly related to particle size and density. This is easier to grasp if one considers measurement dropout. Dropout describes the interruption of data acquisition while no particles cross the measurement volume [151]. Equation (2.15) gives the dropout percentage for gas flows.

$$DO = 100\left(1 - \eta\frac{\rho_g}{\rho_p}\frac{V_m}{V_p}\right) \tag{2.15}$$

Where V_m and V_p stand for the volume of measurement region and particle respectively, ρ_g and ρ_p are densities of gas and particle respectively, while η denotes ratio of particle to gas mass flow. The glycol material used in Paper 2 was released in the flow as fog through a vaporizer. The particle size distribution from this method was not very narrow ($0.2 - 10\ \mu m$), according to the manufacturer. This distribution coupled with measurement conditions (temperature, pressure and humidity) which affected the evaporation of the fog, led to high dropout percentages. Consequently measurement times were prolonged in order to increase the total number of measured samples.

Determination of measurement time when using LDA also depends on the presence of the velocity bias effect. This effect concerns the dependency of velocity sampling rate in LDA measurements, on the velocity magnitude. In particular the sampling of high velocity particles will be more frequent than low velocity ones [141], thus estimators of statistical moments including mean flow velocity, will be biased.

One way of avoiding the velocity bias is by obtaining statistically independent samples. Statistically independent samples are obtained when the temporal distance between consecutive samples, is greater than two times the flow's integral time scale (T_u) [140], [152]. A good approximation of T_u is the ratio of macro-length scale (L_u) of the problem to the mean velocity ($\bar{u}$), as given in equation (2.16) readjusted from [140].

$$T_u = \frac{L_u}{\bar{u}} \tag{2.16}$$

A more precise estimation of T_u can be based on the autocovariance ($C_{uu}(\tau)$) of the measured velocity time signal, given in equation (2.17) adjusted from [152].

$$T_u = \int_0^\infty \frac{C_{uu}(\tau)}{C_{uu}(0)}\,d\tau = \int_0^\infty \rho_{uu}(\tau)\,d\tau \tag{2.17}$$

Where τ stands for the time lag considered when calculating autocovariance. The parameter $\rho_{uu}(\tau)$ showcases a rapid decay towards zero, after which it stabilizes. The first crossing of $\rho_{uu}(\tau)$ is usually considered as the upper integration limit [152] of equation (2.17). A typical estimation of $\rho_{uu}(\tau)$ is given in Fig. 2.10. The estimation was made for data taken from Paper 2. It should be noted that estimation of T_u has to be made across all positions of the measurement grid. Subsequently the maximum T_u will dictate the allowable

temporal distance for independent consecutive samples [152].

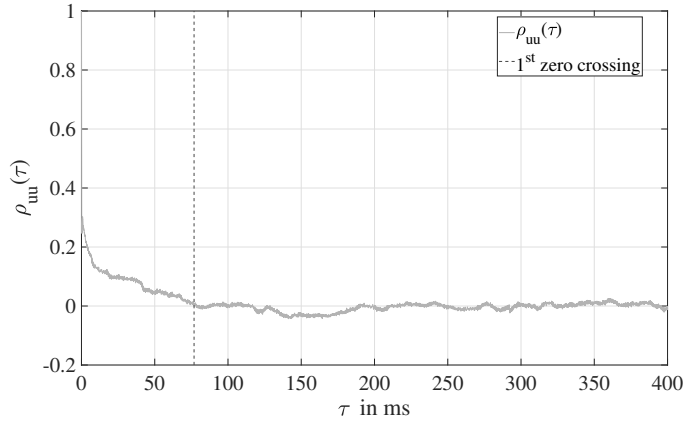

Figure 2.10: Representative estimate of $\rho_{uu}(\tau)$ upstream of low-speed axial fan. Data from measurements conducted in Paper 2.

Another way of treating the velocity bias is by using the transit time [140], [141], [152] which corresponds to each measured seeding particle. The transit time (t_i) of a measured particle, refers to its corresponding signal duration while crossing the measurement volume [140]. This time information can be used for estimating a weighting factor (η_i) for each measured particle, as shown in equation (2.18) adjusted from [152]. Subsequently η_i is utilized as a multiplication factor for estimating statistical moments of the flow.

$$\eta_i = \frac{t_i}{\sum_{j=0}^{N-1} t_j} \tag{2.18}$$

The small dimensions of the measurement volume, typically 0.1 mm thickness and $0.3 - 3$ mm length, motivate the assumption of uniform flow across its volume [141]. Having already accounted for the velocity bias, there is no need for further weighting of measured samples prior to estimating mean velocities and higher moments. However the assumption of uniform flow may be invalid if a non-uniform fringe spacing is characterizing the measurement volume. Non-uniform fringe spacing may arise from improper optical layout, astigmatism and laser light diffraction via particles intersecting the laser beams [141]. Failing to discover it may result in estimators of mean velocity and turbulence intensity contaminated with systematic errors [140], [141]. The systematic error is generally more important for flow turbulence than mean flow velocity. An overestimation of turbulence intensity is expected due to fringe distortion, which is less significant the higher the turbulence intensity of the flow is [141].

Finally, a practical consideration which concerns the measurement volume and affects measurement accuracy, is the alignment of the measurement volume in relation to the investigated flow field. This consideration is particularly important when multiple lenses are utilized in conjunction with the LDA probe. As noted in Section 2.4, lenses of different focal lengths have been used along with two different setups, in Paper 2. This was done to obtain all three velocity components along the velocity profile of interest. Since a two-component LDA system was used, one of the velocity components (tangential) was obtained twice. Although the agreement between the mean tangential velocity profiles was reasonable (fig. 9 in Paper 2), the level of discrepancies motivate longer measurement times for a sufficiently accurate estimator of the flow field's turbulence intensity.

Chapter 3

Selected results and discussion

3.1 Aspect of environment

In order to evaluate methods for characterizing the sound field of LPAFs at the FTF, the round robin test presented in Paper 1 was performed. The results demonstrated good repeatability in the measurement methods, supporting the use of 3D-printed rotor geometries in subsequent investigations (see Paper 6). However, the findings also indicated potential for improvement in sound characterization methods and raised questions concerning room-acoustical effects at the FTF. Consequently, an investigation employing spherical harmonics of the half-space, presented in Paper 4, was carried out. Sections 3.1.1 and 3.1.2 present and discuss selected results from Papers 1 and 4 respectively.

3.1.1 Round robin test of a low-pressure axial fan

The sound field generated by an LPAF depends on its loading conditions. Consequently, a mandatory step preceding the evaluation of suitable methods for characterizing the sound field of the benchmark fan at the FTF was the assessment of its aerodynamic performance. Figure 3.1 demonstrates the curves of pressure rise over volume flow rate of the 3D-printed fans tested at the FTF, along with the curve from the benchmark study [153]. It is noted that compared to the results reported in Paper 1, the curves corresponding to the 3D-printed fans have been normalized with regard to standard air conditions [154].

The three 3D-printed copies of the benchmark fan exhibited discrepancies largely within the measurement accuracy across the tested operating points. A good quantitative agreement was observed between the curves of the 3D-printed fans and the benchmark case for volume flow rates below 1.5 m^3/s, including the stall region. In contrast, at higher flow rates, the 3D-printed fans consistently underperformed compared to the benchmark. It can be hypothesized that the documented deviations between the benchmark and the 3D-printed fans—such

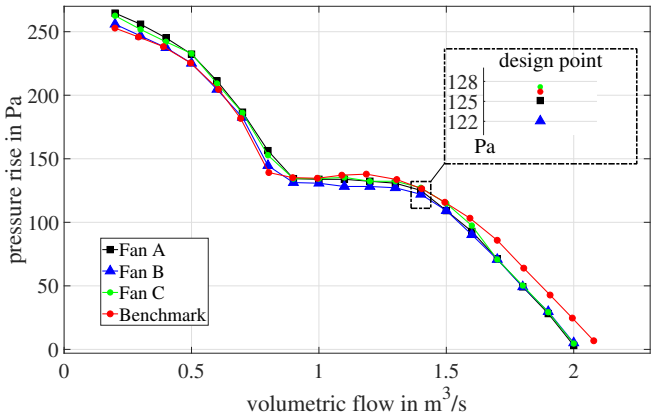

Figure 3.1: Curves of pressure rise over volume flow rate from measurements at FTF and the benchmark study [153]. Data and image adjusted from Paper 1.

as differences in fan geometry and shroud assembly—contributed to increased aerodynamic losses, which became more pronounced at higher volume flow rates.

Following the evaluation of the aerodynamic performance, and given the marginal differences between the 3D-printed fans and the benchmark case at the design point, the SWL from the acoustic measurements at the FTF was estimated. It is noted that ISO 3744:2010 [51] was utilized for estimating the SWL for the benchmark study and the measurements at the FTF. However, an environment correction factor in accordance with the reverberation method [51] was used for the latter.

The narrowband sound power levels (SWL) of the 3D-printed fans and the benchmark fan are shown in Fig. 3.2. A frequency range of 200–2500 Hz is considered. The lower limit of 200 Hz is imposed due to the expected loss of anechoicity below this frequency, while the upper limit of 2500 Hz corresponds to the onset of significant noise contributions from the fan's driving axle. Instances of axle-related tones are indicated in the presented spectra. These contributions were identified via recordings corresponding to the operation of the driving axle without the fan. Although tones unrelated to the fan operation are observed, the selected frequency range encompasses the most relevant portion of the spectra, containing the primary contributors to the benchmark fan's overall sound power level.

The 3D-printed fans show good quantitative agreement across the presented frequencies. Excluding instances of axle noise, the largest discrepancies between the spectra of the benchmark and the 3D-printed fans are observed between the first blade passing frequency (BPF) and the broadband hump at approximately 320 Hz. This part of the spectrum is associated with tip noise [82], [155]. Accordingly, the identified asymmetric tip gap clearance in the 3D-printed fan installations can be linked to these discrepancies. However, the influence of

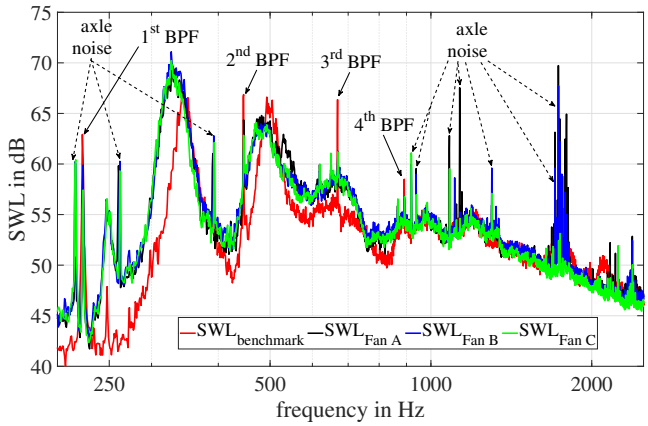

Figure 3.2: SWL at design point from measurements at the FTF and the benchmark study [153]. Data and image adjusted from Paper 1.

the environment correction factor and the integration area on the estimated SWL spectra of the 3D-printed fans should also be considered. Both introduce a constant scaling factor across all frequencies, thereby affecting the relative offset between spectra. It is further noted that significant differences in overall SWL were observed, between 3D-printed fans and benchmark case at volume flow rates between 0.7 and 1.1 m^3/s (see Figure 8 in Paper 1). This observation reinforces the conclusion that installation conditions in the local flow field of the fan, rather than room-acoustical effects, are the dominant cause of the observed discrepancies.

The higher amplitudes observed for the benchmark fan at the first four blade-passing frequencies further highlight the overlap between installation effects in the local flow field of the fan and room-acoustical effects. Given the similarity of the installation configurations, these amplitude deviations could initially be attributed to higher levels of ingested turbulence in the benchmark case. However, subsequent investigations at both facilities under comparable operating conditions [50], [156] indicated similar turbulence levels. Therefore, it can be inferred that the environment correction factor applied in the analysis of the 3D-printed fans primarily accounts for these discrepancies.

3.1.2 Sound characterization with spherical harmonics

The round robin test revealed the presence of room-acoustical effects in the FTF and demonstrated the limitations of the environmental correction factor obtained using the reverberation method specified in ISO 3744:2010 [51]. As an alternative, the two-surface method defined in the same standard can be used to estimate the environmental correction factor. However, this approach provides correction values only in one-third-octave bands, and the spatial constraints of the FTF prevent implementation of the recommended ratio between the two measurement surfaces. Consequently, a monopole-like sound source was

employed in combination with the spherical harmonic decomposition method (see sec. 2.3) to identify room-acoustical effects in the FTF and to support the acoustic characterization of LPAFs.

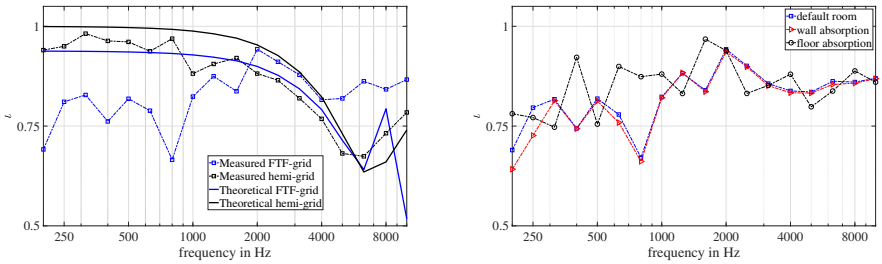

(a) (b)

Figure 3.3: (a) Isotropy of volume source (measured) and point monopole (theoretical), for hemi-anechoic and FTF microphone grid. (b) Isotropy of volume source for different absorption material installations at FTF. Data and images adjusted from Paper 4.

The comparison of the sound field isotropy between the FTF and a hemi-anechoic room, as generated by the monopole, enables the identification of room-acoustical effects at the FTF. Figure 3.3(a) shows the isotropy, estimated according to Eq. 2.9, for both the FTF and the hemi-anechoic room, using a theoretical point monopole source and the measured monopole-like source. It is noted that the microphone grids between the FTF and the hemi-anechoic room utilized different arrangements and number of microphones. Within the frequency range of interest (200-1000 Hz) the comparison of the point monopole cases suggest limited microphone grid effects. Furthermore, the comparative amplitudes and good qualitative agreement between theoretical and measured isotropy curves at the hemi-anechoic room, validate the utilization of the monopole-like source in tandem with a second order limited SHD scheme. The significant deviations between the measured and theoretical isotropy curves at the FTF indicate room-acoustical effects within the frequency range of 200–1000 Hz.

Subsequently, the installation of absorption material to mitigate room-acoustical effects at the FTF was investigated. Figure 3.3(b) shows the isotropy curves obtained from measurements at the FTF with different configurations of absorption material. The installation of absorption material on the walls shows only marginal differences compared to the default state of the FTF. On the contrary, an extensive installation of absorption material across the floor of the facility resulted in moderate increases in isotropy at approximately 400 Hz and throughout the range of 550–1000 Hz. However, this installation comes at the expense of accessibility during the setup of measurement equipment and test configurations.

Besides identifying room-acoustical effects at the FTF, SHD can also be applied for the sound characterization of LPAFs. This approach was investig-

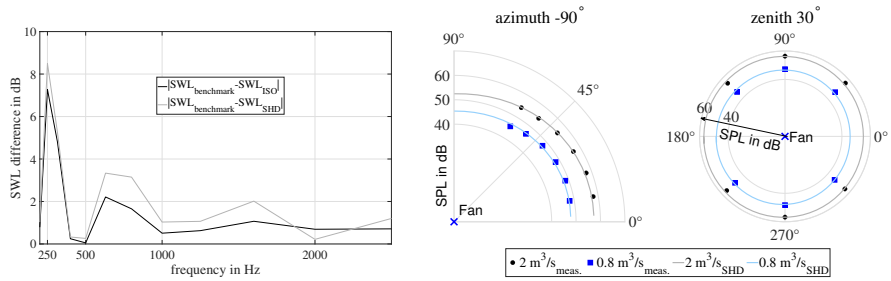

(a) (b)

Figure 3.4: (a) SWL difference at design point between benchmark case and measurements at the FTF estimated with SHD and ISO 3744:2010. (b) Reconstructed and measured SPL in polar coordinates for the first BPF at two operating points. Data and images adjusted from Paper 4.

ated using one of the 3D-printed fans from the round robin test (see previous section). Figure 3.4(a) illustrates the differences between the SWL of the benchmark case study [153] and the SWL measured at the FTF in 1/3-octave bands. The black curve represents differences from SWL estimated according to ISO 3744:2010 [51], while the gray curve corresponds to the SWL estimated via SHD. Both methods yield comparable results across the presented frequency range, despite the second order limit imposed on the SHD and the ambiguity in defining the acoustic center of the source. Furthermore, the SHD method is applicable across different loading conditions. This is demonstrated in Fig. 3.4(b), where the SPL reconstructed at the first BPF under both high-loading and near free-discharge conditions closely matches the microphone measurements.

3.2 Aspect of source

The round robin test and the application of the spherical harmonics scheme revealed room-acoustical effects and limitations in the methods used to characterize the sound field of LPAFs at the FTF. Consequently, the aeroacoustic studies conducted at the FTF are subject to installation effects imposed by the test environment itself. Nevertheless, the evaluation of installation effects in the vicinity of the fan remains feasible, provided that the collective influence of room-acoustical effects on the tested setups is considered. In this context, fan installations that share spatial similarity and identical measurement setups can, through comparison, elucidate installation effects associated with the fan's local flow field.

Installation effects associated with parallel fan operation and inlet geometry were investigated in Paper 2. The study of the parallel fan configuration provided insights into the aspect of spatial similarity for measurements at the FTF, while also revealing significant effects of inlet geometry on aeroacoustic performance. These findings motivated an extended investigation in Paper 5, which included additional loading conditions and inlet geometries. Further-

more, the influence of hub-to-tip ratio and blade loading distribution on the aeroacoustic performance of LPAFs under installation effects was examined in Paper 6. Sections 3.2.1, 3.2.2, and 3.2.3 present and discuss selected results from Papers 2, 5, and 6, respectively.

3.2.1 Parallel fan operation effects

The implications of parallel fan operation are first evaluated from an aerodynamic perspective. Figures 3.5(a) and 3.5(b) present the performance characteristics of the parallel fan systems with different fan spacings for short and long inlet configurations. For reference, the characteristics of a single fan configuration, for which the volume flow rate has been doubled, are also superimposed.

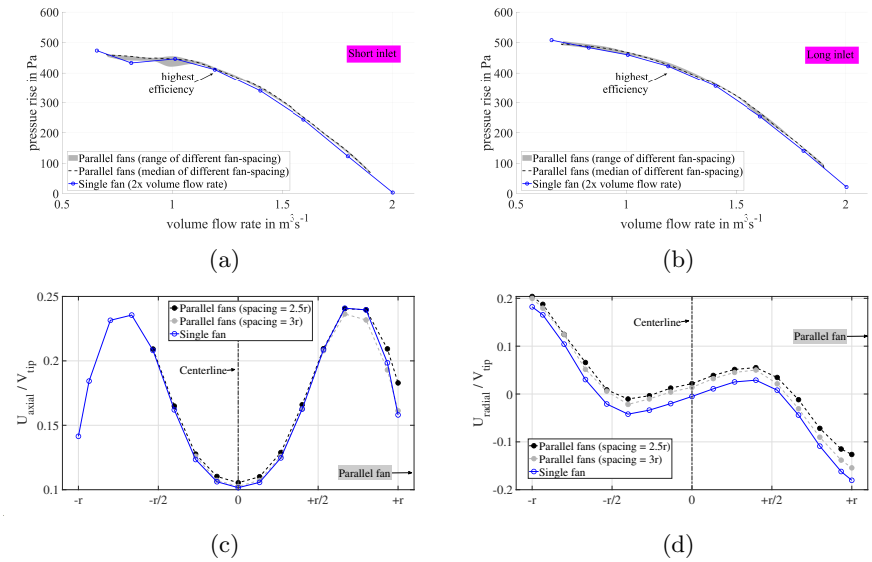

Figure 3.5: Curves of pressure rise over volume flow rate for parallel and single fan installations with short (a) and long inlet (b). Velocity profiles along axial (c) and radial (d) direction for parallel and single fan installations with short inlet. Data and images adjusted from Paper 2.

The minimal discrepancies among the parallel fan installations with different fan spacing suggest limited aerodynamic interaction between the fans, irrespective of the two inlet geometries tested. The consistent scaling of the single fan system, for both inlet geometries further supports this observation. The influence of inlet geometry becomes more apparent in the stall region, where the longer inlet yields a more stable evolution of the performance curve. Moreover, the longer inlet achieves marginally higher pressure gains across the entire operating range.

A more detailed assessment of the aerodynamic interaction between the two parallel fans is obtained by examining the velocity profiles immediately

upstream of one fan's aerodynamic interface plane. Figures 3.5(c) and 3.5(d) present the velocity profiles along the axial and radial directions for both the parallel and single fan installations at the point of highest efficiency. Overall, the velocity profiles of the single fan and parallel fan installations show good quantitative agreement. Minor discrepancies are observed in the axial velocity profiles at locations closer to the neighboring fan. Moreover, the radial velocity profile corresponding to the parallel-fan installations exhibits reduced symmetry compared to that of the single fan installation. Specifically, the saddle point of the radial velocity profile for the parallel-fan systems is shifted slightly to the left of the centerline.

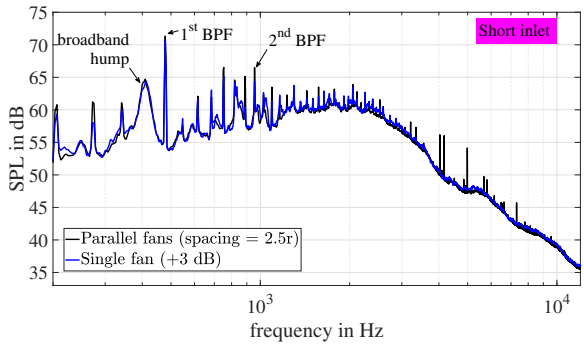

(a)

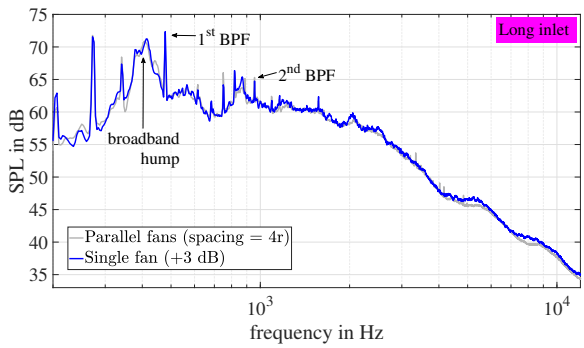

(b)

Figure 3.6: Spatial averaged SPL for parallel and single fan installations with short (a) and long inlet (b). Data and images adjusted from Paper 2.

The absence of significant interaction effects for the parallel fan installation is also confirmed in the spectra obtained from the far-field acoustic measurements. Figures 3.6(a) and 3.6(b) show two representative cases of spatially averaged SPL for parallel-fan installations at the highest efficiency point. In the same figures, the spectra of the corresponding single fan installations, offset by +3 dB to account for doubling of source power, are superimposed for comparison. The agreement between the spectra of the single fan and parallel-fan installations

indicates a consistent scaling of the noise sources across the plotted frequency range. Therefore, the investigated fan spacings did not induce any significant aeroacoustic interaction effects. A byproduct of these results concerns the limits of spatial similarity when conducting far-field acoustic measurements at the FTF. Despite the emergence of room-acoustical effects below 1 kHz, as discussed in the previous sections, the identification of installation effects in the vicinity of the fan remains feasible. For example, the influence of inlet geometry is captured equally well for both single and parallel-fan installations, even when using the same microphone grid.

3.2.2 Inlet geometry effects

The interplay between inlet geometry and aeroacoustic performance observed for the fan in Paper 2, motivated a further study incorporating additional operating conditions and inlet geometries conducted in Paper 5. Figure 3.7 shows the curves of non-dimensional pressure rise, ψ, over non-dimensional volume flow rate, ϕ, for the same fan discussed in the previous section, but with four different inlet shroud geometries.

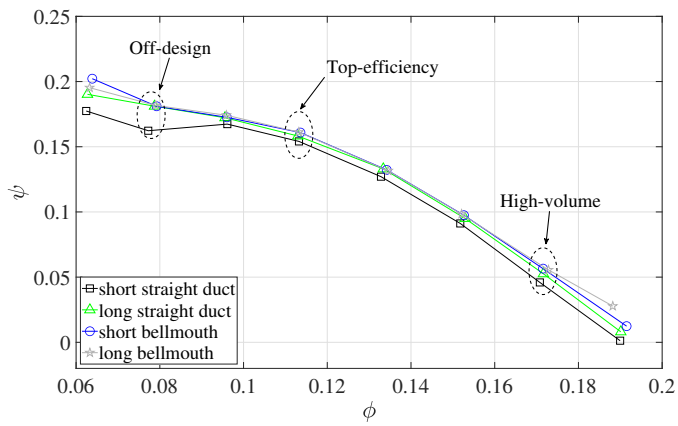

Figure 3.7: Curves of pressure rise (ψ) over volume flow rate (ϕ) for single fan installations with different inlet shroud geometries. Data and image adjusted from Paper 5.

The configurations with bellmouth and the long straight duct exhibit marginal differences across the tested conditions. The configuration with short straight duct showcases consistently lower pressure ($\approx$4%) compared to the other configurations. These deviations are comparable to the values measured in similar studies [55]. Furthermore, the short straight duct exhibits deeper stall conditions, which can be interpreted as a consequence of the sharp shorter inlet [75]. The higher maximum flow rates observed for configurations with bellmouth geometries, are likely linked to the suppression of the vena contracta [157].

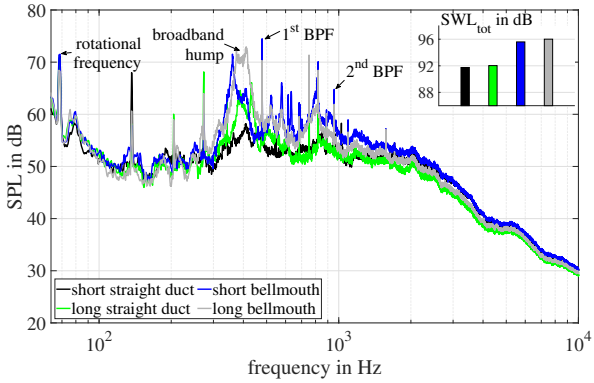

(a)

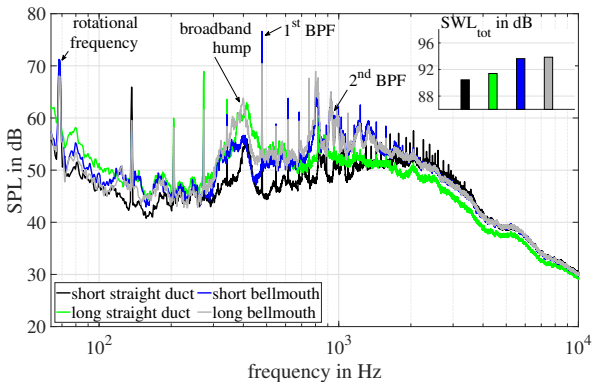

(b)

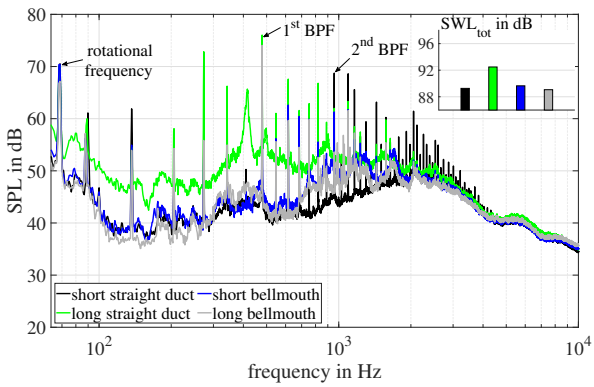

(c)

Figure 3.8: Spatial averaged SPL for single fan installations with different inlet shroud geometries at off-design (a), top-efficiency (b) and high-volume flow rate conditions. Data and images adjusted from Paper 5.

Taking into consideration the performance of the tested configurations, three operating conditions, representing off-design at high load, top-efficiency at intermediate load and high-volume towards free discharge, were selected for investigating the acoustic far-field.

Figure 3.8 presents the spatially averaged SPL measured upstream of the tested configurations under the selected operating conditions. Focusing on the off-design condition in Fig. 3.8(a), the configurations with bellmouth intakes exhibit overall higher noise levels compared to the straight duct configurations. The most pronounced discrepancies occur in the 300–900 Hz range, where the bellmouth configurations display broadband humps of higher amplitude over a wider frequency band. Considering the association of this spectral region with leakage flow between the rotating ring and the shroud [47], [55], [155], [158], the results suggest the presence of different flow regimes. The interaction between the leakage flow and the main flow, shaped differently by the various inlet geometries, may promote backflow vortex generation of varying intensity. Moreover, for the short straight duct, the earlier onset of stall (see Fig. 3.7) compared to the other configurations enforces the anticipation of a distinct flow behavior.

Tonal components of high amplitude, occurring at multiples of the rotational frequency, are present across all configurations. Their common occurrence and established association with the ingestion of large-scale inflow distortions [63], [159] and rotor–stator interactions [85], [86] suggest that the inlet geometry has minimal influence on these features. Above 2 kHz, only marginal discrepancies are observed among all configurations, including a high-frequency hump near 5.5 kHz. The latter is likely associated with vortex shedding at the trailing edge [160], [161] and appears to be independent of the inlet configuration. Furthermore, potential propagation effects emerging at these frequencies also appear insensitive to the inlet geometry, despite the substantial dimensional differences among the tested configurations.

At the top-efficiency condition in Fig. 3.8(b), the higher noise levels of the configurations with bellmouth geometries remain evident. The broadband hump preceding the first BPF exhibits variations in both amplitude and shape among the tested configurations, suggesting differences in the underlying noise-generation mechanisms. The second BPF is obscured by adjacent narrowband contributions for all configurations, while all except the long straight duct show qualitative agreement above 2 kHz. The long straight duct consistently produces lower broadband amplitudes in this range, though it follows the same overall trend. Notably, only the short straight duct displays persistent high-amplitude tones above 2 kHz, which may indicate more efficient acoustic propagation due to the shorter length.

At the high-volume flow rate condition in Fig. 3.8(c), the long straight duct exhibits higher amplitudes up to approximately 1.5 kHz compared to the other configurations. Moreover, it is the only configuration that demonstrates a significant subharmonic feature below the first BPF. At such high flow rates, the persistence of subharmonic humps is generally not expected [39], [155]. The appearance of high-amplitude tones at multiples of the rotational frequency is consistent across all configurations, with quantitative agreement above 3 kHz.

Notably, when examining the evolution of the spectra across different loading conditions, the long straight duct is the only configuration that does not follow the general trend of SWL increase with higher loading.

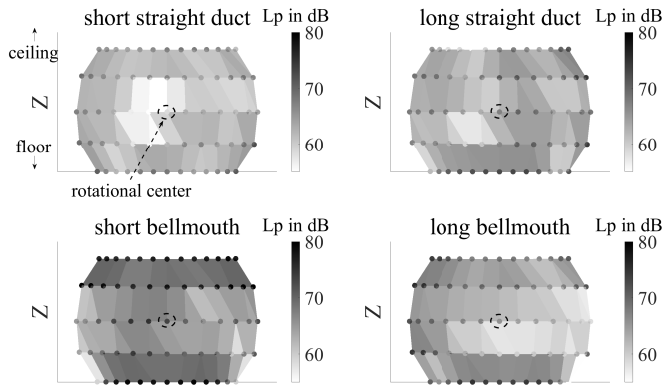

Figure 3.9: Directivity of sound field upstream of fan installations with different inlet shroud geometry at top-efficiency operating conditions. Data and images adjusted from Paper 5.

The prominent tone amplitude at the first BPF for all tested configurations and operating conditions motivates an investigation of the corresponding directivity over the measurement grid. At the first BPF, the wavelength is approximately 0.7 m—more than three times the length of the longest configuration (i.e., the long bellmouth). Consequently, propagation effects associated with inlet geometry are expected to be minimal [1]. Figure 3.9 presents the SPL distribution at the first BPF over the same microphone grid, located 1 m upstream of the fan's rotational center, for the top-efficiency operating point. Overall, the short straight duct exhibits the lowest SPL, with minima occurring near the center of the grid. In contrast, the short bellmouth configuration registers the highest amplitudes, symmetrically distributed from floor to ceiling. The two long configurations display maxima toward the floor and intermediate amplitude levels.

3.2.3 Interplay of installation effects and rotor design

The results presented in Sections 3.2.1 and 3.2.2, addressing parallel fan installations and inlet geometry effects, respectively, represent case studies. Therefore, they provide a limited description of axial fan behavior under the investigated installation effects. Expanding beyond the case-specific investigations, Paper 6 examined different rotor designs within a constrained design space characterized by the hub-to-tip ratio (κ) and the blade loading distribution. The interplay between installation effects—namely, inlet geometry and upstream obstructions—and the design space was investigated.

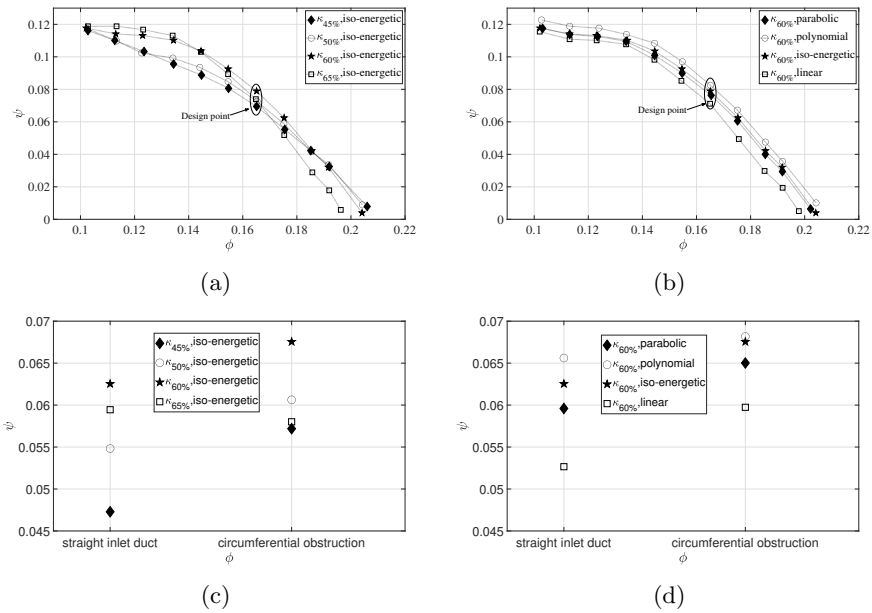

Figure 3.10: Curves of pressure rise (ψ) versus volume flow rate (ϕ) for fans with different hub-to-tip ratios (κ) (a) and blade loading distributions (b). Values of ψ versus ϕ at the design point for fans with different κ (c) and blade loading distributions (d) under various installation conditions. Data and images adapted from Paper 6.

Figure 3.10 shows the ψ–ϕ characteristics of the seven fans investigated in Paper 6, grouped into four fans with varying hub-to-tip ratios (κ) and four fans with different blade loading distributions. It is noted that one fan is common to both groups. Their corresponding design-point performance under various installation conditions is also presented. Overall, the performance characteristics of fans with varying hub-to-tip ratios (κ) (Fig. 3.10(a)) and different blade loading distributions (Fig. 3.10(b)) exhibit similar trends.

Focusing on the design point, the maximum deviations in the pressure coefficient are approximately 0.01 for both groups of fans. These deviations are likely associated with effects not accounted for in the design process, such as secondary flow phenomena. Among the fans with varying hub-to-tip ratios (Fig. 3.10(a)), the fan with $\kappa = 0.6$ demonstrates the best performance, while the fan with $\kappa = 0.45$ performs the worst. The latter behavior can likely be attributed to a breach of the solidity limit required to avoid aerodynamic interference between adjacent blades [1]. The superior performance of the fan with $\kappa = 0.6$ motivated the investigation of fans with different blade loading distributions in the same study. Within this group, the fan with polynomial loading exhibits the highest pressure rise, whereas the fan with linear loading shows the lowest. The latter performance can be partly attributed to the fan's relatively high work output at large blade spans, which is disproportionately

affected by aerodynamic losses associated with secondary flows in that region.

The installation of a straight inlet duct (see Fig. 3.10(c) and Fig. 3.10(d)) at the design point preserves the relative performance order within both fan groups, although the overall magnitudes are substantially lower ($\sim 20\%$) and the spread is wider. This reduction can be attributed to the fans' exposure to separated inlet flow conditions caused by the sharp-edged inlet. In general, the introduction of an upstream circumferential obstruction reduces the performance spread within both fan groups. However, for the fans with varying hub-to-tip ratios, the superiority of the $\kappa = 0.6$ fan becomes more pronounced, whereas for the fans with different blade loading distributions, the advantage of the fan with polynomial loading is only marginally retained.

Figure 3.11 presents the narrowband SWL spectra together with bar plots of the corresponding total SWL at the design point for fans with varying hub-to-tip ratios (κ) under different installation conditions. Overall, lower κ values result in higher total sound power levels ($\mathrm{SWL_{tot}}$) under nominal installation conditions (Fig. 3.11(a)). Focusing on the corresponding narrowband SWL, the qualitative agreement among the spectra suggests the presence of similar noise generation mechanisms. Furthermore, fans with closer κ values exhibit smaller amplitude deviations. The pronounced amplitudes at the blade passing frequencies ($\mathrm{BPF_1}$ to $\mathrm{BPF_5}$), consistently observed across these fans, indicate exposure to unsteady and inhomogeneous inflow conditions [1], [12], [13], which is unsurprising given the absence of any inlet flow conditioner [63]. The subharmonic components (denoted as BH_i), associated with subharmonic tip-noise mechanisms [47], [48], [155], are also prominent for all tested fans. Fans with smaller κ values exhibit substantially higher amplitudes at $\mathrm{BH_2}$ and $\mathrm{BH_3}$, whereas all fans show similar amplitude levels at $\mathrm{BH_1}$.

Examination of the broadband-shaped spectra between approximately 1–7 kHz reveals an upward scaling of the spectral levels as κ decreases. Considering the imposed installation conditions, turbulence-ingestion noise together with trailing-edge noise are expected to dominate the broadband contribution. The increased radiating area at lower κ, particularly relevant for trailing-edge noise, can account for the observed upward scaling of the spectra. Beyond approximately 9 kHz, the spectra of all fans exhibit a similar decay with frequency, following an approximate $\sim \omega^{-2}$ trend.

The introduction of a straight inlet duct (see Fig. 3.11(b)) significantly alters the spectral shape for all fans. Overall, the deviations in total SWL are reduced, as the fans with higher κ (i.e., $\kappa = 0.60$ and 0.65) exhibit substantial increases in amplitude. However, the fan with the highest κ still exhibits the lowest total SWL. The BPF tones are comparable across all fans, and the broadband spectra are similar above $\sim$2 kHz. For frequencies above $\sim$4 kHz, the broadband part exhibits a common decay rate of approximately $\omega^{-1.7}$. Furthermore, the amplitudes of the first subharmonic hump ($\mathrm{BH_1}$) are substantially higher for the fans with lower κ values (i.e., $\kappa = 0.45$ and 0.50). This suggests an intensification of coherent flow structures emanating from the tip region at low frequencies, driven by the flow regime imposed by this installation, which differs from the nominal case (see Fig. 3.10(a)).

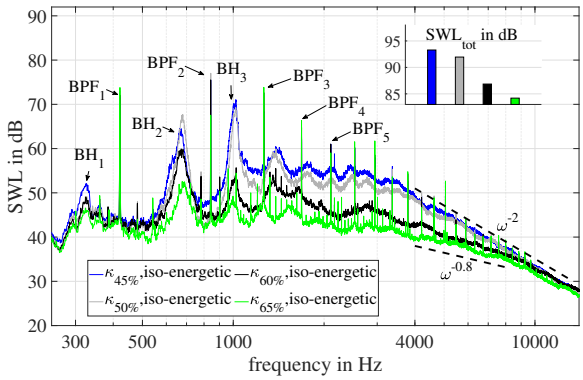

(a)

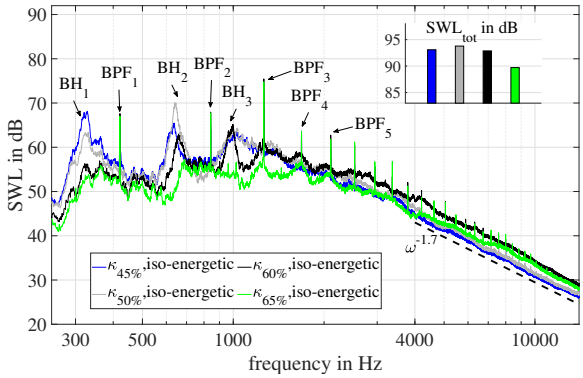

(b)

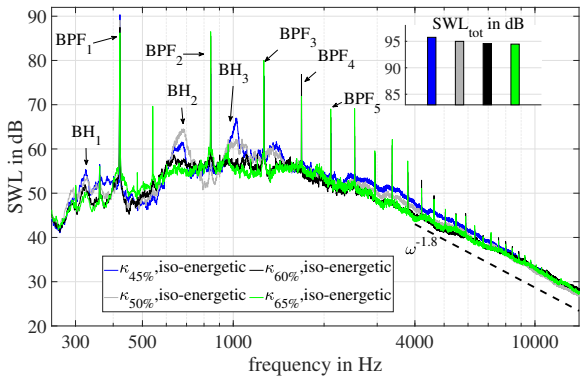

(c)

Figure 3.11: SWL for fans of different κ at the design point for nominal bellmouth inlet (a), straight inlet duct(b) and bellmouth inlet with circumferential obstruction. Data and images adjusted from Paper 6.

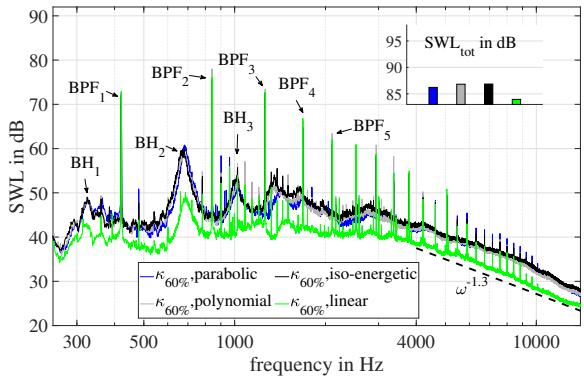

(a)

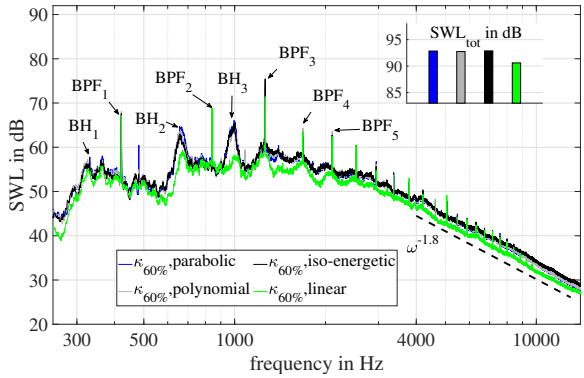

(b)

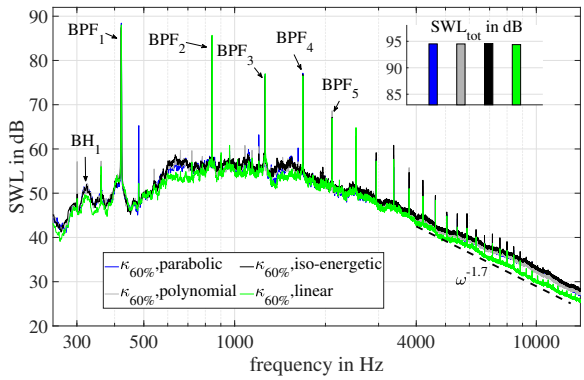

(c)

Figure 3.12: SWL for fans of different blade loading distribution at the design point for nominal bellmouth inlet (a), straight inlet duct(b) and bellmouth inlet with circumferential obstruction. Data and images adjusted from Paper 6.

Installations with a circumferential upstream obstruction (see Fig. 3.11(c)) exhibit a substantial increase in total SWL. A closer examination of the narrowband spectra reveals a significant rise in tonal components, likely due to distorted inlet flow conditions caused by the obstruction [1]. The largest deviations among the tested fans occur at the second and third subharmonic humps, with fans of lower κ exhibiting higher amplitudes. Given the persistence of this trend under nominal conditions, it can be inferred that the upstream obstruction did not significantly affect the noise generation mechanisms in this spectral region. In contrast, the broadband spectra of all fans converge closely above approximately 2 kHz. Finally, significant tonal components besides the BPF and its harmonics—at both low and high frequencies—are observed, likely associated with rotor-stator interaction effects [1], [85].

Figure 3.12 presents the narrowband SWL spectra alongside bar plots of the corresponding total SWL at the design point for fans with varying blade loading distributions under different installation conditions. At nominal conditions (see Fig. 3.12(a)) except for the fan with linear blade loading, the other fans exhibit quantitative agreement across the narrowband SWL spectra. The fan with linear blade loading exhibits the lowest SWL across the spectrum, although its amplitude levels at the first BPFs are comparable to those of the other fans. It also shows qualitative agreement at the second subharmonic hump and at frequencies above 4 kHz. In contrast, the fan with linear blade loading exhibits a greater number of tonal components, and its spectral shape between BPF_2 and BPF_4 differs substantially from that of the other fans. Considering its aerodynamic performance at the design point relative to the other fans (see Fig. 3.10(b)), these discrepancies can be partly attributed to the fan operating under a different flow regime (i.e., loading conditions). In conclusion, these results highlight a trade-off between aerodynamic efficiency and acoustic performance associated with the linear blade loading distribution.

The use of straight inlet ducts (see Fig. 3.12(b)) does not alter the similarity of the narrowband spectra among fans with polynomial, iso-energetic, and parabolic blade loading. Although the fan with linear blade loading continues to exhibit lower amplitudes and remains distinct from the others, its spectral similarities with the other fans improve. Overall, compared to nominal installations, all fans exhibit significant amplitude increases across the frequency range, accompanied by a steeper common decay slope above 4 kHz. These changes are driven by the altered inlet conditions imposed by the straight duct. The impact of altered inlet conditions on noise generation is further emphasized in the obstructed installations (see Fig. 3.12(c)). A qualitative agreement in narrowband SWL is observed across all fans, with significantly elevated amplitudes in both tonal components and the broadband spectrum. Additionally, subharmonic humps beyond the first are indistinguishable. This suggests that noise generation mechanisms associated with distorted inflow ingestion dominate over those related to secondary flows.

The combined analysis of narrowband SWL and aerodynamic performance between nominal and modified installations for all fans tested in Paper 6, highlights the interplay between rotor design and installation effects on LPAF acoustics, revealing the emergence of complex trade-offs. These trade-offs

become more complicated when considering operating conditions beyond the design point (see Paper 6), and are likely to differ further in realistic installations compared with the generic configurations studied in this work.

3.3 Aspect of receiver

The results presented in the previous sections (see Sections 3.1 and 3.2) discussed the implications of installation effects on the acoustics of LPAFs, focusing on SWL and SPL. While these metrics are relevant for investigating installation effects, evaluating their impact from the perspective of human perception requires the use of psychoacoustic metrics. In this context, the investigations presented in Papers 3 and 5 employed psychoacoustic metrics to examine the implications of inlet geometry and parallel fan operation, and upstream obstructions, respectively.

3.3.1 Effects of parallel fan operation and inlet geometry

The psychoacoustic metrics of loudness and sharpness are the primary contributors to the overall objective metric of psychoacoustic annoyance (PA), as defined by Di et al. [127]. Although fluctuation strength is a secondary contributor in PA, it can serve as an indicator of acoustic interference effects in parallel fan installations. These interference effects can be pronounced when the rotational speeds of the parallel fans are deliberately offset. For comparison, the superposition of two incoherent single fan installations is used as a reference condition.

Figure 3.13 presents the statistics for fluctuation strength for the parallel fan configuration, along with loudness, sharpness, and roughness for single fan installations with different inlet geometries. For fluctuation strength, the comparison includes a case with a larger rotational speed difference between the fans (i.e., rpm deviation of 1%), as well as the case of two incoherent fans (i.e., zero rpm deviation).

The case of incoherent sound sources exhibits significantly higher values at off-design conditions and slightly higher values at high-volume flow rates compared to the parallel fan operation with a ≈0.3% rotational speed deviation. In addition, both cases register similar values at top-efficiency conditions. Considering the above, the fluctuation strength of the two incoherent fan sources is not representative of the parallel fan system set to operate at the same rotational speeds. This discrepancy is likely attributed to the slight rotational speed variation (≈0.3%) between the fans. Moreover, the unequal blade spacing employed in the tested fan design may also influence the fluctuation strength observed in the parallel configuration. The anticipated redistribution of sound energy from the fundamental components (i.e., the first and second BPFs) to adjacent harmonics due to unequal blade spacing [162] has been confirmed in the spectra of the single fan installation (see Fig. 3.8). Consequently, the reduced energy at the fundamental frequencies does not provide a basis for substantial increases in fluctuation strength within the parallel fan system. When the rotational speed of one fan was deliberately increased to ≈ 1%, a higher fluctuation strength was observed, though only at high-volume flow rate conditions. Therefore, a further increase in the rotational speed difference—from ≈0.3% to ≈1%—did not result in a significant enhancement of modulation effects.

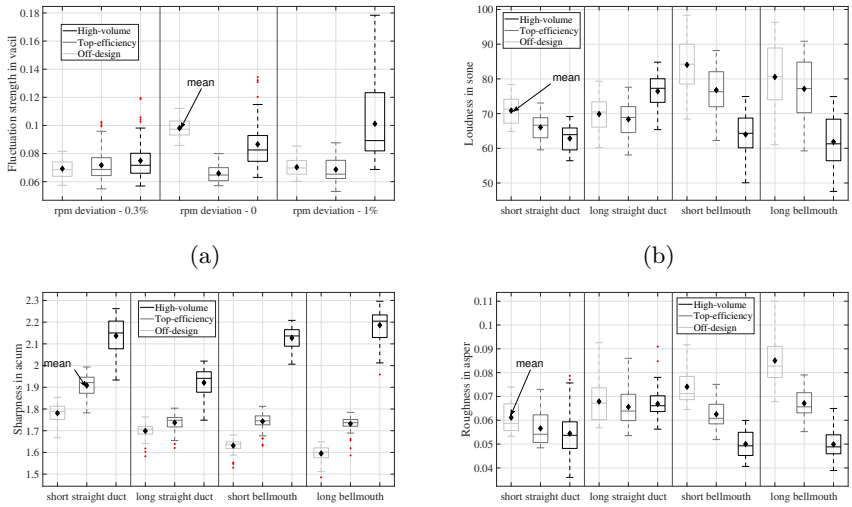

Figure 3.13: Statistics of fluctuation strength for parallel fan installation (a) and loudness (b) sharpness (c), roughness (d) for single fan installations. The horizontal line in the boxes indicates the median across the microphone grid, while the bottom and top edges of the boxes indicate the 25^{th} and 75^{th} percentiles, respectively. The whiskers extend to extreme data points, while + indicates outliers. Diamonds represent the mean values. Data and images adjusted from Paper 5.

Switching the focus to the single fan installations (see Fig. 3.13(b)), mean loudness decreases with increasing flow rate for all inlet geometries except the long straight duct. This trend has also been reported in other LPAFs [106], [107]. It should be noted that the dependence of loudness on loading aligns with the corresponding dependence of SWL on loading, as shown in Fig. 3.8 and in the aforementioned studies. Consequently, the steeper reduction in loudness observed for the bellmouth geometries is consistent with this behavior, whereas the long straight duct exhibits an increase in loudness from top-efficiency to high-volume flow rate conditions.

The sharpness values presented in Fig. 3.13(c) indicate a clear dependence on loading, with magnitudes increasing toward high-volume flow rate conditions for all tested inlet geometries. This relationship has also been reported in LPAFs featuring blade sweep but without a rotating ring [107]. The bellmouth inlet geometries exhibit a steeper increase in sharpness between top-efficiency and high-volume flow rate conditions compared to the straight duct configurations. Overall, the obtained values are consistent with those reported in relevant studies estimating this metric [39], [59], [106], [107].

The mean roughness values, shown in Fig. 3.13(d), exhibit the same dependence on loading as loudness, although the long straight duct geometry appears largely insensitive to variations in loading conditions. It should be noted that

the estimated roughness values are approximately an order of magnitude lower than those reported in other studies on low-pressure axial fans [39], [59], [107]. This discrepancy can be attributed to differences in fan design, as well as in the models and parameter settings employed for roughness estimation in the aforementioned studies.

Figure 3.14 presents the specific fluctuation strength for the parallel fan installations at top-efficiency and high-volume flow rate conditions. Similar to the previous figure (see fig. 3.13(a)) the cases of incoherent sources and parallel fan installation with speed difference of ≈1% is included. Furthermore, the mean specific values of loudness at top-efficiency and high-volume flow rate conditions for single fan installations are presented.

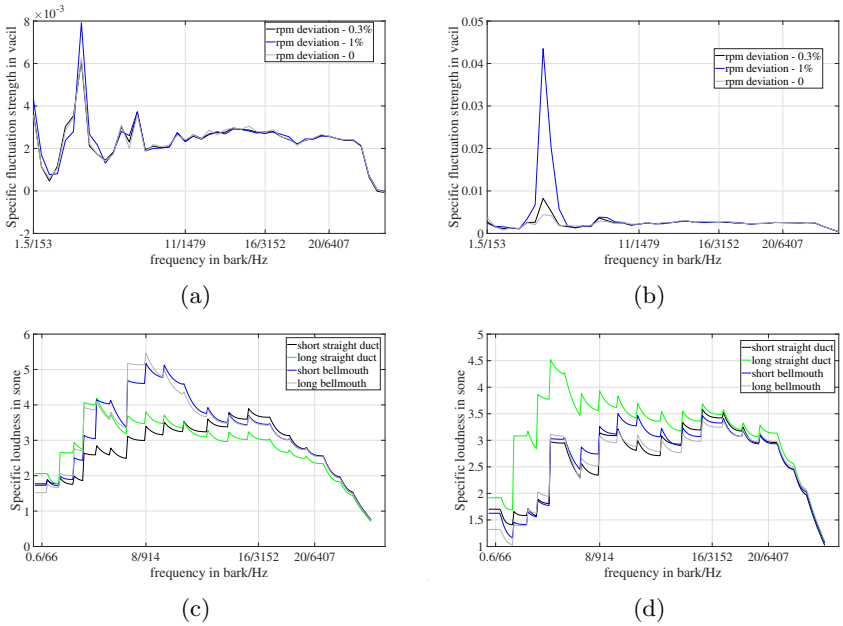

Figure 3.14: Mean specific fluctuation strength for parallel fan installations at top-efficiency (a) and high-volume flow rate conditions (b). Mean specific loudness at top-efficiency (c) and high-volume flow rate conditions (d) for single fan installations of different inlet geometries. Data and images adjusted from Paper 5.

Overall, the highest amplitudes of fluctuation strength (see fig. 3.14(a) and 3.14(b)) are observed around 5 Bark at both operating points. This trend also holds for the single fan installation and is consistent with previous studies on similar configurations [39], [100]. At top-efficiency conditions (see fig. 3.14(a)), the fluctuation strengths of the parallel fan system and the two incoherent fan sources are quantitatively comparable, while increasing the rotational speed deviation to 1% results in noticeable differences only at the maximum value. Similar behavior is observed under high-volume flow rate conditions (see fig. 3.14(b)); however, the case with a 1% rotational speed

difference yields a pronounced increase in maximum fluctuation strength at approximately 5 Bark.

The configurations with bellmouth inlets exhibit a clear dependence of the loudness maximum location on operating conditions (see fig. 3.14(c) and 3.14(d)). Specifically, at top-efficiency, maxima occur around 8 Bark, while at high-volume flow rates they shift to approximately 15 Bark. In contrast, the maxima for the short and long straight duct configurations remain largely insensitive to loading, appearing at about 4 and 15 Bark, respectively. Maxima of loudness near 15 Bark under free-discharge conditions for an axial fan with a rotating ring have also been reported by Cattanei et al. [59]. Furthermore, the occurrence of maximum specific loudness below 10 Bark is considered less unpleasant according to Töpken and Van de Par [101]; hence, the observed behavior is favorable for the long straight duct configuration.

Another notable aspect is the evolution of specific loudness across frequency in accordance with the SPL spectrum. At top-efficiency conditions, the subharmonic humps and first harmonics contribute substantial acoustic power below 500 Hz (see Fig. 3.8) for the bellmouth configurations. However, at high-volume flow rates, these low-frequency contributions diminish significantly, while the broadband high-frequency content increases. Consequently, the variations in specific loudness can be associated with the changing relative importance of the underlying noise mechanisms, including leakage flow, trailing-edge noise, rotor–stator interaction, and inflow turbulence noise.

3.3.2 Effects of upstream obstructions

Besides inlet geometry and parallel fan operation, the perceived sound of LPAF installations can also be influenced by the presence of upstream obstructions, which introduce distortions on the inlet flow. This effect was investigated in Paper 3 using installations with generic upstream obstructions. The same LPAF with a rotating ring as in Paper 5 was examined across different loading conditions.

Figure 3.15 presents the statistics for loudness, sharpness and tonality for the short and long inlet configurations across different loading conditions. The effect of upstream obstructions on mean loudness (Fig. 3.15(a)) under high-pressure conditions is marginal. In contrast, a significant increase in loudness is observed toward free-discharge conditions for the obstructed installations. For the free inlet installation, loudness generally decreases with increasing volume flow rate [39], [106], [107], in close correspondence with SPL. However, the increasing influence of the obstructions at higher flow rates alters the acoustic character of the installations, leading to higher SPL and consequently higher loudness values.

Overall, the tested obstructions appear to offer an advantage in terms of sharpness. A weak dependence of mean sharpness (Fig. 3.15(b)) on loading is observed for installations with upstream obstructions. In contrast, the free inlet case exhibits a distinct increase in sharpness as loading decreases, a behavior typical of LPAFs [106]. Furthermore, the sharpness levels observed for the obstructed installations are close to the minimum values recorded for the free

inlet configuration.

The mean tonality values for the short inlet shroud installations at median-pressure and free-discharge conditions (Fig. 3.15(c)) show a significant increase in the presence of upstream obstructions. The elongation of the inlet shroud (Fig. 3.15(d)) exhibits different effects across the three tested installations. Specifically, the free inlet configuration demonstrates a weak dependence on inlet shroud length. The installation with a radial obstruction shows a slight decrease in tonality under free-discharge conditions but a minor increase at high-pressure conditions. In contrast, the installation with a circumferential obstruction displays a clear decrease in tonality at median-pressure and free-discharge conditions, while only a marginal reduction is observed at high pressure. Overall, these variations in tonality can be interpreted as corresponding changes in the unsteady blade forces experienced by the fan [13]. Such variations arise from the spatially non-uniform inlet flow induced by the upstream obstructions. However, when the obstructions are positioned further upstream, the non-uniformity of the ingested flow is attenuated, resulting in less pronounced tonal variations.

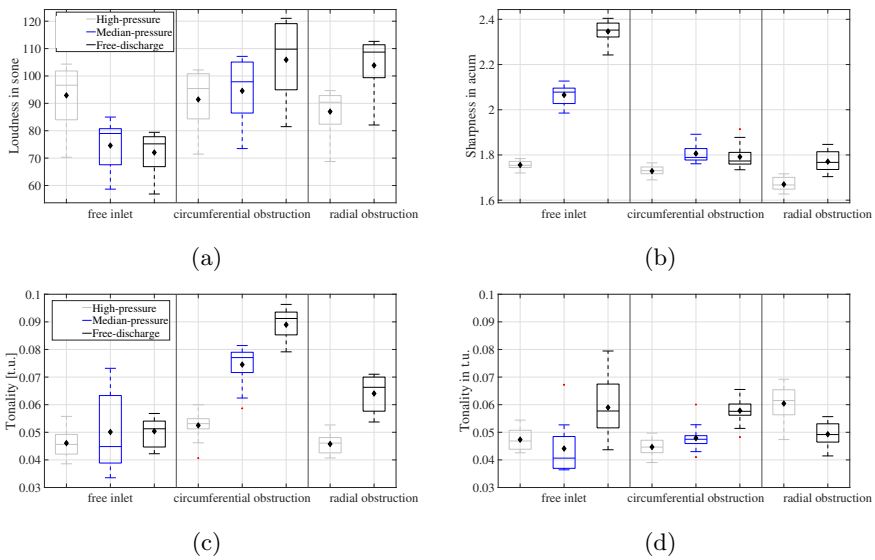

Figure 3.15: Statistics of loudness (a) sharpness (b) and tonality for short (c) and long (d) inlet. The horizontal line in the boxes indicates the median across the microphone grid, while the bottom and top edges of the boxes indicate the 25^{th} and 75^{th} percentiles, respectively. The whiskers extend to extreme data points, while + indicates outliers. Diamonds represent the mean values. Data and images adjusted from Paper 3.

Figure 3.16 presents the mean specific loudness at selected operating conditions for the different installations featuring a short inlet shroud. Although the mean loudness values are similar across configurations at high-pressure conditions (see Fig. 3.15(a)), discrepancies appear across the frequency range

of specific loudness (Fig. 3.16(a)). Specifically, the absence of upstream obstructions results in a slight reduction of specific loudness below 1 kHz, while at higher frequencies the free inlet configuration exhibits marginally higher values than the obstructed cases.

At free-discharge conditions (see Fig. 3.16(b)), the installations with upstream obstructions exhibit substantially higher specific loudness levels than the free inlet configuration up to approximately 2 kHz. The differences observed between the two obstructed configurations can be partly attributed to the distinct flow losses and inlet velocity profiles they induce.

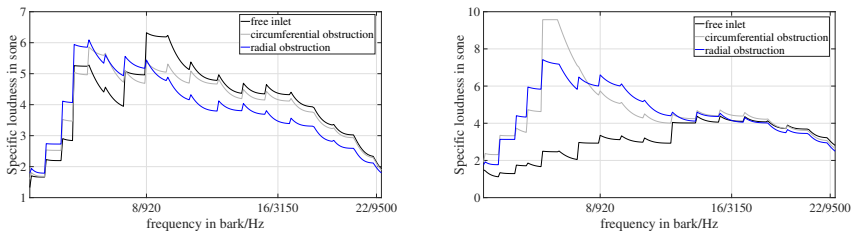

Figure 3.16: Mean specific loudness at high-pressure (a) and free-discharge (b) for single fan installations with different upstream obstructions. Data and images adjusted from Paper 3.

Chapter 4

Summary of Papers

4.1 Paper 1

Vourakis, M., & Karlsson, M. (2022). *A round robin test of a low-pressure axial fan.* In International Congress on Fan Noise, Aerodynamics, Applications and Systems 2022, 27-29 June, Senlis, France, 2022.

4.1.1 Scope

In Paper 1, a round robin test of a low-pressure axial fan (LPAF) was performed. The main objective of the study was the evaluation of measurement setup and methods for sound characterization of LPAFs at the fan test facility (FTF).

4.1.2 Methodology

Three copies of the benchmark fan along with one copy of the stator, inlet and outlet shroud were 3D-printed via laser sintering. Sanding and paint filling were applied to the stationary components of the installation and to one of the fan copies, while the second copy was only painted and the third remained unprocessed. All fan copies were compared to the original CAD design via 3D scanning. The characteristic curves of the three fan installations were obtained at the FTF. In addition far-field acoustic measurements were obtained upstream of the fans for estimating the sound characteristics and the sound directivity of the installations. The microphones were distributed over two spherical surfaces of different radii. The estimation of sound power level (SWL) was made by utilizing ISO 3744:2010 [51] with an environment correction factor in accordance with the reverberation method.

4.1.3 Main findings

The pressure rise curves of the three tested fans showcased discrepancies within the expected measurement accuracy across the operation map. However, the efficiency curves did not register the same degree of repeatability across

the operation range, mainly attributed to the low accuracy of the torque sensor. The sound characteristic curves of the fans showed good repeatability with the highest magnitude of discrepancies registered towards free discharge. Furthermore, the narrowband spectra of SWL at the design point showed good agreement for the three fans. Overall, the repeatability of the measurements was perceived as satisfactory.

The pressure rise curve of the benchmark study [153] was quantitatively reproduced for the majority of the operating points, though considerable discrepancies were found towards free discharge. Moreover, the efficiency curve was reproduced qualitatively, showing a relatively stable discrepancy when compared to those obtained. The sound characteristic curve was reproduced well at the design point onward, as well as at flow rates corresponding to deep stall. However, significant discrepancies were observed at early stall and towards free discharge. At the design point, comparison of the narrowband spectra, between obtained measurements and the benchmark study, revealed phase and magnitude mismatch between the first two blade passing frequencies. The observed mismatch was linked to dimensional deviations arising during installation, including asymmetries in the tip-gap clearance. Finally the evaluation of sound directivity showed retention of the sound field's symmetry, along the polar angle range measured. Conclusively, the reproducibility of the attained results with regard to the reference study was deemed improvable.

4.1.4 Division of work

The author of the thesis performed the measurements, post-processed the results and wrote the original draft of the paper. Mikael Karlsson provided technical supervision, discussed the results and provided feedback on the manuscript.

4.2 Paper 2

Vourakis, M., & Karlsson, M. (2023). *Aeroacoustic interaction effects between parallel low-pressure axial flow fans.* In Tenth Convention of the European Acoustics Association, Forum Acusticum (pp. 3865-3872).

4.2.1 Scope

In Paper 2, an aeroacoustic investigation of parallel low-pressure axial fans, with rotating rings, under varied installation conditions was performed. The aim of the study was to identify interaction effects within the range of tested installation conditions, which could alter the acoustic or aerodynamic performance of the parallel fan system.

4.2.2 Methodology

Two identical low-speed/pressure electric axial fans with a rotating rings, used in automotive cooling modules, were studied in the FTF. The parallel fan installation was tested for different distances between the fans and straight inlet shrouds of different length. A single fan case was also tested as reference. Acoustic measurements were performed upstream of the fan system's inlet, over spherical surface segments corresponding to two radii. SWL estimation was made by utilizing ISO 3744:2010 [51] with an environment correction factor in accordance with the two surface method. Moreover, aerodynamic measurements were performed, in proximity to the fan's aerodynamic interface plane, for one case of inlet shroud length. The aerodynamic measurements were performed with an LDA system, allowing the estimation of velocity profiles as well as investigation of corresponding power spectral density.

4.2.3 Main findings

The inlet velocity profiles obtained demonstrated an increasing asymmetry as the distance between fans decreased. However, these effects did not translate to noticeable discrepancies when examining the characteristic curve or the sound spectra of the system.

Furthermore, the inlet shroud length constituted alterations to both aerodynamic and acoustic performance of the system. Both the parallel fan system and the single fan reference case registered gains along their characteristic curves and exhibited a more predictable stall region when fitted with the longer inlet shroud. Conversely, the longer inlet shroud increased the SWL across the lower frequencies substantially while attenuating levels slightly at higher frequencies. Moreover, low-frequency spectra of broadband character showcased broadening over frequency. This behavior was attributed to the alteration of the fan/shroud radiation impedance with the introduction of the longer inlet shroud.

Finally the spectral density analysis of the inlet velocity profiles showcased the persistence of energy at frequencies corresponding to the first motor orders.

4.2.4 Division of work

The author of the thesis performed the measurements, post-processed the results and wrote the original draft of the paper. Mikael Karlsson provided technical supervision, discussed the results and provided feedback on the manuscript.

4.3 Paper 3

Vourakis, M., Zea, E., Etemad, S., Karlsson, M., & Andersson, N. (2025). *Impact of distorted inlet flow on axial fan psychoacoustics.* In International Congress on Fan Noise, Aerodynamics, Applications and Systems 2025, 9-11 April, Antibes/Juan-les-Pins, France, 2025.

4.3.1 Scope

In Paper 3, a low-pressure axial fan with rotating ring installed downstream from obstructions of generic geometry was investigated. The study examined different inlet shroud lengths under varied loading conditions. The aim of the study was to assess the impact of distorted inlet flow, imposed by the upstream obstructions, on the psychoacoustics of the fan.

4.3.2 Methodology

All measurements were performed at the FTF. The fan installation consisted of a bellmouth intake, followed by an obstruction and a straight duct section upstream of the fan. The tested fan featured a rotating ring and is utilized in automotive cooling modules. Two obstructions, one of radial and second of circumferential geometry, were tested together with three straight duct sections of varying length. Furthermore, a reference non-obstructed fan installation was tested, and a configuration including the obstructions but excluding the fan, to evaluate self-noise and aerodynamic losses. Far-field acoustic measurements were conducted at three operating points, representing high-efficiency, intermediate-pressure, and free-discharge conditions. The psychoacoustic analysis was performed via the open-source toolbox SQAT [121].

4.3.3 Main findings

Comparison of the sound spectra between installations with and without the fan indicated minor self-noise effects. Installations with obstructions exhibited a notable increase in loudness compared to the non-obstructed installation, under intermediate and free discharge conditions. Furthermore, the specific loudness analysis revealed obstruction-induced effects below 1 kHz and 2 kHz at intermediate and free discharge conditions, respectively. On the contrary, sharpness levels decreased for obstructed installations towards free discharge.

Inlet shroud length effects were primarily observed for the metric of tonality under upstream obstructions. This behavior was attributed to the persistence of a non-uniform inlet flow topology, which becomes pronounced as the obstruction approaches the fan's aerodynamic interface, thereby leading to elevated tonality levels.

4.3.4 Division of work

The author of the thesis performed the measurements, post-processed the results and wrote the original draft of the paper. Elias Zea supervised the

work, discussed the results and provided feedback on the manuscript. Sassan Etemad provided project supervision and feedback on the manuscript. Mikael Karlsson supervised the work and provided feedback on the manuscript. Niklas Andersson provided supervision and feedback on the manuscript.

4.4 Paper 4

Vourakis, M., Zotter, F., Brandão, E., & Zea, E. (2025). *Aeroacoustic source characterization at fan test facility with spherical harmonics of the half-space.* JASA Express Letters, 5(5).

4.4.1 Scope

In Paper 4, a scheme of spherical harmonics of the half-space was employed for aeroacoustic source characterization at the FTF. The primary objective of the study was to use this scheme for identifying room-acoustical effects, while the secondary objective was to evaluate its applicability for sound characterization of a LPAF.

4.4.2 Methodology

The theoretical case of a point monopole source radiating in a free field above a reflecting surface was first considered. The sound field was then expanded in spherical harmonic basis functions for the half-space, where only even-order spherical harmonics were retained. The spherical harmonic coefficients were expressed both for a measurement scenario and in analytical form. A second-order truncation was applied to the former and a fortieth-order truncation to the latter. The room-acoustical effects were subsequently evaluated using an isotropy estimator. Measurements of a compact monopole-like sound source were obtained at a hemi-anechoic room and at the fan test facility. The microphone grid at the hemi-anechoic facility utilized 19 microphones over a half-sphere, while the grid at the FTF comprised 65 microphones over a quarter sphere. Different absorption material installations were tested at the FTF.

Furthermore, the SWL of a benchmark case fan [153] was estimated utilizing ISO 3744:2010 [51] with an environment correction factor according to the reverberation method. An alternative method for estimating SWL of the fan, based on the spherical harmonic decomposition, was also assessed.

4.4.3 Main findings

The comparison of isotropy between the theoretical monopole and the measured volume source at the hemi-anechoic room showcased good qualitative agreement. On the contrary, the isotropy curve obtained from the measurements in the FTF revealed significant discrepancies, especially at lower frequencies. This was primarily attributed to room-acoustical effects, while uncertainty regarding the location of the volume source's acoustic center was also acknowledged.

The investigated SWL estimators for the low-pressure axial fan measured at the FTF, showcased marginal differences across the evaluated frequency range. The discrepancies between the measured cases at the FTF and the benchmark data were mainly attributed to installation and geometry deviations of the fan and inlet shroud, while a compounding effect from room-acoustical effects was hypothesized.

The reconstruction of the directivity maps at the first and second BPF, based on the SHD scheme, retained the measured pattern. Furthermore, applicability of the scheme was showcased at different operating points, namely unsteady (stall) and free discharge.

4.4.4 Division of work

The author of the thesis performed the measurements, post-processed the results and wrote the original draft of the paper. Franz Zotter provided technical supervision for the scheme of spherical harmonic decomposition, discussed the results, reviewed and provided feedback on the manuscript. Eric Brandão discussed the results, reviewed and provided feedback on the manuscript. Elias Zea supervised the work, discussed the results, reviewed and provided feedback on the manuscript.

4.5 Paper 5

Vourakis, M., Zea, E., Karlsson, M., Andersson, N., & Etemad, S. (2025). *Installation effects on axial fans: Combined aeroacoustic and psychoacoustic perspective.* Applied Acoustics, 240, 110872.

4.5.1 Scope

In Paper 5, installation effects on the aeroacoustic and psychoacoustic performance of a low-pressure axial fan with a rotating ring were investigated. The study examined different inlet shrouds and a parallel fan configuration under varied loading conditions. The objective was to advance the understanding of the interplay between inlet geometry and the aerodynamic, acoustic, and psychoacoustic performance of such fans.

4.5.2 Methodology

All measurements were conducted at the FTF. Two copies of an electric axial cooling fan with a rotating ring were used for the single and parallel fan configurations. Four inlet shroud geometries, 3D-printed via laser sintering, were tested: two with bellmouths and two with straight ducts. In the parallel fan configuration, the spacing between the two fans was also varied. The aerodynamic performance of all configurations was evaluated across a wide operating range. Far-field acoustic measurements were performed upstream of the fans using microphones arranged on two spherical segments of different

radii. The sound power level (SWL) was estimated in accordance with ISO 3744:2010 [51], applying an environmental correction factor based on the two-surface method. Psychoacoustic metrics were obtained using the open-source toolbox SQAT [121].

4.5.3 Main findings

A marginal performance improvement was observed for the elongated inlet geometries, resulting in a more stable operation onset stall. In the case of bellmouth configurations the improvement was attributed to the suppression of vena contracta effects. Furthermore, three distinctive trends were identified regarding the acoustic performance across different inlet configurations. Firstly, the use of the bellmouth configuration resulted in the highest overall SWL at high-loading conditions, but also in the steepest amplitude reduction toward free-discharge. Thus, a trade-off arose between aerodynamic and acoustic performance. Secondly, a weak coupling between SWL and loading conditions was observed for the elongated straight duct. Lastly, the shortest inlet configuration exhibited the best acoustic performance overall, particularly at high loading.

At high-loading conditions instances of the SPL, including tones and broadband humps, demonstrated qualitative similarities for different inlet geometries. Moreover, a quantitative agreement was observed at broadband spectra above 2.5 kHz irrespective of inlet geometry or loading conditions. The directivity of the upstream sound field at the first BPF indicated a dependence on the inlet geometry.

The psychoacoustic metrics of loudness and roughness demonstrated similar dependencies to loading conditions as the total SWL for the tested inlet geometries. Moreover, the bellmouth installations exhibited the steepest reduction of these metrics with decreased loading. A common trend of increased sharpness with reduced loading was observed for all inlet geometries. Tonality and fluctuation strength demonstrated a dependence on operating conditions only for the shortest inlet geometry.

The evolution of specific loudness showcased a transition of maxima towards higher frequencies as loading decreased for all installations with bellmouths and the shortest inlet. On the contrary, the elongated straight duct installation exhibited weak synergy to loading. The specific roughness showcased a trend of increasing maxima with increasing loading for configurations with bellmouths. Moreover, both specific loudness and roughness exhibited quantitative agreement for all configurations above $\approx$2.5 kHz. Lastly, the specific fluctuation strength demonstrated the same trends for all tested configurations.

The parallel fan system's aerodynamic performance demonstrated no sensitivity to the tested fan spacings irrespective of inlet geometry. Specifically, the SWL spectra of the parallel fan system scaled in accordance with the spectra of two incoherent fan sources for the tested loading conditions and inlet geometries. Furthermore, for the parallel fan system the mean values of all psychoacoustic metrics, with the exception of fluctuation strength, showcased a good agreement with values from the two incoherent fan sources. Finally, the maxima of specific fluctuation strength towards free-discharge conditions

increased as the difference of rotational speeds approached 1 %.

4.5.4 Division of work

The author of the thesis performed the measurements, post-processed the results and wrote the original draft of the paper. Elias Zea supervised the work, discussed the results and provided feedback on the manuscript. Sassan Etemad provided project supervision and feedback on the manuscript. Mikael Karlsson supervised the work and provided feedback on the manuscript. Niklas Andersson provided supervision and feedback on the manuscript.

4.6 Paper 6

Vourakis, M., Ghosh, D., Andersson, N., Etemad, S., Karlsson, M., & Zea, E. (2025). *Experimental investigation of installation effects on the aeroacoustics of low-pressure axial fans: on the impact of blade loading distribution and hub-to-tip ratio.* Manuscript.

4.6.1 Scope

In Paper 6, seven 3D-printed LPAFs were investigated, comprising one group of fans with varying hub-to-tip ratios and a second group with different blade loading distributions. The study aimed to advance the understanding of blade loading distribution and hub-to-tip ratio in the aeroacoustic performance of LPAFs under installation effects.

4.6.2 Methodology

The fans were designed according to the blade element momentum method for low-solidity fans via the Python code *C-Fan* [113]. Three different inlet geometries were tested, including bellmouth, straight duct and shortened bellmouth. All inlet shrouds and fans were 3D-printed via laser sintering. The electric brushless motor driving the fans was integrated into their hubs. Two different upstream obstructions made from plexiglass were tested in tandem with the bellmouth inlet. One of the obstructions represented a circular sector and the other a radial ring.

All measurements were conducted at the FTF. Acoustic measurements were performed upstream of the fans via microphones distributed over a sphere segment of ≈ 1 m radius. The aerodynamic performance of nominal installations, i.e. fans with bellmouth inlet and free intake, was evaluated across a wide operational range. Three operating conditions were chosen for investigating the aerodynamic performance under installation effects, namely the optimum efficiency point, design point, and overload condition. Furthermore, the acoustic performance of all installations was recorded at these points. The SWL was estimated in accordance with ISO 3744:2010 [51], applying an environmental correction factor based on the reverberation method.

4.6.3 Main findings

Similar aerodynamic performance was observed for all fans at the design point and throughout the consider operation range, under nominal installation conditions. The fan with polynomial blade loading distribution and 0.6 hub-to-tip ratio demonstrated the best performance. On the contrary, fans with linear blade loading and 0.45 hub-to-tip ratio showcased the worst performance.

The fan with 0.6 hub-to-tip ratio and linear blade loading exhibited the lowest noise emissions at the design and optimum efficiency operating conditions, while the fans with other blade loading distributions (same hub-to-tip ratio) registered similar spectra. Consequently, a trade-off between aerodynamic and acoustic performance was observed for the linear blade loading distribution. At the optimum efficiency point, fans with lower hub-to-tip ratios demonstrated lower noise emissions, while at the design point fans with higher hub-to-tip ratios. Furthermore, both design parameters showed negligible effects on noise emissions at overload conditions.

Overall, the impact of the tested inlet geometries on aerodynamic performance followed the dependencies observed under nominal installations. Furthermore, the tested obstructions imposed similar relative losses across all fans at the measured conditions. Consequently, a weak coupling between the imposed aerodynamic effects and the study parameters was suggested.

Significant increases of noise emissions were registered at the design and overload conditions for all fans, under modified installations. Moreover, a weak dependence of blade loading distribution on noise emissions under installation effects was observed. Lastly, fans with higher hub-to-tip ratios showcased increased noise emissions at the design point, albeit reduced emissions at overload conditions.

4.6.4 Division of work

The author of the thesis performed the measurements, post-processed the results and wrote the original draft. Debarshee Ghosh designed the fans, discussed the results and provided feedback on the manuscript. Sassan Etemad provided project supervision and feedback on the manuscript. Mikael Karlsson supervised the work and provided feedback on the manuscript. Niklas Andersson provided supervision and feedback on the manuscript. Elias Zea supervised the work, discussed the results and provided feedback on the manuscript.

Chapter 5

Concluding remarks

5.1 Summary

The present thesis has investigated installation effects on the acoustics of low-pressure axial fans, addressing the aspects of source, environment and receiver. The aspect of environment was motivated by the non-ideal acoustic test environment employed in all experimental investigations. The source aspect concerned installation conditions in the vicinity of the fan, including inlet geometry, upstream obstructions and paralell fan operation. Several of these installation conditions were further evaluated from the perspective of the receiver through the use of psychoacoustic metrics.

Initially, a round robin test of a benchmark fan was conducted in Paper 1 to evaluate the acoustic and aerodynamic measurement capabilities of a bespoke fan test facility. Obtained results of aerodynamic and sound characteristics demonstrated the repeatability of the employed measurement methods, as well as the potential of 3D-printed rotor geometries for aeroacoustic investigations on rotor design. However, the assessment of reproducibility revealed sensitivities to room-acoustical effects and the suitability of the employed sound-characterization methods. This led to a complementary study in Paper 4, where spherical harmonics of the half-space were used for source characterization and to identify room-acoustical effects at the employed facility. The evaluation of isotropy using a monopole-like source demonstrated the emergence of room-acoustical effects in the 200–1000 Hz frequency range. In addition, the feasibility of using a second-order spherical harmonic decomposition to reconstruct the directivity and SWL of the benchmark fan, across different loading conditions, was established.

The feasibility to conduct aeroacoustic investigations on installation effects in the vicinity of the fan was assumed based on the collective influence of room-acoustical effects in spatially similar test setups. This assumption was put to the test in Paper 2, while studying the effects of parallel fan operation and inlet geometry. Only minor interaction effects were observed in the aerodynamic performance and inlet flow field of the tested parallel fan installations. These results, combined with the acoustic far-field measurements, suggested that

the installation behaved like two incoherent sound sources. Additionally, the identification of similar changes in the acoustic far-field between single and parallel fan installations across different inlet geometries supported the assumption of a collective influence of room-acoustical effects in comparable test setups.

The significant acoustic alterations resulting from inlet geometry changes in the fan case study of Paper 2 were further examined in Paper 5, which included additional operating conditions and inlet geometries. Discrepancies in the acoustic far-field between installations with bellmouth geometries and straight ducts were observed in the frequency range of 300–2000 Hz, particularly under high loading conditions. Furthermore, the shortest inlet configuration was identified as the case where a trade-off between aerodynamic performance and noise emissions becomes apparent. The installation with an elongated straight duct also exhibited the least sensitivity of sound emissions to operating conditions.

The incorporation of a BEM method for low-solidity LPAFs in Paper 6 enabled investigation of installation effects and rotor design, extending the scope beyond the fan study case of Paper 2 and 5. The design space included hub-to-tip ratio and blade loading distributions, while installation effects comprised inlet geometry and upstream obstructions. The two groups of fans (i.e., varying hub-to-tip ratio and blade loading distribution) showcased comparable aerodynamic performance at design conditions; however, when varied loading conditions and installation effects were considered, complex aeroacoustic dependencies emerged, particularly for the hub-to-tip ratio. For the group of fans with varying blade loading distributions, a distinct trade-off between aerodynamic and acoustic performance was observed for the fan with linear blade loading, whereas the remaining fans exhibited only minor discrepancies. Moreover, the acoustic performance showed lower sensitivity to the investigated blade-design parameters when the fans were subjected to upstream obstructions compared with inlet geometry variations. Still, a substantial increase of noise emissions was registered for all installations with upstream obstructions from design conditions towards free discharge.

The interplay between psychoacoustics and installation effects was initially examined for the fan study case of Paper 5. The loudness and roughness metrics showed strong sensitivity to the inlet geometry, whereas the trend of increasing sharpness towards free discharge was consistent across all tested inlet geometries. In the case of parallel fan operation, the analysis of fluctuation strength revealed deviations from the behavior expected of two incoherent sound sources. This deviation was attributed to rotational speed variations during parallel fan operation, as well as to the unequal blade spacing of the tested fan.

Subsequently, the same fan study case from Paper 5 was used in Paper 3 to evaluate the interplay between upstream obstructions and psychoacoustics. Unexpectedly, installations with upstream obstructions showed a significant increase in loudness from median and free-discharge conditions. In contrast to free inlet installations, obstructed installations exhibited lower sharpness values at median and free-discharge conditions, along with an overall insensitivity

to loading variations. Moreover, tonality showed dependence on inlet shroud length for the obstructed installations, attributed to the persistence of non-uniform inlet flow and the resulting unsteady blade forces on the fan.

Overall, the combined investigations in this work, addressing the test environment, the vicinity of the fan, and the receiver perspective, advance the understanding of installation effects on the acoustics of low-pressure axial fans. The insights gained contribute to the assessment and mitigation of noise emissions in low-pressure axial fan installations.

5.2 Future work

The inherent limitations of this work, identified within the methods and the assumptions imposed, provide a starting ground for future research. In the following a number of suggestions for future research are given. This list focuses on pathways related to the work performed and is therefore not exhaustive with regards to the research problem.

The characterization of aeroacoustic sound sources in non-ideal acoustic environments challenges the reproducibility of obtained results. As mentioned in Section 3.2, this problem can be partly circumnavigated by relying on relative comparisons of similar measurement setups, under the assumption of a collective influence of room-acoustical effects. However, this assumption does not constitute a reliable basis for acquiring absolute levels of the investigated quantities (e.g., sound pressure levels), and its suitability for model development (i.e., linked to aeroacoustic source processes) or verification of numerical simulations therefore can be limited. The round robin test presented in Paper 1 provided a basis for quantifying discrepancies between the two acoustic environments (i.e., the fan test facility and the standardized measurement facility of the benchmark case [153]), following an approach analogous to the absolute comparison test defined in ISO 3744:2010 [51]. Nevertheless, the feasibility of this approach can be strengthened by using an identical fan copy, maintaining identical microphone positions relative to the fan's rotational center, and employing multiple loading conditions. The latter could provide a measure of sensitivity to amplitude variations. Alternatively, employing different fans could pursue the same objective, though the practical realization of such measurements would be more difficult. Besides the definition of an environment correction factor (i.e., K_2 in ISO 3744:2010 [51]) the listed approach can be utilized on the basis of reciprocal frequency response functions under the assumption of linearity [163].

The method of spherical harmonic decomposition as described in section 2.3 and implemented in Paper 4, demonstrated promising potential for sound characterization of low-pressure axial fans at the fan test facility. The validity of the method could be improved by employing a microphone array with higher accuracy in the average distance to the fan's rotational center. Furthermore, employing alternative sampling strategies (i.e., different spatial distribution of the microphones over the spherical segment) could optimize the use of the limited number of microphones while enabling higher expansion orders [164].

The fan study case investigated in Papers 2 and 5 revealed a complex dependence of the acoustic far-field for installations tested, on both loading conditions and inlet geometry. The limited installation cases investigated with concurrent aerodynamic measurements, however, prevented a comprehensive analysis of these observations. Consequently, a complementary experimental investigation aimed at identifying discrepancies in the flow topology of the tested installations can be motivated. This investigation can incorporate LDA measurements over the blade path and at the fan's aerodynamic interface plane. Alternatively, the incorporation of computational methods (e.g., hybrid computational aeroacoustic methods [165]), validated against measured fan performance (i.e., aerodynamic and acoustic) could enable the identification of inherent flow phenomena and their ties to prevalent noise sources of investigated installations. It is also noted, that despite the short duct length of the installations, an investigation on ducts effects on acoustic source radiation [166], can be suggested.

The investigation in Paper 6 of the interplay between design parameters and installation effects on the aeroacoustics of low-pressure axial fans can be extended by leveraging the capabilities of *C-Fan* [113]. Furthermore, building a larger measurement dataset that includes fan performance, acoustic far-field data, and inlet-flow conditions for a variety of fan installations and loading conditions would enable the development of a semi-empirical prediction model. This model could be developed on the basis of machine learning methods, such as transfer learning random forest [167], and used to predict the acoustic performance of modified fan installations based on measurement data from the nominal installation.

The psychoacoustic evaluation of installation effects on low-pressure axial fans performed in Papers 3 and 5 can be expanded by incorporating subjective listening tests. The representativeness of the acoustic recordings could be improved by integrating a binaural head into the measurement setup. The acquired dataset can be subsequently used to develop predictive models of sound quality, as demonstrated in recent psychoacoustic studies [57].

Bibliography

[1] T. Carolus, *Fans: aerodynamic design-noise reduction-optimization*. Springer Nature, 2023 (cit. on pp. 1, 7, 8, 23, 25, 26, 45–47, 50).

[2] S. Castegnaro, "Aerodynamic design of low-speed axial-flow fans: A historical overview", *Designs*, vol. 2, no. 3, p. 20, 2018 (cit. on p. 1).

[3] G. Agricola, *De re Metallica (English Edition)*. Dover Publications Inc.: Washington, DC, USA, 1950 (cit. on p. 1).

[4] M. Piwowarski and D. Jakowski, "Areas of fan research—a review of the literature in terms of improving operating efficiency and reducing noise emissions", *Energies*, vol. 16, no. 3, p. 1042, 2023 (cit. on p. 1).

[5] K. Bamberger and T. Carolus, "Efficiency limits of fans", *Proceedings of the Institution of Mechanical Engineers, Part A: Journal of Power and Energy*, vol. 234, no. 5, pp. 739–748, 2020 (cit. on p. 1).

[6] C. L. Themann and E. A. Masterson, "Occupational noise exposure: A review of its effects, epidemiology, and impact with recommendations for reducing its burden", *The Journal of the acoustical society of America*, vol. 146, no. 5, pp. 3879–3905, 2019 (cit. on p. 1).

[7] A. Timmis, P. Vardas, N. Townsend *et al.*, "European society of cardiology: Cardiovascular disease statistics 2021", *European heart journal*, vol. 43, no. 8, pp. 716–799, 2022 (cit. on p. 1).

[8] S. Moreau, "The third golden age of aeroacoustics", *Physics of Fluids*, vol. 34, no. 3, 2022 (cit. on p. 1).

[9] I. J. Sharland, "Sources of noise in axial flow fans", *Journal of Sound and Vibration*, vol. 1, no. 3, pp. 302–322, 1964 (cit. on pp. 2, 5).

[10] B. Mugridge and C. Morfey, "Sources of noise in axial flow fans", *The Journal of the Acoustical Society of America*, vol. 51, no. 5A, pp. 1411–1426, 1972 (cit. on pp. 2, 5).

[11] R. E. Longhouse, "Noise mechanism separation and design considerations for low tip-speed, axial-flow fans", *Journal of Sound and Vibration*, vol. 48, no. 4, pp. 461–474, 1976 (cit. on p. 2).

[12] S. Wright, "The acoustic spectrum of axial flow machines", *Journal of Sound and Vibration*, vol. 45, no. 2, pp. 165–223, 1976 (cit. on pp. 2, 47).

[13] W. Neise and U. Michel, "Aerodynamic noise of turbomachines", *Deutsche Forschungsanstalt für Luft- und Raumfahrt e.V., DLR, Institut für Strömungsmechanik, Abt. Turbulenzforschung, Berlin*, vol. 5, 1994 (cit. on pp. 2, 47, 56).

[14] W. K. Blake, *Mechanics of flow-induced sound and vibration, Volume 2: Complex flow-structure interactions*. Academic press, 2017 (cit. on p. 3).

[15] T. J. Mueller, *Aeroacoustic measurements*. Springer Science & Business Media, 2002 (cit. on pp. 4, 16, 18, 21, 31).

[16] D. Ragni, F. Avallone and D. Casalino, "Measurement techniques for aeroacoustics: From aerodynamic comparisons to aeroacoustic assimilations", *Measurement Science and Technology*, vol. 33, no. 6, p. 062 001, 2022 (cit. on p. 4).

[17] L. Botero-Bolívar, F. L. Dos Santos, C. H. Venner and L. D. de Santana, "Trailing-edge far-field noise and noise source characterization in high inflow turbulence conditions", *The Journal of the Acoustical Society of America*, vol. 155, no. 2, pp. 803–816, 2024 (cit. on p. 4).

[18] L. Bowen, A. Celik, B. Zhou, M. F. Westin and M. Azarpeyvand, "The effect of leading edge porosity on airfoil turbulence interaction noise", *The Journal of the Acoustical Society of America*, vol. 152, no. 3, pp. 1437–1448, 2022 (cit. on p. 4).

[19] A. J. Torija, Z. Li and P. Chaitanya, "Psychoacoustic modelling of rotor noise", *The Journal of the Acoustical Society of America*, vol. 151, no. 3, pp. 1804–1815, 2022 (cit. on p. 4).

[20] W. Chen, B. Peng, R. P. Liem and X. Huang, "Experimental study of airfoil-rotor interaction noise by wavelet beamforming", *The Journal of the Acoustical Society of America*, vol. 147, no. 5, pp. 3248–3259, 2020 (cit. on p. 4).

[21] A. J. Torija, P. Chaitanya and Z. Li, "Psychoacoustic analysis of contra-rotating propeller noise for unmanned aerial vehicles", *The Journal of the Acoustical Society of America*, vol. 149, no. 2, pp. 835–846, 2021 (cit. on p. 4).

[22] B. Turhan, H. K. Jawahar, A. Gautam *et al.*, "Acoustic characteristics of phase-synchronized adjacent propellers", *The Journal of the Acoustical Society of America*, vol. 155, no. 5, pp. 3242–3253, 2024 (cit. on p. 4).

[23] R. Merino-Martínez, P. Sijtsma, M. Snellen *et al.*, "A review of acoustic imaging methods using phased microphone arrays: Part of the "aircraft noise generation and assessment" special issue", *CEAS Aeronautical Journal*, vol. 10, pp. 197–230, 2019 (cit. on pp. 4, 21).

[24] X. Niu, H. Chen, Y. Li *et al.*, "Design and performance of a small-scale acoustic wind tunnel at wenzhou university for aerodynamic noise studies", *Applied Acoustics*, vol. 199, p. 109 010, 2022 (cit. on p. 4).

[25] P. Sijtsma and H. Holthusen, "Source location by phased array measurements in closed wind tunnel test sections", in *5th AIAA/CEAS Aeroacoustics Conference and Exhibit*, 1999, p. 1814 (cit. on p. 4).

[26] S. Jaeger, W. Home and C. Allen, "Effect of surface treatment on array microphone self-noise. 6th aiaa", in *CAES Aeroacoustics Conference, Lahaina, Hawaii, AIAA2000–1937*, 2000 (cit. on p. 4).

[27] V. Fleury, L. Coste, R. Davy, A. Mignosi, C Cariou and J.-M. Prosper, "Optimization of microphone array wall mountings in closed-section wind tunnels", *AIAA journal*, vol. 50, no. 11, pp. 2325–2335, 2012 (cit. on p. 4).

[28] L Koop and K Ehrenfried, "Microphone-array processing for wind-tunnel measurements with strong background noise. 14th aiaa/ceas aeroacoustics conference, vancouver, bc, canada", AIAA-2008-2907, Tech. Rep., 2008 (cit. on p. 4).

[29] A. Defreitas and W. N. Alexander, "Identification of anomalies in microphone array measurements of trailing edge noise by eigenstructure analysis", *The Journal of the Acoustical Society of America*, vol. 153, no. 2, pp. 1073–1083, 2023 (cit. on p. 4).

[30] M Bilka, J Anthoine and C Schram, "Design and evaluation of an aeroacoustic wind tunnel for measurement of axial flow fans", *The Journal of the Acoustical Society of America*, vol. 130, no. 6, pp. 3788–3796, 2011 (cit. on p. 4).

[31] L. Huang and J. Wang, "Acoustic analysis of a computer cooling fan", *The Journal of the Acoustical Society of America*, vol. 118, no. 4, pp. 2190–2200, 2005 (cit. on p. 4).

[32] O. Amoiridis, A. Zarri, R. Zamponi *et al.*, "Experimental analysis of the sound radiated by an automotive cooling module working at different operational conditions", in *AIAA AVIATION 2020 FORUM*, 2020, p. 2598 (cit. on pp. 4, 7).

[33] F. Casagrande Hirono, A. Torija Martinez, A. Elliott, J. Taylor, S. Grimshaw and D. Lefas, "Aeroacoustic design and optimisation of an all-electric ducted fan propulsion module for low-noise impact", in *28th AIAA/CEAS Aeroacoustics 2022 Conference*, 2022, p. 3034 (cit. on p. 4).

[34] Y. Sun, R. Li, L. Wang, C. Liu, Z. Yang and F. Ma, "Bionic noise reduction design of axial fan impeller", *Journal of Physics D: Applied Physics*, vol. 57, no. 34, p. 345 501, 2024 (cit. on p. 4).

[35] T. Zhong, C. Yang and M. Åbom, "Tonal noise reduction of an electric ducted fan using over-the-rotor acoustic treatment", *Applied Acoustics*, vol. 205, p. 109 298, 2023 (cit. on pp. 4, 8).

[36] *ISO 5136:2003 Acoustics — Determination of sound power radiated into a duct by fans and other air-moving devices — In-duct method.* International Organization for Standardization, 2003 (cit. on p. 4).

[37] *ISO 5801:2017 Fans — Performance testing using standardized airways.* International Organization for Standardization, 2017 (cit. on pp. 4, 5).

[38] A Maaloum, S Kouidri and R Rey, "Aeroacoustic performance evaluation of axial flow fans based on the unsteady pressure field on the blade surface", *Applied Acoustics*, vol. 65, no. 4, pp. 367–384, 2004 (cit. on pp. 4, 24).

[39] T. Novaković, L. Čurović, M. Hočevar and J. Prezelj, "Impact of geometric modifications of small axial fans on psychoacoustic metrics", *Applied Acoustics*, vol. 218, p. 109 913, 2024 (cit. on pp. 4, 10, 44, 53–55).

[40] E. Canepa, A. Cattanei, F. Jafelice, F. M. Zecchin and D. Parodi, "Effect of rotor deformation and blade loading on the leakage noise in low-speed axial fans", *Journal of Sound and Vibration*, vol. 433, pp. 99–123, 2018 (cit. on p. 4).

[41] A. Cattanei, E. Canepa, G. Milanese and D. Parodi, "Further study on the test configuration for axial flow fans noise measurements", in *16th AIAA/CEAS Aeroacoustics Conference*, 2010, p. 3810 (cit. on p. 4).

[42] S. Wu, S Su and H Shah, "Noise radiation from engine cooling fans", *Journal of Sound and Vibration*, vol. 216, no. 1, pp. 107–132, 1998 (cit. on p. 4).

[43] ISO Central Secretary, "ISO 3745:2012 Acoustics — Determination of sound power levels and sound energy levels of noise sources using sound pressure — Precision methods for anechoic rooms and hemianechoic rooms", en, International Organization for Standardization, Geneva, CH, Standard ISO 3745:2012, 2012. [Online]. Available: `https://www.iso.org/standard/45362.html` (cit. on pp. 4, 5, 17, 18, 21, 29).

[44] A. Rynell, G. Efraimsson, M. Chevalier and M. Abom, "Acoustic characteristics of a heavy duty vehicle cooling module", *Applied acoustics*, vol. 111, pp. 67–76, 2016 (cit. on pp. 4, 7).

[45] A. Corsini, F. Rispoli and A. Sheard, "Aerodynamic performance of blade tip end-plates designed for low-noise operation in axial flow fans", 2009 (cit. on p. 4).

[46] Y. Lai, C. Weng, Y.-Y. Lu, M. Karlsson, M. Abom and M. Knutsson, "Study of installation effects on automotive cooling fan noise", *SAE International Journal of Advances and Current Practices in Mobility*, vol. 5, no. 2022-01-0935, pp. 803–809, 2022 (cit. on pp. 4, 5).

[47] S. Moreau and M. Sanjose, "Sub-harmonic broadband humps and tip noise in low-speed ring fans", *The Journal of the Acoustical Society of America*, vol. 139, no. 1, pp. 118–127, 2016 (cit. on pp. 4, 44, 47).

[48] T. Zhu, D. Lallier-Daniels, M. Sanjosé, S. Moreau and T. Carolus, "Rotating coherent flow structures as a source for narrowband tip clearance noise from axial fans", *Journal of Sound and Vibration*, vol. 417, pp. 198–215, 2018 (cit. on pp. 4, 6, 47).

[49] K. Tokaji and C. Horváth, "Acoustically transparent duct", *International Journal of Aeroacoustics*, vol. 17, no. 3, pp. 238–258, 2018 (cit. on p. 5).

[50] F. J. Zenger, A. Renz, M. Becher and S. Becker, "Experimental investigation of the noise emission of axial fans under distorted inflow conditions", *Journal of Sound and Vibration*, vol. 383, pp. 124–145, 2016 (cit. on pp. 5, 6, 11, 22, 24, 37).

[51] ISO Central Secretary, "ISO 3744:2010 Acoustics — Determination of sound power levels and sound energy levels of noise sources using sound pressure — Engineering methods for an essentially free field over a reflecting plane", en, International Organization for Standardization, Geneva, CH, Standard ISO 3744:2010, 2010. [Online]. Available: `https://www.iso.org/standard/52055.html` (cit. on pp. 5, 16–18, 29–31, 36, 37, 39, 59, 61, 63, 65, 66, 71).

[52] *ISO 10302-1:2011 acoustics – measurement of airborne noise emitted and structure - borne vibration induced by small air - moving devices – part 1: airborne noise measurement*. International Organization for Standardization, 2011 (cit. on p. 5).

[53] M. Hodgson and I. Li, "Experimental study of the noise emission of personal computer cooling fans", *Applied Acoustics*, vol. 67, no. 9, pp. 849–863, 2006 (cit. on p. 5).

[54] J. Hickey, W. Zhao and T. Persoons, "Experimental and numerical investigation of winglet designs for optimized performance of small axial fans", *Applied Acoustics*, vol. 231, p. 110 448, 2025 (cit. on p. 5).

[55] E. Canepa, A. Cattanei, F. M. Zecchin, G. Milanese and D. Parodi, "An experimental investigation on the tip leakage noise in axial-flow fans with rotating shroud", *Journal of Sound and Vibration*, vol. 375, pp. 115–131, 2016 (cit. on pp. 5, 22, 24, 42, 44).

[56] S. Qingyi, X. Haodong, C. Jian and Z. Jiangtao, "Experimental and numerical study on a new noise reduction design for a small axial fan", *Applied Acoustics*, vol. 211, p. 109 535, 2023 (cit. on p. 5).

[57] N. Cerkovnik, J. Murovec, T. Novaković and J. Prezelj, "A psychoacoustic evaluation and predictive model for computer axial fan sound quality", *Applied Acoustics*, vol. 237, p. 110 749, 2025 (cit. on pp. 5, 10, 72).

[58] M. Yadegari, F. Ommi, S. K. Aliabadi and Z. Saboohi, "Reducing the aerodynamic noise of the axial flow fan with perforated surface", *Applied Acoustics*, vol. 215, p. 109 720, 2024 (cit. on p. 5).

[59] A. Cattanei, F. M. Zecchin, A. Di Pasquali and A. Lazari, "Effect of the uneven blade spacing on the noise annoyance of axial-flow fans and side channel blowers", *Applied Acoustics*, vol. 177, p. 107 924, 2021 (cit. on pp. 5, 10, 53–55).

[60] Z. Sun, J. Tian, Y. Zheng, X. Zhu, Z. Du and H. Ouyang, "Design of sinusoidal-shaped inlet duct for acoustic mode modulation noise reduction of cooling fan", *Applied Acoustics*, vol. 216, p. 109 741, 2024 (cit. on pp. 5, 6).

[61] Z. Peng, Y. Wu, J. Tian and H. Ouyang, "Discrete noise control of cooling fan module: Stator and rotor interaction", *Applied Acoustics*, vol. 165, p. 107 308, 2020 (cit. on pp. 5, 7).

[62] Y. Huo, Z. Wang, L. Du *et al.*, "Experimental study on noise reduction of a compact axial fan with leaned vanes", *Applied Acoustics*, vol. 231, p. 110 509, 2025 (cit. on p. 5).

[63] M. Sturm and T. Carolus, "Tonal fan noise of an isolated axial fan rotor due to inhomogeneous coherent structures at the intake", *Noise Control Engineering Journal*, vol. 60, no. 6, pp. 699–706, 2012 (cit. on pp. 5, 22, 44, 47).

[64] M. Sturm and T. Carolus, "Impact of the large-scale environment on the tonal noise of axial fans", *Proceedings of the Institution of Mechanical Engineers, Part A: Journal of Power and Energy*, vol. 227, no. 6, pp. 703–710, 2013 (cit. on p. 5).

[65] F. Bellelli, R. Arina and F. Avallone, "On the impact of operating condition and testing environment on the noise sources in an industrial engine cooling fan", *Applied Acoustics*, vol. 227, p. 110 252, 2025 (cit. on p. 5).

[66] C. Morfey, "The acoustics of axial flow machines", *Journal of Sound and Vibration*, vol. 22, no. 4, pp. 445–466, 1972 (cit. on p. 5).

[67] B. Mugridge, "Acoustic radiation from aerofoils with turbulent boundary layers", *Journal of Sound and Vibration*, vol. 16, no. 4, pp. 593–614, 1971 (cit. on p. 5).

[68] N Chandrashekhara, "Tone radiation from axial flow fans running in turbulent flow", *Journal of Sound and Vibration*, vol. 18, no. 4, pp. 533–543, 1971 (cit. on p. 5).

[69] F. Zenger, G. Herold and S. Becker, "Acoustic characterization of forward-and backward-skewed axial fans under increased inflow turbulence", *AIAA Journal*, vol. 55, no. 4, pp. 1241–1250, 2017 (cit. on pp. 5, 6, 11).

[70] F. Czwielong, C. Ocker, L. Tieghi *et al.*, "Experimental investigations of the aeroacoustic interactions of fan blade skew, leading edge serrations and inflow turbulence", in *30th AIAA/CEAS Aeroacoustics Conference (2024)*, 2024, p. 3391 (cit. on pp. 5, 6, 11).

[71] C. Ocker, T. F. Geyer, F. Czwielong *et al.*, "Permeable leading edges for airfoil and fan noise reduction in disturbed inflow", *AIAA Journal*, vol. 59, no. 12, pp. 4969–4986, 2021 (cit. on pp. 5, 6, 11).

[72] R. A. Wallis, *Axial Flow Fans: Design and Practice*. Academic Press, 2014 (cit. on p. 6).

[73] I. E. Idelchik, M. Steinberg and O. G. Martynenko, *Handbook of Hydraulic Resistance*. Hemisphere Publishing Corporation, New York, 1986, vol. 2 (cit. on p. 6).

[74] W. C. Osborne and C. G. Turner, Eds., *Woods Practical Guide to Fan Engineering*, 5th ed. Woods of Colchester Limited, 1969 (cit. on p. 6).

[75] A Maaloum, S Kouidri, F Bakir and R Rey, "Effect of inlet duct contour and lack thereof on the noise generated of an axial flow fan", *Applied Acoustics*, vol. 64, no. 10, pp. 999–1010, 2003 (cit. on pp. 6, 42).

[76] J. Tian, Z. Sun, P. Chai and H. Ouyang, "Study on the influence of inlet asymmetry on aerodynamic noise of cooling fan", *Journal of Engineering for Gas Turbines and Power*, vol. 142, no. 12, p. 121 014, 2020 (cit. on p. 6).

[77] T. Benedek, J. Vad and B. Lendvai, "Combined acoustic and aerodynamic investigation of the effect of inlet geometry on tip leakage flow noise of free-inlet free-exhaust low-speed axial flow fans", *Applied Acoustics*, vol. 187, p. 108 488, 2022 (cit. on pp. 6, 22, 24).

[78] Z. Sun, J. Tian, T. Zhang, Z. Du and H. Ouyang, "Cooling fan aerodynamic noise reduction with short inlet duct and its applicability", *International Journal of Refrigeration*, vol. 148, pp. 117–130, 2023 (cit. on p. 6).

[79] R. Longhouse, "Control of tip-vortex noise of axial flow fans by rotating shrouds", *Journal of sound and vibration*, vol. 58, no. 2, pp. 201–214, 1978 (cit. on p. 6).

[80] T. Fukano, Y. Takamatsu and Y. Kodama, "The effects of tip clearance on the noise of low pressure axial and mixed flow fans", *Journal of sound and vibration*, vol. 105, no. 2, pp. 291–308, 1986 (cit. on p. 6).

[81] F. Kameier and W. Neise, "Rotating blade flow instability as a source of noise in axial turbomachines", *Journal of sound and vibration*, vol. 203, no. 5, pp. 833–853, 1997 (cit. on p. 6).

[82] T. Fukano and C.-M. Jang, "Tip clearance noise of axial flow fans operating at design and off-design condition", *Journal of sound and vibration*, vol. 275, no. 3-5, pp. 1027–1050, 2004 (cit. on pp. 6, 36).

[83] B. Luo, W. Chu and H. Zhang, "Tip leakage flow and aeroacoustics analysis of a low-speed axial fan", *Aerospace Science and Technology*, vol. 98, p. 105 700, 2020 (cit. on p. 6).

[84] B. Lendvai and T. Benedek, "Experimental and numerical investigation of the blade tip-related aeroacoustic sound source mechanisms of a ducted low-speed axial flow fan", *Applied Acoustics*, vol. 215, p. 109 705, 2024 (cit. on p. 7).

[85] J. M. Tyler and T. G. Sofrin, "Axial flow compressor noise studies", SAE Technical Paper, Tech. Rep., 1962 (cit. on pp. 7, 8, 44, 50).

[86] S Kaji and T Okazaki, "Generation of sound by rotor-stator interaction", *Journal of Sound and Vibration*, vol. 13, no. 3, pp. 281–307, 1970 (cit. on pp. 7, 44).

[87] E. Canepa, A. Cattanei and F. M. Zecchin, "Effect of the rotor–stator gap variation on the tonal noise generated by axial-flow fans", *Applied Acoustics*, vol. 94, pp. 29–38, 2015 (cit. on p. 7).

[88] P. Duncan and B Dawson, "Reduction of interaction tones from axial flow fans by non-uniform distribution of the stator vanes", *Journal of Sound and Vibration*, vol. 38, no. 3, pp. 357–371, 1975 (cit. on p. 7).

[89] P. Duncan and B Dawson, "Reduction of interaction tones from axial flow fans by suitable design of rotor configuration", *Journal of Sound and Vibration*, vol. 33, no. 2, pp. 143–154, 1974 (cit. on p. 7).

[90] F. Czwielong, F. Krömer and S. Becker, "Experimental investigations of the sound emission of axial fans under the influence of suction-side heat exchangers", in *25th AIAA/CEAS aeroacoustics conference*, 2019, p. 2618 (cit. on pp. 7, 22, 24).

[91] F. Czwielong, J. Soldat and S. Becker, "On the interactions of the induced flow field of heat exchangers with axial fans", *Experimental Thermal and Fluid Science*, vol. 139, p. 110 697, 2022 (cit. on pp. 7, 22).

[92] M. Park, D.-J. Lee and H. Lee, "Inflow effects on tonal noise of axial fan under system resistances", *Applied Acoustics*, vol. 192, p. 108 737, 2022 (cit. on pp. 7, 23, 24).

[93] A. Gérard, S. Moreau, A. Berry and P. Masson, "Design of multi-modal obstruction to control tonal fan noise using modulation principles", *Journal of Sound and Vibration*, vol. 356, pp. 34–47, 2015 (cit. on p. 7).

[94] F. Czwielong, S. Floss, M. Kaltenbacher and S. Becker, "Influence of a micro-perforated duct absorber on sound emission and performance of axial fans", *Applied Acoustics*, vol. 174, p. 107 746, 2021 (cit. on p. 8).

[95] N. Liu, C. Jiang, L. Huang and C. Wang, "Effect of porous casing on small axial-flow fan noise", *Applied Acoustics*, vol. 175, p. 107 808, 2021 (cit. on p. 8).

[96] R. Guo, T. Mi, L. Li and R. Luo, "Research on aerodynamic performance and noise reduction of high-voltage fans on fuel cell vehicles", *Applied Acoustics*, vol. 186, p. 108 454, 2022 (cit. on p. 8).

[97] W. Dong, D. Hu, Y. Shen, J. Li and Q. Yang, "Feasibility verification of reducing the total sound pressure level of multiple cooling fans for fuel cell vehicle", *International Journal of Green Energy*, vol. 21, no. 1, pp. 26–42, 2024 (cit. on p. 8).

[98] D. Hu, W. Dong, P. Gao *et al.*, "Noise reduction optimization for numerous radiator fans for fuel cell vehicle considering thermal-fluid-acoustic synergy", *International Journal of Heat and Mass Transfer*, vol. 223, p. 125 231, 2024 (cit. on p. 8).

[99] S. K. Tang and M. Wong, "On noise indices for domestic air conditioners", *Journal of sound and vibration*, vol. 274, no. 1-2, pp. 1–12, 2004 (cit. on p. 9).

[100] M. Schneider and C. Feldmann, "Psychoacoustic evaluation of fan noise", in *Proc. of Fan*, 2015, pp. 1–12 (cit. on pp. 9, 54).

[101] S. Töpken and S. Van de Par, "Perceptual dimensions of fan noise and their relationship to indexes based on the specific loudness", *Acta Acustica united with Acustica*, vol. 105, no. 1, pp. 195–209, 2019 (cit. on pp. 9, 55).

[102] S. Töpken and S. van de Par, "Determination of preference-equivalent levels for fan noise and their prediction by indices based on specific loudness patterns", *The Journal of the Acoustical Society of America*, vol. 145, no. 6, pp. 3399–3409, 2019 (cit. on p. 9).

[103] E. Claaßen, S. Töpken and S. van de Par, "The influence of the reference level on loudness and preference judgements for spectrally manipulated fan sounds", *The Journal of the Acoustical Society of America*, vol. 155, no. 3, pp. 1735–1746, 2024 (cit. on p. 9).

[104] G. Rong, T. Mi, S. Ye, Y. Jiang, J. Lv and Z. Wang, "Modelling and intelligent prediction of sound quality for high-voltage fans on fuel cell vehicles", *Proceedings of the Institution of Mechanical Engineers, Part D: Journal of Automobile Engineering*, vol. 236, no. 6, pp. 1246–1258, 2022 (cit. on p. 9).

[105] Y. Huang and Q. Zheng, "Sound quality modelling of hairdryer noise", *Applied Acoustics*, vol. 197, p. 108 904, 2022 (cit. on p. 9).

[106] F. Zenger, S. Münsterjohann and S. Becker, "Efficient and noise reduced design of axial fans considering psychoacoustic evaluation criteria", *Applied Mechanics and Materials*, vol. 856, pp. 181–187, 2017 (cit. on pp. 10, 53, 55).

[107] J. Muiyser, J. van der Spuy and A. Bekker, "Comparison of sound quality metrics for axial flow fans with straight and forward swept blades", in *Proc. of Fan*, 2018, pp. 1–11 (cit. on pp. 10, 53–55).

[108] *IEA 2025, Global EV Outlook 2025, IEA, Paris 2025, License: CC BY 4.0*, 2025 (cit. on p. 10).

[109] G. Cerrato, "Automotive sound quality-powertrain, road and wind noise", *Sound and Vibration*, vol. 43, no. 4, 16 – 24, 2009 (cit. on pp. 10, 18).

[110] J. Jabben, E. Verheijen and C. Potma, "Noise reduction by electric vehicles in the netherlands", in *Inter-Noise and Noise-Con Congress and Conference Proceedings*, Institute of Noise Control Engineering, vol. 2012, 2012, pp. 6958–6965 (cit. on p. 10).

[111] K. Genuit and A. Fiebig, "Sound design of electric vehicles-challenges and risks", in *INTER-NOISE and NOISE-CON Congress and Conference Proceedings*, Institute of Noise Control Engineering, vol. 249, 2014, pp. 3492–3501 (cit. on pp. 10, 18).

[112] N. C. Otto, R. Simpson and J. Wiederhold, "Electric vehicle sound quality", SAE Technical Paper, Tech. Rep., 1999 (cit. on pp. 10, 18).

[113] D. Ghosh, *Computational aerodynamics and aeroacoustics of low pressure axial fans*. Chalmers Tekniska Hogskola (Sweden), 2025 (cit. on pp. 11, 25–28, 66, 72).

[114] P. V. Gullberg, *Optimisation of the flow process in engine bays-3d modelling of cooling airflow*. Chalmers Tekniska Hogskola (Sweden), 2011 (cit. on p. 16).

[115] ISO Central Secretary, "ISO 26101-1:2021 Acoustics - Test methods for the qualification of the acoustic environment - Part 1: Qualification of free-field environments", en, International Organization for Standardization, Geneva, CH, Standard ISO 26101-1:2021, 2021. [Online]. Available: `https://www.iso.org/standard/80877.html` (cit. on p. 16).

[116] H.-P. Wallin, U. Carlsson, M. Åbom, H. Bodén, R. Glav and R. Hildebrand, *Sound and vibration*, eng, 2., rev. uppl. Stockholm: Institutionen för farkostteknik, Tekniska högskolan, 2010, ISBN: 978-91-7415-553-2 (cit. on pp. 17, 19, 24).

[117] L. Feng, *Acoustical measurements* (Trita-AVE (Department of Aeronautical and Vehicle Engineering, Royal Institute of Technology), 2007:07), eng. Stockholm: KTH Engineering Sciences, 2007 (cit. on pp. 17, 18, 29).

[118] M. Long, *Architectural acoustics*. Elsevier, 2005 (cit. on p. 18).

[119] M. J. Crocker, *Handbook of noise and vibration control*. John Wiley & Sons, 2007 (cit. on p. 18).

[120] O Amoiridis, A Zarri, R Zamponi *et al.*, "Sound localization and quantification analysis of an automotive engine cooling module", *Journal of Sound and Vibration*, vol. 517, p. 116 534, 2022 (cit. on pp. 18, 22).

[121] G. F. Greco, R. Merino-Martínez, A. Osses and S. C. Langer, "Sqat: A matlab-based toolbox for quantitative sound quality analysis", in *INTER-NOISE and NOISE-CON Congress and Conference Proceedings*, Institute of Noise Control Engineering, vol. 268, 2023, pp. 7172–7183 (cit. on pp. 19, 62, 65).

[122] *ISO 532-1:2017 Acoustics Methods for calculating loudness - Part 1: Zwicker method*. International Organization for Standardization, 2017 (cit. on p. 19).

[123] *DIN 45692:2009-08: Measurement technique for the simulation of the auditory sensation of sharpness*. Deutsches Institut für Normung: Berlin, Germany, 2009 (cit. on p. 19).

[124] P. Daniel and R. Weber, "Psychoacoustical roughness: Implementation of an optimized model", *Acta Acustica united with Acustica*, vol. 83, no. 1, pp. 113–123, 1997 (cit. on p. 19).

[125] W. Aures, "Berechnungsverfahren für den sensorischen wohlklang beliebiger schallsignale", *Acta Acustica united with Acustica*, vol. 59, no. 2, pp. 130–141, 1985 (cit. on p. 19).

[126] A. Osses Vecchi, R. García León and A. Kohlrausch, "Modelling the sensation of fluctuation strength", *Proceedings of Meetings on Acoustics*, vol. 28, no. 1, p. 050 005, Apr. 2017 (cit. on p. 19).

[127] G.-Q. Di, X.-W. Chen, K. Song, B. Zhou and C.-M. Pei, "Improvement of zwicker's psychoacoustic annoyance model aiming at tonal noises", *Applied Acoustics*, vol. 105, pp. 164–170, 2016 (cit. on pp. 19, 52).

[128] B. Rafaely, Y. Peled, M. Agmon, D. Khaykin and E. Fisher, "Spherical microphone array beamforming", *Speech Processing in Modern Communication: Challenges and Perspectives*, pp. 281–305, 2010 (cit. on p. 19).

[129] E. G. Williams, *Fourier acoustics: sound radiation and nearfield acoustical holography*. Academic press, 1999 (cit. on pp. 19, 20).

[130] P. Filippi, *Acoustics: basic physics, theory, and methods*. Academic Press, 1999 (cit. on p. 19).

[131] J. B. Allen and D. A. Berkley, "Image method for efficiently simulating small-room acoustics", *The Journal of the Acoustical Society of America*, vol. 65, no. 4, pp. 943–950, 1979 (cit. on p. 20).

[132] F. Zotter, A. Sontacchi, M. Noisternig and R. Höldrich, "Capturing the radiation characteristics of the bonang barung", in *Proc. of the 3rd AAAA Congress*, 2007, pp. 27–28 (cit. on p. 20).

[133] M. Nolan, M. Berzborn and E. Fernandez-Grande, "Isotropy in decaying reverberant sound fields", *The Journal of the Acoustical Society of America*, vol. 148, no. 2, pp. 1077–1088, 2020 (cit. on p. 21).

[134] H. Pomberger, A. Sontacchi, M. Brandner, M. Resch, S. Brandl and R. Höldrich, "Free-field pressure-based sound power measurement procedure with low spatial-sampling-and near-field-induced uncertainty", in *INTER-NOISE and NOISE-CON Congress and Conference Proceedings*, Institute of Noise Control Engineering, vol. 253, 2016, pp. 4318–4327 (cit. on p. 21).

[135] G. Herold and E. Sarradj, "Microphone array method for the characterization of rotating sound sources in axial fans", *Noise Control Engineering Journal*, vol. 63, no. 6, pp. 546–551, 2015 (cit. on p. 22).

[136] F. J. Krömer, S. Moreau and S. Becker, "Experimental investigation of the interplay between the sound field and the flow field in skewed low-pressure axial fans", *Journal of Sound and Vibration*, vol. 442, pp. 220–236, 2019 (cit. on p. 22).

[137] T. Benedek and J. Vad, "An industrial onsite methodology for combined acoustic-aerodynamic diagnostics of axial fans, involving the phased array microphone technique", *International Journal of Aeroacoustics*, vol. 15, no. 1-2, pp. 81–102, 2016 (cit. on p. 22).

[138] C. Ocker, F. Czwielong, P. Chaitanya, W. Pannert and S. Becker, "Aerodynamic and aeroacoustic properties of axial fan blades with slitted leading edges", *Acta Acustica*, vol. 6, p. 48, 2022 (cit. on p. 22).

[139] F. Krömer, F. Czwielong and S. Becker, "Experimental investigation of the sound emission of skewed axial fans with leading-edge serrations", *Aiaa Journal*, vol. 57, no. 12, pp. 5182–5196, 2019 (cit. on p. 22).

[140] H.-E. Albrecht, N. Damaschke, M. Borys and C. Tropea, *Laser Doppler and phase Doppler measurement techniques*. Springer Science & Business Media, 2013 (cit. on pp. 22, 32, 33).

[141] Z. Zhang, *LDA application methods: laser Doppler anemometry for fluid dynamics*. Springer Science & Business Media, 2010 (cit. on pp. 22, 31–33).

[142] R. Franzke, *Experimental and numerical investigations of underhood flow for vehicle thermal management*. Chalmers Tekniska Hogskola (Sweden), 2021 (cit. on p. 22).

[143] M. Vourakis and M. Karlsson, "Aeroacoustic interaction effects between parallel low-pressure axial flow fans", in *10th Convention of the European Acoustics Association, Forum Acusticum 2023*, Torino,Italy 10-15 Septeber 2023 (cit. on p. 23).

[144] F. J. Krömer, "Sound emission of low-pressure axial fans under distorted inflow conditions", Ph.D. dissertation, Dissertation, Erlangen, Friedrich-Alexander-Universität Erlangen-Nürnberg ..., 2018 (cit. on pp. 23, 24).

[145] L. N. Quaroni, R. Merino-Martinez, F. d. Monteiro and S. S. Kumar, "Collective blade pitch angle effect on grid turbulence ingestion noise by an isolated propeller", in *30th AIAA/CEAS Aeroacoustics Conference (2024)*, 2024, p. 3209 (cit. on p. 24).

[146] M. Drela, "Xfoil: An analysis and design system for low reynolds number airfoils", in *Low Reynolds number aerodynamics: proceedings of the conference notre dame, Indiana, USA, 5–7 June 1989*, Springer, 1989, pp. 1–12 (cit. on p. 27).

[147] P. de Haller, "Das verhalten von tragflügelgittern in axialverdichtern und im windkanal", *Brennstoff-Wärme-Kraft (BWK)*, vol. 5, no. 333, p. 24, 1953 (cit. on p. 27).

[148] D. Ragni, *EAA Summer school 2023,lecture notes: Advanced non-intrusive techniques for aeroacosutics*, 2023 (cit. on p. 29).

[149] M. Handbook, "Technical documentation", *Brüel&Kjaer, Naerum*, 2019 (cit. on p. 29).

[150] *Signals and Mechanical Systems,Lecture notes,KTH Royal Institute of Technology*, 2018 (cit. on p. 30).

[151] T. Arts, H. Boerrigter, M. Carbonaro *et al.*, "Measurement techniques in fluid dynamics. an introduction, von karman institute for fluid dynamics", *Rhode-Saint-Genese*, pp. 43–274, Jan. 2001 (cit. on p. 31).

[152] *LDA and PDA Reference Manual,Dantec Dynamics*, 2011 (cit. on pp. 31–33).

[153] F. Zenger, C. Junger, M. Kaltenbacher and S. Becker, "A benchmark case for aerodynamics and aeroacoustics of a low pressure axial fan", SAE Technical Paper, Tech. Rep., 2016 (cit. on pp. 35–37, 39, 60, 63, 71).

[154] F. M. White, *Fluid mechanics*, 1999 (cit. on p. 35).

[155] S. Magne, S. Moreau and A. Berry, "Subharmonic tonal noise from backflow vortices radiated by a low-speed ring fan in uniform inlet flow", *The Journal of the Acoustical Society of America*, vol. 137, no. 1, pp. 228–237, 2015 (cit. on pp. 36, 44, 47).

[156] M. Vourakis, E. Zea, M. Karlsson, N. Andersson and S. Etemad, "Installation effects on axial fans: Combined aeroacoustic and psychoacoustic perspective", *Applied Acoustics*, vol. 240, p. 110 872, 2025 (cit. on p. 37).

[157] W. Cory, *Fans and Ventilation: A Practical Guide*. Elsevier, 2010 (cit. on p. 42).

[158] M. Piellard, B. B. Coutty, V. Le Goff, V. Vidal and F. Pérot, "Direct aeroacoustics simulation of automotive engine cooling fan system: Effect of upstream geometry on broadband noise", in *20th AIAA/CEAS Aeroacoustics Conference*, 2014, p. 2455 (cit. on p. 44).

[159] G. Homicz and A. George, "Broadband and discrete frequency radiation from subsonic rotors", *Journal of Sound and Vibration*, vol. 36, no. 2, pp. 151–177, 1974 (cit. on p. 44).

[160] M. Henner, F. Franquelin, B. Demory, Y. Beddadi, C. Roland and A. Serran, "Hump-shaped broadband noise on a fan at off-design conditions", *Journal of Mathematics and System Science*, vol. 5, pp. 376–384, 2015 (cit. on p. 44).

[161] E. Canepa, A. Cattanei and F. Mazzocut Zecchin, "Leakage noise and related flow pattern in a low-speed axial fan with rotating shroud", *International Journal of Turbomachinery, Propulsion and Power*, vol. 4, no. 3, p. 17, 2019 (cit. on p. 44).

[162] R. Mellin and G. Sovran, "Controlling the tonal characteristics of the aerodynamic noise generated by fan rotors", *Journal of Fluids Engineering, Transactions of the ASME*, vol. 92, no. 1, 143 – 154, 1970. DOI: 10.1115/1.3424923 (cit. on p. 52).

[163] M. Vourakis, *Experimental Studies on the Aeroacoustics of Low-Speed Axial Fans*. Chalmers Tekniska Hogskola (Sweden), 2023 (cit. on p. 71).

[164] F. Zotter and M. Frank, *Ambisonics: A practical 3D audio theory for recording, studio production, sound reinforcement, and virtual reality*. Springer Nature, 2019 (cit. on p. 71).

[165] D. Ghosh, M. Vourakis, A. Boström, N. Andersson, A. Roy and S. Etemad, "Evaluation of hybrid computational aeroacoustic methods applied to automotive cooling-fans", in *International Congress on Fan Noise, Aerodynamics, Applications and Systems 2025, 9-11 April, Antibes/Juan-les-Pins, France*, 2025. [Online]. Available: http://www.fan2025.org/doc/FAN2025%20-PROCEEDINGS%20-%20ISBN%20978-1-905941-32-2.pdf (cit. on p. 72).

[166] B. Baddour, P. Joseph, A. McAlpine and R. Leung, "Duct effects on acoustic source radiation", *AIAA Journal*, vol. 62, no. 3, pp. 1037–1051, 2024 (cit. on p. 72).

[167] X. Zhan, C. Liu, A. Zhang, Y. Liu and Y. Cao, "Prediction of compressor aerodynamic noise based on transfer learning random forest", *The Journal of the Acoustical Society of America*, vol. 158, no. 1, pp. 336–351, 2025 (cit. on p. 72).

Αν τ΄όνειρα που έκαμες είναι ακόμη αλάργα,
μη χάνεις το κουράγιο σου δεν είναι όλα μαύρα,
στη τόλμη και επιμονή που έχεις εντρυφήσει,
ήυρες αξίες φυλακτά για τη παντέρμη ζήση!
Μ.Β.

Appended Papers